Journal Pre-proof

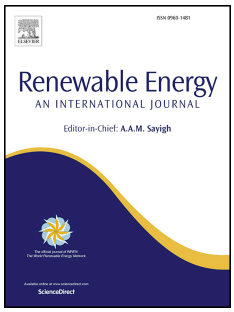

Thermophysical properties of hydrogen mixtures relevant for the development of the hydrogen economy: Review of available experimental data and thermodynamic models

Daniel Lozano-Martín, Alejandro Moreau, César R. Chamorro

PII: S0960-1481(22)01271-X

DOI: https://doi.org/10.1016/j.renene.2022.08.096

Reference: RENE 17617

To appear in: *Renewable Energy*

Received Date: 10 December 2021

Revised Date: 2 April 2022

Accepted Date: 19 August 2022

Please cite this article as: Lozano-Martín D, Moreau A, Chamorro CéR, Thermophysical properties of hydrogen mixtures relevant for the development of the hydrogen economy: Review of available experimental data and thermodynamic models, *Renewable Energy* (2022), doi: https://doi.org/10.1016/j.renene.2022.08.096.

Thermophysical properties of hydrogen mixtures relevant for the development of the hydrogen economy: Review of available experimental data and thermodynamic models.

Daniel Lozano-Martín, Alejandro Moreau, and César R. Chamorro*

Grupo de Termodinámica y Calibración (TERMOCAL), Research Institute on Bioeconomy (BioEcoUVa), Escuela de Ingenierías Industriales, Universidad de Valladolid, Paseo del Cauce, 59, E-47011 Valladolid, Spain.

Abstract

The accurate knowledge of thermophysical and thermodynamic properties of pure hydrogen and hydrogen mixtures plays an important role in the design and operation of many processes involved in hydrogen production, transport, storage, and use. These data are needed for the development of theoretical models necessary for the introduction of hydrogen as a promising energy carrier in the near future. A literature survey on both the available experimental data and the theoretical models associated with the thermodynamic properties of hydrogen mixtures, within the operational ranges of industrial interest for composition, temperature, and pressure, is presented in this work. Considering the available experimental data and the requirements for the design and operation of hydrogen systems, the most relevant gaps in temperature, pressure and composition are identified.

Keywords: hydrogen mixtures; thermophysical properties; equations of state.

Highlights:

Design of hydrogen production and use processes need reliable thermodynamic models.

A literature survey on equations of state for hydrogen mixtures is reported.

Available experimental data are tested against thermodynamic models.

The more relevant data needed to improve equations of state are identified.

* Corresponding author e-mail: cescha@eii.uva.es. Tel.: +34 983423756. Fax: +34 983423363

1. Introduction

In recent years, hydrogen is being pursued as a sustainable energy carrier. Hydrogen allows renewable energy sources to contribute more efficiently to the future energy mix, helping to match the variable output from the main renewable sources (wind and solar) with the demand. Hydrogen gives a way to decarbonize the economy in a broad range of sectors, not only energy and transport, but also in such fields as chemicals or iron and steel production, where it is difficult to search for alternatives that can reduce emissions.

Hydrogen is already in use in a number of important industrial sectors. Pure hydrogen, with only small amounts of contaminants allowed, is demanded for oil refining and fertilizer manufacturing. Hydrogen without prior separation from other gases, mainly in the form of synthesis gas (H_2, CO, CO_2), is also broadly used in industry.

Industry has already proved that hydrogen can be produced, stored and distributed on a large scale [1], but unfortunately, almost all hydrogen for industrial use is nowadays produced from fossil fuels. Hydrogen obtained using renewable energy and sustainable processes, usually called 'green' hydrogen, is currently more expensive. For hydrogen to have a role in future low-carbon energy systems, it is necessary to demonstrate that it can be obtained economically from low-carbon-emission processes, and it also needs to be adopted in sectors where it is almost completely absent at the moment, such as transport, heat supply for buildings and power generation [2].

Hydrogen, like electricity, is an energy carrier rather than an energy source. But unlike electricity, it is a chemical energy carrier, which gives it important advantages. Hydrogen has a higher energy content per unit of mass than most of the conventional fossil fuels and the possibility of higher energy conversion efficiencies when used in fuel cells. On the other hand, most of the 'green' hydrogen production methods are not mature enough, resulting in high production costs.

Hydrogen can be used in its pure form or it can also be combined with other inputs to produce hydrogen-based fuels and feedstock. Hydrogen-based fuels include products such as synthetic methane, synthetic liquid fuels and methanol, all of which require carbon as an input, alongside hydrogen. Hydrogen-based feedstock include such products as ammonia, which can be used as a chemical feedstock or potentially as a fuel.

One of the key elements to permit the hydrogen economy to progress is the development of appropriate thermodynamic models describing the behavior of hydrogen mixtures. The accurate knowledge of thermophysical and thermodynamic properties, such as PVTx, speed of sound, and vapor-liquid equilibrium (VLE), plays an important role in the design and operation of any chemical plant in general [3][4], and of many processes involved in hydrogen production, transport and use in particular [5]. Generally speaking, the precise knowledge of the thermodynamic and transport properties allows to determine the feasibility of a given process, the design of the plant, the sizing of the equipment, and is particularly relevant for the optimization of processes. The requirement for accuracy and reliability varies depending on the application [3].

This work presents a review of both the experimental data and models for the thermodynamic properties of hydrogen mixtures needed in industry and by the energy sector for the development of the hydrogen economy and supersedes our preliminary research advanced in a previous report [6]. The components of the studied mixtures have been selected from among the main components involved in the processes to obtain, transport and use hydrogen with current and foreseeable technologies. The paper is focused on VLE, density, speed of sound and other caloric properties of binary hydrogen mixtures, as those are the main experimental data needed for the improvement of existing reference equations of state and the development of new ones. Phase equilibria data are limited to VLE. Liquid-liquid, solid-liquid, or solid-vapor equilibrium data are not considered in this review. The purpose of the work is to summarize the available experimental data and

theoretical models, evaluate their quality, and identify knowledge gaps, providing suggestions for future research on H_2 mixtures.

2. Obtaining, storing, transporting, and using hydrogen.

Hydrogen is an abundant element but, unfortunately, it is not found as a pure substance in nature. Hydrogen must be extracted from fossil fuels, biomass or water, for which energy is needed and (if fossil fuels are used) CO_2 is emitted. Attending the primary energy source used to produce hydrogen, we can consider thermal, electrical, photonic and biochemical processes. Hydrogen that meets certain sustainability criteria has been termed "green" hydrogen, but there is no universally agreed definition yet, as there is no international green hydrogen standard [2].

2.1. Production processes, components, and compositions

The main technologies for obtaining hydrogen from fossil fuels are hydrocarbon reforming and pyrolysis. These methods are the most commonly used today. Currently, up to 48 % of hydrogen comes from natural gas steam reforming and another 48 % comes from oil reforming and from coal gasification. In hydrocarbon reforming, the other component involved, besides the hydrocarbon, can be steam (steam reforming) or oxygen (partial oxidation). Both processes can be combined (autothermal reaction). Carbon monoxide appears as a byproduct of these processes. The main components that may be involved in all of these processes, besides H_2, are CH_4 (or higher hydrocarbons), CO, CO_2 and H_2O. Hydrocarbon pyrolysis consists in the thermal decomposition (temperatures around 1000 ºC) of the hydrocarbon in an oxygen free environment, producing hydrogen and pure carbon. No CO_2 or CO is produced [7].

Biomass can also be used as the raw material for hydrogen production. Two kinds of processes, thermochemical and biological, can be used. Thermochemical processes, which are much faster and effective than the biological ones, mainly involve pyrolysis and gasification. The main gaseous products are H_2, CH_4, CO, and CO_2. Nitrogen also appears in biomass gasification in the presence of air (syngas).

Biological processes are more environmentally friendly and less energy intensive, as they usually operate at ambient temperature, but they are less efficient. The main biological technologies used for the production of hydrogen are bio-photolysis (direct or indirect) and fermentation (dark or photo-fermentation, simple or multi-stage). The raw material for obtaining hydrogen is water for the bio-photolysis processes and biomass for the fermentation processes. Hydrogen appears accompanied by oxygen in the photolysis processes and by CO_2 in the fermentative processes [8].

Water can be used as an abundant and inexpensive raw material for hydrogen production, but today less than 4 % of hydrogen comes from water splitting, although its relevance is expected to increase in the future. Three main processes can be used: electrolysis, thermolysis or photo-electrolysis. Water electrolysis uses electricity as the required energy input. In the case where the electricity comes from renewable or nuclear sources, the hydrogen produced does not involve the emission of greenhouse gases (GHG) into the atmosphere. Water thermolysis is the decomposition of water into hydrogen and oxygen at very high temperatures (over 2500 ºC). In photo-electrolysis, water is decomposed into hydrogen and oxygen when visible light is absorbed with the help of some photo-catalyst [9][10]. Hydrogen can also be produced by mimicking photosynthesis reactions.

Various comprehensive reviews of the techniques for hydrogen production can be found in [11], [12], [13], and [14].

2.2. Transport and storage

Hydrogen, like electricity, is an energy carrier rather than an energy source, but unlike electricity, it is a chemical energy carrier, which gives it important advantages. Hydrogen has a higher energy content per unit of mass than conventional fossil fuels and, when used in fuel cells, higher energy conversion efficiencies. Hydrogen contains 33.33 kWh energy per kg, compared to 12 kWh for petrol and diesel [15]. However, due to its very low density, storing the same amount of energy requires larger volumes. The development of hydrogen storage technologies is fundamental for the generalization of the use of hydrogen as a fuel. For small-scale applications hydrogen can be stored as a compressed gas, at pressures up to 70 MPa, or as a cryogenic liquid, at temperatures below 20 K [16][17]. For large-scale applications, underground storage is a viable solution. A knowledge of the solubility of hydrogen in water is necessary for the optimization of underground storage, as in some cases the stored gas will be in direct contact with water or brine [18]. Solid-state hydrogen storage has obtained increasing attention in recent years, as it is considered a safer hydrogen storage mode. A classification and description of different technologies of hydrogen storage can be found in [19] and [20].

Hydrogen can be transported in its pure form but blending hydrogen into the natural gas pipelines has important benefits for its transport, making use of the widespread natural gas network. Hydrogen-enriched natural gas can be used directly by the consumer, or alternatively, hydrogen can be separated again from the natural gas at the end of the transport line. The use of hydrogen-enriched natural gas will result in lower carbon dioxide emissions, assuming the hydrogen is produced in a low carbon manner [21]. Used as an alternative fuel, natural gas–hydrogen mixtures represent an intermediate step on the path to an ultimate hydrogen economy.

2.3. Use of hydrogen

Hydrogen can be used in its pure form, or it can also be combined with other inputs to produce hydrogen-based fuels for the energy sector, and feedstock for industry. Hydrogen-based fuels include such products as synthetic methane, synthetic liquid fuels and methanol, all of which require carbon as an input, alongside hydrogen. Hydrogen-based feedstock include such products as ammonia, which can be used as a chemical feedstock or potentially as a fuel.

The use of hydrogen in the energy sector may play a key role in achieving ambitious climate targets, but it is also central to industrial development. Hydrogen is one of the limited options for the decarbonization of many industrial sectors, particularly those that require chemical transformations that may not be amenable to other clean energy sources [22].

There are numerous possibilities of integrating the use of hydrogen into the current power systems: power-to-gas systems as a way to store surplus renewable electricity, stationary fuel cells, vehicular applications, co-generation systems, or even as an alternative fuel for the aviation sector [23]. A review of some examples of the use of hydrogen in different applications can be found in [19].

3. Existing models for pure hydrogen and hydrogen mixtures.

3.1. Equations of state for pure hydrogen.

The current reference equation of state (EoS) for hydrogen is the one proposed in 2009 by Leachman et al. [24], which developed three different forms, one for orthohydrogen, one for parahydrogen, and one for normal-hydrogen. This EoS is included in commercial software of industrial and scientific use such as REFPROP [25]. The equation of state is explicit in the

Helmholtz free energy, with 14 terms, and is valid for temperatures from the triple point (13.957 K) to 1000 K and for pressures up to 2000 MPa.

Actually, hydrogen is a mixture of two different kinds of molecules, namely ortho- and parahydrogen. The differentiating feature of the two forms is the relative orientation of the nuclear spin of the individual atoms, with orthohydrogen existing at higher energy states with parallel nuclear spins and parahydrogen at lower energy states with anti-parallel nuclear spins. Its equilibrium composition for temperatures higher than 200 K approximately is about 75% ortho- and 25% parahydrogen, which is the so-called normal-hydrogen. At lower temperatures, the concentration of parahydrogen continuously increases, although the conversion of nonequilibrium orthohydrogen into parahydrogen composition to an equilibrium hydrogen mixture is quite slow in the absence of a proper catalyst. In any case, the reference EoS of Leachman et al. [24] consider normal-hydrogen as a pure fluid, since the non-idealities associated with the mixing of orthohydrogen and parahydrogen are negligibly small.

The uncertainty in density for this reference equation of state is 0.1 % at temperatures from the triple point to 250 K and at pressures up to 40 MPa, except in the critical region, where the uncertainty rises to 0.2%. In the region between 250 and 450 K and at pressures up to 300 MPa, the uncertainty in density is 0.04%. At temperatures between 450 and 1000 K, the uncertainty in density increases up to 1%. At pressures between 300 and 2000 MPa, the uncertainty in density is 8%. The speed of sound data are represented within 0.5% below 100 MPa. The claimed uncertainty for heat capacities is 1.0%. The estimated uncertainties of vapor pressures and saturated liquid densities are 0.2% for each property [24].

These uncertainties are estimated based on the comparison with the available experimental data sets in the literature, which include PVT, vapor pressure and speed of sound data for each kind of hydrogen, despite several experimental gaps: the most noteworthy are density data at temperatures lower than 50 K for normal-hydrogen, and density and speed of sound data at temperatures higher than 100 K for parahydrogen [26]. The data for orthohydrogen are based on a transformation of the para- and normal-hydrogen data using the quantum law of corresponding states. It should be noted, for the case of the claimed uncertainty of 1.0 % for heat capacities, that only isochoric and isobaric data for parahydrogen are available, showing deviations between (1 to 2) %. However, for normal hydrogen it may be assumed that the uncertainty for the heat capacity will be twice the uncertainty of the speed of sound data in the limit of low pressures, which is also around the value of 1 % mentioned above.

More questionable is the stated uncertainty of 0.2 % of vapor pressures for normal-hydrogen, because the deviations from the literature data are mostly around 1% and even higher, both far from and near the critical point of 33.145 K.

The previous reference equation of state for hydrogen, used as a reference in former versions of NIST's standard properties package REFPROP, was the one proposed in 1982 by Younglove [27]. This equation was based on experimental data for the thermodynamic properties of pure parahydrogen and was modified to predict the thermodynamic properties of normal hydrogen by replacing the ideal-gas heat capacity equation and fixed-point properties of the parahydrogen model with values for normal hydrogen. The range of applicability of the equation of Younglove was pressures up to 121 MPa and temperatures up to 400 K. The model used the International Practical Temperature Scale of 1968. This pressure explicit equation of state for hydrogen was based on the well-known modified Benedict-Webb-Rubin (mBWR) equation of state which uses 32 terms.

Another equation of state for hydrogen, with reference quality, was developed in 2000 by Klimeck [28] for normal hydrogen, specifically designed for the development of the multicomponent

GERG equation of state (GERG 2004 [29] and GERG 2008 [30], which will be described later). The requirements for this equation were a similar structure to that of the other components and of the mixture, good accuracy, and a reasonable simplicity to achieve low computation times. This equation of state was developed by using multi-property fitting and optimization methods. It has an individually optimized structure with 14 terms. This equation is valid for temperatures of (14 to 700) K and pressures up to 300 MPa. The uncertainty in density at pressures up to 30 MPa is less than 0.2% over the temperature range (65 to 270) K and less than 0.1% at temperatures above 270 K. At pressures over 30 MPa, the uncertainty in density is less than (0.2 – 0.3) %.

All the EoS existing to date for hydrogen have been studied in terms of their uncertainty in the work of Sakoda et al. [31]. Briefly, with respect to density the EoS of Leachman et al. [24] for parahydrogen agrees within 0.2 % with that of Younglove [27] at temperatures below 100 K and pressures up to 45 MPa. Above that, the differences between the two EoS grow quickly up to 0.9 %, with a better agreement to the experimental data of the EoS of Leachman et al. For temperatures above than 473 K, the EoS of Younglove [27], Klimeck [28], and Leachman et al. [24] are in agreement also within 0.2 % at pressures up to 120 MPa. However, the limited data available do not allow us to know more. Regarding the vapor pressures, the mutual agreement between the EoS of Leachman et al. and Younglove is good and below 0.4 % for parahydrogen; on the contrary, the EoS of Klimeck deviates significantly from the EoS of Leachman et al. and from the experimental data for normal hydrogen. The saturated liquid densities calculated from the EoS of Leachman et al. and from the one of Younglove match within 0.3 % below the critical point, although the EoS of Leachman et al. yields better estimations of both saturated vapor and liquid densities. According to the speed of sound and heat capacity, the representation of experimental data by the EoS of Leachman et al. is much better than that of Younglove for parahydrogen, especially at temperatures below 100 K and pressures above 100 MPa. This is also true for the EoS of Leachman et al. with respect to the EoS of Klimeck for normal-hydrogen. The maximum deviations for both properties between the three EoS occur at temperatures near 50 K, with differences up to 5 %.

3.2. EoS for hydrogen mixtures

3.2.1. EoS for binary hydrogen mixtures

A model for hydrogen with ammonia binary mixtures was proposed by Neumann et al. [32] in 2020. The model is explicit in the reduced Helmholtz free energy as a function of temperature, density, and composition. The equation of state can be used to calculate all thermodynamic properties over the entire fluid region covering vapor, liquid, phase equilibria, and supercritical states. Most of the experimental data used for the development of the EoS are reproduced within their experimental uncertainty. The range of validity is linked to the available data for each system; however, reasonable extrapolation behavior was ensured with the use of constraints during the fitting process.

A model for the hydrogen with carbon dioxide binary mixture was proposed by Demetriades and Graham in 2016 [33], developed from experimental data measured by Fandiño et al. [34]. The aim of this pressure explicit model was to improve the understanding of the thermodynamic behavior of carbon dioxide and relevant impurities (nitrogen, oxygen, and hydrogen) during the pipeline transport stage of carbon capture and storage (CCS) processes.

In the same year, Blackham [35] developed a reduced Helmholtz EoS for the thermodynamic properties of cryogenic mixtures composed of hydrogen + helium and hydrogen + neon. The application range for mixtures of hydrogen + helium is at temperature range from (14 to 33) K and pressures up to 11 MPa, and for mixtures of hydrogen + neon from (24.6 to 42.5) K and up

to 2.5 MPa. The extrapolation ranges were tested up to 1000 K and 750 MPa for hydrogen + helium, and up to 330 K and 750 MPa for hydrogen + neon.

Cubic EoS (Peng–Robinson, PR, and Soave–Redlich–Kwong, SRK) with quantum corrections for hydrogen, deuterium, helium, neon and their binary mixtures are presented by Aasen et al. [36]. Quantum corrections are needed for quantum fluids such as hydrogen and helium at very low temperatures. The quantum corrections result in a significant better accuracy, especially for caloric properties.

Aasen et al. [37,38] have also developed an Statistical Associating Fluid Theory for Mie potentials of variable range corrected for quantum effects (SAFT-VRQ-Mie) EOS for pure hydrogen, deuterium, helium and neon [37], and for their binary mixtures [38].

Four new equations of state for the binary mixtures of hydrogen with methane, nitrogen, carbon dioxide and carbon monoxide have recently been proposed by Beckmüller et al. [39] as part of research to improve the GERG-2008 EoS [30] for the description of hydrogen enriched natural gas mixtures. These EoS are expressed in terms of the reduced Helmholtz energy and have the same mathematical structure and ranges of validity as the GERG-2008, which allows a direct implementation into the existing framework of the GERG-2008 model.

3.2.2. EoS for multicomponent hydrogen mixtures

The GERG-2008 Equation of State (EoS) [30], an expanded version of the previous GERG-2004 [29], is a valid model for multicomponent mixtures of 21 of the most frequent components of natural gas, hydrogen being one of them. The 21 components are classified as *main components* (methane, nitrogen, carbon dioxide and ethane), *secondary alkanes* (linear alkanes, from propane to n-decane, and branched alkanes, such as isobutane and isopentane) and *other secondary components*. Hydrogen was included in the category of *other secondary components*, together with oxygen, carbon monoxide, water, hydrogen sulfide, helium and argon. The GERG-2008 EoS currently serves as the ISO standard (ISO 20765-2) for the calculation of the thermodynamic properties of natural gases [40].

The GERG-2008 EoS is based on fundamental equations of state for each of the 21 pure substances considered in the model and the correlation equations specifically developed for the 210 possible binary mixtures of the 21 components considered. This structure allows for a description of multicomponent mixtures over a wide range of compositions. Thermal and caloric properties of the most accurate experimental data are represented by the EoS within their accuracy for temperatures from (90 to 450) K and pressures up to 35 MPa. The range of validity can be extended, but with higher uncertainties, for temperatures from (60 to 700) K and pressures up to 70 MPa.

The GERG-2008 is a fundamental equation for multicomponent mixtures explicit in the Helmholtz free energy, with density, temperature and composition as independent variables. The development of a model like this for a multicomponent mixture requires[41][42]:

- pure substance equations of state for all considered components,
- departure functions for each binary function (adjustable from experimental binary data),
- reducing functions for the mixture density and temperature, dependent on the composition (adjustable from experimental binary data, or obtained from combining rules, without any fitting).

Equations of state for hydrogen, carbon monoxide, water and helium were developed specifically for the development of the GERG equation of state. For the rest of the pure constituents, existing

equations of state were used [28] [43] [44]. The range of validity for the new hydrogen EoS [29], developed for this purpose, is (14 to 700) K at pressures up to 300 MPa. The new equation of state is explicit in the Helmholtz free energy, with 14 terms. At the time of the development of the GERG 2004 there was already a pressure explicit equation for hydrogen [27], based on the modified BWR equation of state with 32 terms. The complex structure of this equation and its poor performance in the liquid phase and the supercritical region were the reasons for the necessity to develop a new equation of state for hydrogen.

Departure functions were developed from binary experimental data for 15 of the 210 possible binary mixtures. Seven of these departure functions are *binary specific departure functions*, and the other eight are less accurate *generalized departure functions*. For the other 205 binary systems, no departure functions were adjusted from experimental data, due to the lack of accurate and reliable binary data.

The experimental data available for the binary mixture consisting of hydrogen with methane at the time of the development of the GERG 2004 were considered satisfactory and a binary specific departure function was developed. This binary specific departure function consists of only four polynomial terms, when most of the other departure functions have 10 or even 12 terms (polynomial and exponential). The parameters of the reducing functions were also fitted to the experimental data.

For the 19 other binary mixtures with hydrogen, no departure functions were developed, only the reducing functions were obtained. For the binary mixtures of hydrogen with nitrogen, carbon dioxide, ethane, propane, n-butane, n-hexane, n-heptane and carbon monoxide, the parameters of the reducing functions were fitted to the experimental data, while, for the other ten binary systems, linear or Lorentz-Berthelot combining rules were used to obtain the reducing functions (without any fitting to experimental data). Table 1 summarizes the number of experimental data points used for the fitting of these reducing functions.

The basis for the development of the GERG-2008 EoS was the simultaneous fitting of the coefficients of the equations (departure functions and reducing functions) to experimental data for several thermodynamic properties of binary mixtures (density, speed of sound, isobaric and isochoric heat capacities, enthalpy differences, saturated liquid densities, and VLE data), following the so-called multi-property fitting. The quality and extent of these data determine the accuracy of the model. Approximately 53 000 binary data were used for the development of the GERG-2008, and other 42 000 were used to check the resulting model. For the hydrogen binary mixtures, only 3851 density data and 689 VLE data were used. No speed of sound or other thermodynamic properties were used.

Hassanpouryouzband et al. [5] used the GERG-2008 EoS to predict the thermo-physical properties of H_2 mixed with a typical natural gas from the North Sea and for binary mixtures of hydrogen with selected components of natural gas (CH_4, N_2, CO_2). The predictions are performed over wide ranges of mole fraction of H_2 (10–90 mol %), pressures (0.01–100 MPa), and temperatures (200–500 K). Results are available through a free-access software called H2Themobank [5].

The AGA8-DC92 [45] is another EoS that enables the calculation of thermodynamic properties of multicomponent mixtures of up to 21 components of natural gas, hydrogen among them. This equation is applicable only to the gas phase and has several limitations compared to the GERG-2008 [30].

Demetriades and Graham [33] have proposed a general framework for deriving pressure-explicit EoS for impure CO_2. This framework generalizes a previous EoS for pure CO_2 [46] to binary mixtures with N_2, O_2 and H_2. This model is valid for pressures up to 16 MPa and temperatures

between 273 K and the critical temperature of pure CO_2. In this region, the model achieves close agreement with experimental data. When compared to the GERG EoS, the authors state that this model has a comparable level of agreement with (CO_2 + N_2) VLE experiments and superior agreement with the (CO_2 + O_2) and (CO_2 + H_2) VLE data.

Other simpler EoS, such as the Peng-Robinson EoS or other pressure-explicit cubic EoS, are often used in industrial applications to describe multicomponent hydrogen mixtures. The accuracy obtained with this simpler EoS are not comparable to the more complex models described before within the range for which the latter have been designed.

Binary, ternary and quaternary mixtures of hydrogen, water, and the three main components of air, nitrogen, oxygen and argon, have been studied using molecular modeling through the Monte Carlo approach and simulation, the PC-SAFT equation of state, and sophisticated empirical equations of state by Köster et al. [47]. For that study a new force field for hydrogen was developed. The results obtained for the thermodynamic properties including the phase behavior were compared to experimental data with excellent agreement in many cases.

3.3. Analysis of existing models for binary and multicomponent hydrogen mixtures

Even when it is stated that the GERG-2008 model is valid for hydrogen-enriched natural gas mixtures, with the same level of accuracy in the main ranges of temperature and pressure, the model was initially developed in order to characterize conventional natural gas mixtures, which usually only contain hydrogen in very small amounts, if any. Some papers [48] [49] have evaluated the performance of the GERG and AGA equations of state when dealing with hydrogen-enriched natural gas samples. The results presented in [49] for hydrogen-enriched natural gas mixtures, with up to 30 % of hydrogen, suggests that both equations of state are suitable for hydrogen-enriched natural-gas mixtures in the investigated temperature and pressure ranges. However, the results presented in [48] for a hydrogen enriched natural gas mixture gravimetrically prepared, with only 3 % of hydrogen, show that even when the GERG-2008 EoS displays a better performance than AGA8-DC92 when applied to natural gas-type mixtures without hydrogen, it presents higher deviations for the hydrogen-enriched natural gas mixtures, even for such a low hydrogen concentration as 3 %, mainly at low temperatures and high pressures. Deviations of experimental density data for that 3 % hydrogen-enriched natural gas mixture from the GERG-2008 EoS can be seen in Figure 1.

A problematic aspect of GERG-2008 EoS has been recently reported in the research of Deiters et al. [50]. When the GERG-2208 model is applied to high asymmetric mixtures, i.e, mixtures of components with a high difference between their critical points, it leads to unexpected shapes of the phase envelope. This is the case for many of the mixtures containing hydrogen, and it is revealed as erroneously predicted open phase envelopes, which means unphysical regions of liquid-liquid equilibrium (LLE) phase separation, as depicted in Figure S1. The problem becomes more evident at lower temperatures and corresponding higher pressures, predicting in the worst scenario an unreasonable maximum in the critical line with the temperature. Deiters et al. [50] studied the source of this distortion of the phase envelope shape in the multiparametric GERG models, and concluded that the origin was in the use of empirically corrected critical exponents in the terms applied to the pure-fluid EoS to ensure the accurate prediction of the properties of pure fluid in the vicinity of the critical point. These non-classical terms do not have to be the same for the mixture model as for the pure fluids, and considering them may have a negative side effect, as described above. Thus, they proposed to build the mixture models using classical critical exponents in the pure fluid EoS and introduce the corrected exponents in the final stage of the fitting procedure of the mixture model.

In the work of Beckmüller et al. [39], the known open-phase issues of the GERG-2008 were solved for the systems $H_2 + CH_4$ at temperatures below 120 K, $H_2 + N_2$ at temperatures below 100 K, $H_2 + CO$ at temperatures below 80 K and $H_2 + CO_2$ at temperatures below 260 K. The solution was to: (i) replace the Klimeck [28] EoS of pure hydrogen used in the GERG-2008 model with the current reference EoS of Leachman et al. [24], and (ii) reparametrize the departure function of $H_2 + CH_4$, as well as build three new specific departures equations for $H_2 + N_2$, $H_2 + CO$ and $H_2 + CO_2$, respectively, based on more data sets of accurate VLE and density values than the used in the original model, now covering the whole pressure and temperature ranges where this problem occurred.

The works of Köster et al. [47] and Alkhatib et al. [51] tackle the performance of the widely used cubic EoS and the statistical associating fluid theory (SAFT) EoS compared to GERG-2008 EoS. In these two studies the assessment of the cubic and SAFT EoS compared to the GERG-2008 EoS is made without applying the improvements made to the GERG EoS by Beckmüller et al. [39] considering new binary functions for the mixtures of H_2 with CH_4, N_2, CO and CO_2.

The research of Köster et al. [47] deals with all the subsystems containing H_2, N_2, O_2, Ar, and H_2O. The version of the cubic EoS chosen was Peng-Robinson (PR) [52,53], with the alpha function of Twu et al. [54], the quadratic van der Waals one-fluid mixing rules and no volume translation. The version of the SAFT EoS used was the perturbed chain PC-SAFT [55–57], with Lorentz-Berthelot mixing rule for the energy parameter exclusively, modeling H_2 as a spherical molecule. Pure fluid parameters were taken from literature, and only one binary temperature-independent interaction parameter was fitted to vapor pressure data for the PR and PC-SAFT EoS.

Focusing on hydrogen binary systems and regarding the several VLE data, PR agrees better than the other EoS with the experimental data of both the liquid and vapor saturation lines for the $H_2 + N_2$ system, and with the liquid saturation line for H_2 + Ar. On the contrary, PC-SAFT overestimates the critical point and the pressures of the liquid saturation line for both $H_2 + N_2$ and H_2 + Ar systems, and also shows large discrepancies in the vapor saturation line for H_2 + Ar. GERG-2008 yields a nonphysical open phase envelope for both $H_2 + N_2$ and H_2 + Ar. This issue for the $H_2 + N_2$ system was subsequently corrected in the work of Beckmüller et al. [39], but remains for the mixtures of H_2 + Ar. All the EoS perform well for the vapor saturation line of $H_2 + H_2O$, with PC-SAFT deviating less than PR in the liquid saturation line and GERG-2008 yielding a nonreal open phase envelope again, not yet solved.

Density was evaluated against several equimolar mixtures, where unlike molecular interactions are more significant. For $H_2 + N_2$, PR, SAFT and GERG-2008 EoS perform well for temperatures below T = 273 K, but show increasing deviations at high pressures and densities, overestimating the density at T = (323 up to 373) K. Concerning the H_2 + Ar system, PC-SAFT and GERG-2008 yield low discrepancies, however PR behave worst. In addition, PR fails reproducing the saturated liquid density as expected from a cubic EoS. The results reveal that neither the PR nor the PC-SAFT EoS were able to qualitatively predict the very low experimental values of hydrogen solubility into water and, hence, of the Henry's law constant. Not enough VLE data for $H_2 + O_2$ and density data for $H_2 + O_2$ and $H_2 + H_2O$ were available for comparison.

Furthermore, Köster et al. [47] used molecular simulation through the Monte Carlo method and nonpolarizable force fields taken from literature for Ar, N_2, and O_2, with two different force fields for H_2, a new one developed for H_2 in their work and another from literature. Overall, the Monte Carlo simulation reveals as the more versatile and accurate of all the models analyzed for these systems.

Alkhatib et al. [51] also used the PR EoS with the same alpha function of Twu et al. [54], van der Waals mixing rules and no volume translation such as Köster et al. [47]. But they shifted to the

polar Soft-SAFT EoS [58,59], with again Lorentz-Berthelot mixing rule for only the energy parameter, modeling H_2 as a non-spherical molecule in this case. They studied the binary mixtures of H_2 with CH_4, C_2H_6, C_3H_8, N_2, and CO_2 in terms of VLE, density and some calorific properties, such as isobaric heat capacity, speed of sound and Joule-Thomson coefficient, selecting only one representative data source for each property and system.

PR and polar Soft-SAFT are the only models reproducing the entire phase envelopes for all the binary systems containing hydrogen studied, with higher accuracy from polar Soft-SAFT, although both models overestimate the critical points. For the PR EoS, the deviations systematically increase as the temperature is reduced away from the temperature of the data used in fitting the binary parameter, while for the polar Soft-SAFT EoS this is less notorious. Thus, the predictive behavior of the polar Sof-SAFT is better than PR. They found that GERG-2008 was the least accurate, mainly due to prediction of open phase envelopes with decreasing temperatures and increasing pressure for most of these mixtures. These unexpected shapes of the phase boundary were announced in the work of Deiters et al. [50] and corrected in the work of Beckmüller et al. [39], reparametrizing the GERG-2008 with a wider range and more accurate experimental database than the original one used for the binary mixtures of H_2 + CH_4, H_2 + N_2, and H_2 + CO_2. Surprisingly, Alkhatib et al. [51] also report an open phase envelope in the case of H_2 + CO_2, not saw in the research of Köster et al. [47], even when dealing also with this system at similar temperatures around 80 K.

Regarding the system H_2 + CH_4, both PR, polar Soft-SAFT and GERG-2008 reproduce the density and isobaric heat capacity experimental data with similar deviations. These deviations are constant with the hydrogen content for the density but tend to increase rapidly with the hydrogen molar fraction for the heat capacity. Moreover, GERG-2008 model clearly outperforms in estimating the speed of sound data, while the polar Soft-SAFT model performs with smaller deviations with respect to the Joule-Thomson coefficients (JT). Similar qualitative discrepancies are found for the other systems: H_2 + C_2H_6, H_2 + C_3H_8, H_2 + N_2, and H_2 + CO_2, with similar agreement for density and speed of sound of all the models, while polar Soft-SAFT deviates less for second-order derivative properties, such as the JT coefficient, again.

In addition, Alkhatib et al. [51] computed also viscosity values through the Chapman-Enskog theory for the dilute gas contribution and the residual part from either PR + friction theory, or polar Soft-SAFT + free volume theory, or GERG-2008 + extended corresponding states.

The inclusion of quantum corrections in the alpha function of the cubics EoS and in the framework of the SAFT EoS, as well as temperature dependent binary interaction parameters, is suggested to enhance the accuracy of both models, specially at low temperatures, with the disadvantage of losing simplicity and predictive capabilities, and requiring a much larger experimental database for reparameterization.

Although, cubic EoS with classical expressions accurately reproduce the VLE data, they clearly fail reproducing the interaction second virial coefficients and densities of the mixtures at most ultra-cryogenic states. This stems mainly in the poor description of these properties for the pure components at low temperatures. Aasen et al. deal with this issue in a subsequent work [36], adding temperature dependent quantum corrections into the covolume parameter for both PR and SRK EoS. This results in an overall improvement of the predictive capabilities of these models, highlighting the reduction of the error representing the isochoric heat capacity of liquid hydrogen at saturation from 80 % to less than 4 %.

The implementation of quantum corrections in the framework of the SAFT-type EoS has been addressed in the works of Aasen et al. focusing on ultra-cryogenic conditions, first for the pure hydrogen, helium, neon, and deuterium [37], and then extended for their mixtures [38]. The

strategy followed has been to use Monte Carlo simulations via Mie potential with Feynman-Hibbs quantum corrections to optimize the parameters of two different force fields by fitting to experimental VLE data and interaction second virial coefficients B_{ij} (from the literature and ab initio calculations) for the mixtures of the mentioned fluids. Then, the already adjusted force field was introduced into the statistical associating fluid theory-variable range (SAFT-VR) EoS by a proper perturbation theory to yield the statistical associating fluid theory of quantum corrected Mie potentials (SAFT-VRQ Mie) EoS. In this work, the cubic EoS of Soave–Redlich–Kwong (SKR) is used in the comparison as a reference classical and simple model to know if the increase of accuracy of the SAFT-VRQ Mie EoS is justified by the increase in complexity by adding quantum corrections.

Regarding the mixtures containing hydrogen, for H_2 + Ne both the simulations, the SAFT-VRQ Mie EoS and SRK EoS reproduce well the phase envelopes data, with SRK EoS been slightly more accurate. However, SAFT-VRQ Mie EoS shows a great improvement representing B_{ij}, and the liquid densities: SRK EoS overestimate liquid densities at low temperatures and underestimate them at high temperatures systematically. SAFT-VRQ Mie EoS also overcomes SRK EoS at estimating experimental speeds of sound. With respect to H_2 + He mixtures, there is a close agreement between experimental phase envelopes data and both simulations and SRK EoS, though SRK overpredicts systematically the concentration of helium in the saturated liquid line. SAFT-VRQ Mie performs excellent away from the critical region, but sharply overpredicts the critical pressure. Despite this, the quantum corrections do represent an improvement for the estimation of saturated liquid density. Finally, the comparison with ab initio computations of B_{ij} for these mixtures is satisfactory for SAFT-VRQ Mie EoS and the simulations with one of the force fields, showing clear deviations with the SRK EoS.

4. Available experimental data for hydrogen binary mixtures

High-quality experimental data are needed to develop reliable thermodynamic models, but obtaining high-quality experimental data is expensive and time-consuming, and in general, such data are scarce [3]. This scarcity of experimental data is more acute in emerging fields such as the hydrogen economy.

The GERG 2008 EoS was developed as a reference for natural gas mixtures. In any case, the main components that accompany hydrogen in the vast majority of processes for the production, storage, transport and final use of hydrogen, are included in the list of the 21 components considered in this EoS. For this reason, we have taken the list of components of the GERG-2008 as starting point for this literature search.

For this literature search, we have considered only binary mixtures of hydrogen with the 20 other elements included in the GERG-2008 EoS and additionally we have considered the binary mixtures of hydrogen with neon and ammonia. The thermophysical properties object of this survey are VLE equilibrium data, density, and speed of sound and other calorific properties, in the main range of applicability of the GERG-2008 EoS, as these are the more relevant data sets of data for the development of multiparametric EoS.

Table 2 shows the available experimental data on VLE for hydrogen binary mixtures, indicating the authors, the experimental technique used, composition of the binary mixture, ranges of temperature and pressure, and estimated uncertainty for each magnitude, for each reference. Tables 3 and 4 present the same information for the available experimental data on density and speed of sound, respectively. The experimental techniques used to obtain these data are usually described in detail in the original sources, but a comprehensive review of the available

experimental techniques can be found in the works of Wagner and Kleinrahm [60] and Cheng et al. [61].

The experimental data sets presented in Tables 2, 3, and 4 have been classified in two categories based on an estimate of their quality. The ranks or priorities of the data sets are given in the third column of these tables. The rank (1 is primary, 2 is secondary) of the data set is determined based on the apparatus used for the measurements and its stated achievable uncertainty, the expertise and trajectory of the laboratory, the agreement with other data sets, and the year the data were taken. In some cases, a rank value of 1 indicates that the experimental data set was weighted during the fitting process and a rank value of 2 indicates that the experimental data sets were used as supplementary measurements in determining real fluid behavior of the system.

The reported uncertainty in the last column of Tables 2, 3, and 4 are taken from the references, when available. In general, modern references clearly indicate the experimental expanded (k = 2) uncertainty of the measurement and the state point. For all other works, it has been considered any indication of error, accuracy, or precision as the best estimation of what we currently understand by standard uncertainty of measurement. And they are collected in Tables 2, 3, and 4, after multiplying these values by two.

4.1. Analysis of the available experimental data

Tables 5, 6 and 7 present the statistical analysis of the deviations of the experimental data sets presented in Tables 2, 3 and 4 with respect to the GERG-2008 EoS with the improvements developed by Beckmüller et al. [39]. The mixture model used for estimating the properties of helium + hydrogen and neon + hydrogen is the one proposed by Blackham [35] and the mixture model used for estimating the properties of ammonia + hydrogen is the one proposed by Neumann et al. [32]. Unless otherwise stated, all calculations are made considering hydrogen as normal hydrogen. Data where deviations could be not calculated because the equation of state does not converge or where the equation of state does converge, but with relative deviations greater than 100%, clearly out of agreement, are not considered in the statistical analysis. Data for pure fluids are also discarded. It is indicated in Tables 5, 6 and 7 if the deviations are within the reported experimental expanded (k = 2) uncertainty for every data set.

We have analyzed the deviations with respect to the GERG EoS in terms of Average Absolute Relative Deviations (AARD), Bias, Root Mean Square (RMS), and Maximum Absolute Relative Deviation (Max ARD), defined as follows:

$$\mathrm{AARD} = \frac{1}{n}\sum_{i=1}^{n}\left|10^2 \cdot \frac{x_{\mathrm{i,exp}} - x_{\mathrm{i,EoS}}}{x_{\mathrm{i,EoS}}}\right| \quad (1)$$

$$\mathrm{Bias} = \frac{1}{n}\sum_{i=1}^{n}\left(10^2 \cdot \frac{x_{\mathrm{i,exp}} - x_{\mathrm{i,EoS}}}{x_{\mathrm{i,EoS}}}\right) \quad (2)$$

$$\mathrm{RMS} = \sqrt{\frac{1}{n}\sum_{i=1}^{n}\left(10^2 \cdot \frac{x_{\mathrm{i,EoS}} - x_{\mathrm{i,EoS}}}{x_{\mathrm{i,EoS}}}\right)^2} \quad (3)$$

$$\mathrm{Max\ RD} = \max\left(\left|10^2 \cdot \frac{x_{\mathrm{i,exp}} - x_{\mathrm{i,EoS}}}{x_{\mathrm{i,EoS}}}\right|\right) \quad (4)$$

The AARD and Max RD are not meaningful in the case of the VLE data. In this case, the Average Absolute Deviations (AAD) and Maximum Absolute Deviation (Max AD) in mol % are used instead, defined as:

$$\mathrm{AAD} = \frac{1}{n}\sum_{i=1}^{n}\left|10^2 \cdot (x_{\mathrm{i,exp}} - x_{\mathrm{i,EoS}})\right| \quad (5)$$

$$\mathrm{Max\ AD} = \max\left(\left|10^2 \cdot (x_{\mathrm{i,exp}} - x_{\mathrm{i,EoS}})\right|\right) \quad (6)$$

A total of 4854 experimental VLE data, corresponding to 16 binary systems (14 of the 20 possible binary systems with hydrogen considered by the GERG-2008 EoS, see Table 1), are analyzed and the results are summarized in Table 5. In the same way, the results of the analysis of the 5603 experimental density data, corresponding to 12 binary systems (10 of them of those 20 binary systems), are summarized in Table 6; while the results of the analysis of the 1043 experimental speed of sound data or other caloric properties, corresponding to 8 binary systems (7 of them of those 20 binary systems), are presented in Table 7.

Figures 2 to 10 show the deviations of the bubble-point data and the dew-point data (in mol-%) for the binary mixtures of hydrogen analyzed in this work with respect to the improved GERG-2008 EoS [30][39]. In the same way, Figures 11 to 17 depict the percentage deviations of homogeneous density data, and Figures 18 to 21 display the percentage deviations of speed of sound, isobaric heat capacity, excess enthalpy and joule-Thomson coefficient data.

As supplementary material, Figures S2 to S5, show average absolute deviations of vapor-liquid equilibrium (VLE), density and compressibility, and speed of sound and other calorific properties data with respect to the improved GERG-2008 EoS [30][39]. Figures S6 to S11 depict (*p*, *T*), (*p*, *x*), and (*p*, *y*) plots of vapor-liquid equilibrium (VLE) data. Figures S12 to 16 illustrate (*p*, *T*) and (*p*, *x*) plots of density, compressibility, speed of sound, and other calorific properties data.

Near half of the VLE data (2260 of 4854, Figures 2, 3, 4 and 7), and most of the density data (4199 of 5603, Figures 11, 12, 13 and 16) and the speed of sound data, as well as other caloric properties (914 of 1043, Figures 18, 19, 20, and 21), correspond to the binary systems of hydrogen with methane, nitrogen, carbon dioxide and carbon monoxide. The binary system hydrogen with methane is the only one for which a binary specific departure function is included in the GERG-2008 model [30], and new equations of state for the four binary systems of hydrogen with methane, nitrogen, carbon dioxide and carbon monoxide were proposed recently by Beckmüller et al. [39]. A detailed analysis of the available experimental data for these four systems, whose deviations from the GERG-2008 EoS are presented in Figures 2, 3, 4, and 7, can be found in that paper [39].

With respect to the VLE of CH_4 + H_2 (see Figure 2), the AAD ranges between (0.20 to 5.2) mol-%, but most of the differences remain about 1 % for the saturated liquid line and twice for the saturated vapor data. The higher AAD of the saturated vapor line are due to the data at higher temperatures, especially at composition between the critical point and the maximum composition. However, the discrepancies are higher than the stated experimental uncertainties. For example, Tsang et al. [62] indicate an expanded (k = 2) experimental uncertainty of 0.5 mol-% and the AAD are between (1.2 to 1.4)%, while Hong et al. [63] report a 0.33 mol-% of uncertainty and the resulting AAD are above 0.82 mol-%. regarding the density of this system (see Figure 11), the AARD are between (0.014 to 1.4) %, with an average value of 0.5 %, and within the experimental uncertainty for most of the works in non-extreme conditions: Hernández-Gómez et

al. [136] report an expanded (k = 2) uncertainty of 0.5 %, while the AARD are an order of magnitude lower, 0.05 %. At low temperatures and high pressures, up to 100 MPa, the situation is different and the data of Machado et al. [64] gives AARD of 1.4 %, which are outside the claimed uncertainty of 0.2 %. In addition, speed of sound data from Lozano-Martín et al. [176] and Maurer [175] is also well reproduced (see Figure 18).

Regarding the VLE of N_2 + H_2 (see Figure 3), the estimated dew and bubble points of the phase envelopes by the mixture model of Beckmüller et al. [39] result in a good agreement, with deviations as low as for the previous system and AAD = (0.06 to 2.2) mol-%, with an overall AAD of 1 mol-%. Although, these differences are outside the experimental expanded (k = 2) uncertainty reported by several authors, it seems they were determined too optimistically in general. For instance, data sets of Streett et al. [65] show differences below 1.4 mol-% in comparison with an experimental expanded (k = 2) uncertainty of 0.1 mol-%; however, some inconsistencies appear in the saturated vapor line approaching the maximum pressure of the phase boundary which are higher than the claimed uncertainty. A clear improvement over the phase envelope is reflected in the density data of Mastinu et al. [66] at low temperatures, below 100 K, accurately reproduced with an AARD = 0.9 %. Another representative density data sets for this system are those of Jaeschke et al. [149] and Michels et al. [67] at temperatures between (270 to 420) K, which correspond well with an experimental uncertainty below 0.1 % and yield low AARDs (see Figure 12). At even higher temperatures and pressures, the density data of Bennett et al. [68] show deviations that increase with the pressure, in line with an increasing experimental uncertainty. Apart from these properties, also speed of sound data from Van Itterbeek et al. [69] exist (see Figure 18), but as the authors do not report an experimental uncertainty, we only conclude the data are well represented.

For the system CO_2 + H_2 (see Figure 4), the VLE data sets of Fandiño et al. [34] are quite comprehensive and well reproduced by the mixture model of Beckmüller et al. [39], with AAD of (0.13 and 0.45) mol-% for the saturated liquid and vapor lines, respectively. These results are within the corresponding experimental expanded (k = 2) uncertainties of (0.3 and 0.5) mol-% for the bubble and dew points, respectively. Similar good agreement is also present with the data of Tsang et al. [70], which extends the experimental pressure range up to 170 MPa. One reliable data set of density for these mixtures is the work of Souissi et al. [71] (see Figure 13). The AARD is rather low, about 0.2 %; however, the mixture model is not capable of reproducing the data within the extremely low specified uncertainty of 0.06 %. Higher pressure and temperature ranges where studied by Cipollina et al. [72] and Mallu et al. [73], respectively. Unfortunately, both data source show large dispersion of the experimental values or the results show an offset compared to the data of Souissi et al. [71]. Finally, the density data of Cheng et al. [74] at high temperatures up to 670 K do are represented within the experimental expanded (k = 2) uncertainty by the EoS, with an AARD = 0.41 %.

Figure 5 shows the deviations of the bubble-point data and the dew-point data (in mol %) for the binary mixtures ethane + hydrogen and propane + hydrogen. A total of 500 experimental VLE data points are included in this Figure 5. The AAD deviations range from 0.012 for the 70 dew-point data of the system ethane + hydrogen, measured by Hiza et al. [75], to 2.5 for the 54 dew-point data of the system propane + hydrogen, measured by Burris et al. [76]. Mihara et al. [77] measured the density of these two mixtures. A total of 227 density data are analyzed. The results can be seen in Figure 14. The AARD for the 154 data of the ethane + hydrogen system is 0.23 and 0.12 for the 73 data of the propane + hydrogen system. Temperature range for these measurements is (298 – 348) K and pressures up to 9.3 MPa. Mason et al. [78] also give densities for these two systems, but only at atmospheric pressure and 289 K.

In the same way, Figure 6 shows the deviations of the bubble-point data and dew-point data (in mol %) for the binary mixtures n-butane + hydrogen, i-butane + hydrogen, pentane + hydrogen,

and hexane + hydrogen. In this case, a total of 563 experimental VLE data points are included in Figure 6. The AAD for these sets of data range from 0.13 for the 28 dew-point data of the system n-butane + hydrogen, measured by Aroyan et al. [79], to 9.5 for the 22 bubble-point data of the system i-butane + hydrogen, measured by Dean et al. [80]. Figure 15 depicts the deviations of the density data of these mixtures. A total of 482 density data are analyzed, of which 421 correspond to the system hexane + hydrogen, measured by Nichols et al. [81]. These 421 experimental density data for the system hexane + hydrogen cover a temperature range from 278 K to 511 K and pressures up to 68.9 MPa. The AARD of these data is as low as 0.034, with a Max ARD of 13.

According to the VLE of CO + H_2 (see Figure 7), the data base is more limited in the number of points and the temperature, pressure, and composition ranges. In addition, some authors do not report a clear overall experimental uncertainty, as Verschoyle [82]. The most reliable data for comparison is the work of Tsang et al. [83], with the mixture model of Beckmüller et al. [39] representing the data successfully, with AAD = 0.6 mol-% for the saturated liquid line and AAD = 0.8 mol-% for the saturated vapor line. With respect to density data (see Figure 16), the most recent data of Cipollina et al. [72] yield AARD = 2.4 %, which are too high for this system and does not match the AARD from the same authors but for the system CO_2 + H_2 of 0.5 %. Lower differences are obtained in our work when comparing to the data of Scott [84] and Townend et al. [85], with AARD of 0.25 % and 0.16 %, respectively. Although the authors do not report any overall experimental uncertainty, the disagreement could be explained considering the relatively high content of impurities present in the studied mixtures. The same as mentioned above for the speed of sound data (see Figure 18) from Van Itterbeek et al. [69] applies in this system.

The VLE of the system water + hydrogen was studied by Setthanan et al. [86], Kling et al. [87], Wiebe et al. [88], and Shoor et al. [89], while the VLE of the system hydrogen sulfide + hydrogen was studied by Yorizane et al. [90]. There is a total of 55 experimental VLE data for the system with water and 22 for the system with hydrogen sulfide, whose deviations from the GERG-2008 EoS (bubble-point data and dew-point data, in mol %) are presented in Figure 8. The data set from Wiebe et al. [88] is the more numerous (40) and has a broader range in temperature and pressure, from 273 K to 373 K, and up to 101 MPa. The AAD of this set of data is 0.51 with a Max AD of 1.4. Note that the GERG-2008 EoS estimates fairly well the dew points but not the bubble points for the water + hydrogen, even taking into account the low solubility of hydrogen into liquid water. The GERG-2008 model overpredicts by far the liquid saturation line, estimating an open phase envelope contrary to the experimental data. No experimental data on density, speed of sound or other caloric properties have been found for these two binary systems.

A total of 487 experimental VLE data points for the binary systems helium + hydrogen have been published by Yamanishi et al. [91], Hiza [92], Hiza [93], Sneed et al. [94], Streett et al. [95], and Sonntag et al. [96]; and a total of 378 points for the system argon + hydrogen can be found at Calado et al. [97] and Volk et al. [98], and a total of 323 points for the system neon + hydrogen have been reported by Streett et al. [99], Heck et al. [100], and Zelfde et al. [101]. Their deviations can be seen in Figure 9. Most of these data are for pressures below 10 MPa, except the data from Calado et al. [97] that covers a range up to 52 MPa. Temperature ranges for the binary system helium + hydrogen are between 15 K and 30 K, and between 80 K and 140 K for the binary system argon + hydrogen. The AAD for these sets of data range from 0.22 for the 21 bubble-point data of the system helium + hydrogen, measured by Hiza [92], to 19 for the 132 bubble-point data of the system argon + hydrogen, measured by Calado et al. [97]. The weakness of the Blackham [35] mixture model are describing the VLE and density properties in the following conditions: (i) for the hydrogen + helium system, in the critical region and at temperatures below 15 K and above 32 K with pressures below 1 MPa and above 11 MPa, (ii) for the hydrogen + neon system, in the critical region and also for molar fractions of neon between (0.03 to 0.3). It is worth highlighting the really high discrepancy obtained for the argon + hydrogen system in the whole phase envelope

according to the GERG-2008. Again, the GERG EoS yields a false open phase envelope, overestimating the pressures at the cryogenic temperatures of experimental data from Calado et al. [97] and Volk et al. [98]. This can be understood considering that the development of the GERG was focused on natural gas mixtures and its normal range of validity is for T > 90 K. A total of 290 density data points for the system argon + hydrogen are also available in the scientific literature at Scholz et al. [102], Tanner et al. [103], and Zandbergen et al. [104], and a total of 229 density points for the system neon + hydrogen at Streett [105] and Güsewell et al. [106]. Deviations of these density data from the GERG-2008 EoS are represented in Figure 16. The AARD for the sets of density data for argon + hydrogen ranges from 0.32 for the data of Scholz et al. [102] to 1.4 for the data of Zandbergen et al. [104], while the AARD for the sets of density data of neon + hydrogen are around 5.6 %. The absolute deviation for this last set of data can be as high as 9.3 % for the argon + hydrogen system, but this set of data is also the one that reaches the lowest temperature (170 K). In the case of the neon + hydrogen system, the maximum absolute deviation is 27 %, at temperatures between (25 to 31) K. The ranges of pressures for the three sets of data are around 10 MPa. There are also a few speed of sound data, only 8, for these two binary mixtures, published by Van Itterbeek et al. [107] in 1946, and their deviations are shown in Figure 18.

Figure 10 shows the deviations of the bubble-point data and the dew-point data (in mol-%) for the binary mixture ammonia + hydrogen. A total of 246 experimental VLE data points are included in this Figure 10. The AAD deviations range from 0.0004 to 1.1 for the dew-point data and 0.78 for the bubble-point data of the system ammonia + hydrogen. A total of 172 density data are analyzed for ammonia + hydrogen mixtures by Kazarnovskiy et al. [108] and Hongo et al. [109]. These results can be seen in Figure 17.

The huge asymmetry between ammonia and hydrogen, due to their very different critical points (T_c (NH_3) = 405.56 K *vs.* T_c (H_2) = 33.145 K), made necessary to develop a departure function in the EoS of Neumann et al. [32]. In general, the experimental phase envelopes are well described by this model, with overall AAD from all the datasets considered in this work of 0.5 mol-%, even for lower temperatures where the phase boundary becomes steeper. The solubility data sets of Wiebe et al. [110] and Wiebe et al. [111] agree with the model within an AAD of 1.1 mol-% and 0.35 mol-%, respectively. Unfortunately, they do not indicate any experimental uncertainty. Reamer et al. [112] measured dew points and calculated bubble points for this system in the range (280 – 390) K up to 4.2 MPa. They declared an experimental uncertainty of only 0.2 mol-%, too optimistic. A more reasonable uncertainty of 1 mol-% yields that nearly all the deviations remain within the uncertainty, with AAD of 0.15 mol-% for the dew points and 0.78 mol-% for the bubble points. Other data sets found in the literature are of lower quality. With respect to density data, Kazarnovskiy et al. [108] measured molar volumes up to 155 MPa with a 2% experimental expanded (k = 2) uncertainty. This data is represented with deviations half the uncertainty, AARD = 1.1 %. Furthermore, Hongo et al. [109] determined densities up to 6.6 MPa, but they do not claim any uncertainty. In any case, the relative discrepancies are on average of 0.67 %, slightly increasing with the pressure as usual, thus suggesting a good agreement.

Figure 19 depicts the deviation of the 78 available molar heat capacity data for the binary system nitrogen + hydrogen, measured by Knapp et al. [113]. Figure 20 shows the deviation of the molar heat capacities measured by Wormald et al. [114] for the binary systems methane + hydrogen and nitrogen + hydrogen. Finally, Figure 21 shows the percentage deviations of the Joule-Thompson data for the binary system methane + hydrogen, measured by Randelman et al. [115].

5. Conclusions

The basis for the development of multiparameter equations of state is experimental data for several thermodynamic properties. The quality and extent of these data determine the accuracy of the model. The paper describing the GERG 2008 stated that it seems to be worthwhile to develop different generalized departure functions for several binary mixtures, hydrogen with other components among them. For the development of these generalized, or binary-specific, departure functions, as well as for the development of reducing functions for the mixture density and temperature, dependent on the composition, an extended set of high-quality experimental data of thermodynamic properties of binary mixtures of hydrogen with the rest of the components of natural gas is needed.

Only the methane + hydrogen binary system, of the 20 possible binary mixtures of hydrogen with the rest of the components considered by the GERG-2008 model, has a binary specific departure function included in the current GERG-2008 EoS. A recent study by Beckmüller et al. [39] has developed four equations of state for the binary systems of hydrogen with methane, nitrogen, carbon dioxide, and carbon monoxide. Nevertheless, they recognize that new highly accurate data for these systems are still required for further improvements and a more comprehensive validation, especially for the binary system hydrogen + carbon monoxide. For the rest of the binary systems, the amount of experimental data available is very poor. VLE data are available for the binary mixtures of hydrogen with ethane, propane, butane, iso-butane, pentane, hexane, water, hydrogen sulfide, helium, and argon. Density data are available for the binary mixtures of hydrogen with ethane, propane, butane, pentane, hexane, and argon. Finally, very few speed of sound or other caloric properties data are available, and only for the binary mixtures of hydrogen with oxygen, helium, and argon. There is a real need for density and speed of sound data for the binary systems of hydrogen with water, hydrogen sulfide, helium, and argon, besides all the linear hydrocarbons from ethane to decane, including iso-butane and iso-pentane. Not only mixtures of hydrogen with the components of natural gas are of interest for the industry. A recent survey on industrial requirements for thermodynamic and transport properties presented by Kontogeorgis et al. [4], pointed out that accurate prediction of fluid-liquid phase equilibrium and dew point calculations for mixtures including heavier hydrocarbons and hydrogen is crucial.

For the development of new EoS, not only experimental data of binary mixtures with hydrogen will be necessary, but also binary mixtures between the rest of the components of natural gas. As an example, for the binary mixtures with CO_2, a review of available models and experimental data is presented by Li et al. [116][117].

Besides the experimental data of binary mixtures, which are relevant for the development of new equations of state, it is also important to check the capability of the current or newly developed EoS with multicomponent mixtures containing hydrogen. In this sense, it is important to determine the density, speed of sound or phase equilibrium properties of ternary or multicomponent mixtures containing hydrogen. Mixtures of natural gases of known composition (gravimetrically prepared, simulating typical NG mixtures) with varying amounts of hydrogen, not only up to 20 mol % of hydrogen, even with higher hydrogen contents, are of great interest.

It is also very important to extend the ranges of validity of temperature and pressures of the thermodynamic models, in order to cover the working ranges of some hydrogen storage systems. In this sense, it is necessary to obtain high quality experimental data of binary mixtures of hydrogen with other components at high pressures (over 70 MPa) or at very low temperatures (below 20 K). Another research field of great interest is the study of the effect of traces and small amounts of impurities in the behavior of pure hydrogen or hydrogen mixtures.

In conclusion, we can say that there is still an acute need for accurate, reliable, and thermodynamically consistent experimental data of hydrogen and hydrogen mixtures.

819 Nevertheless, quality, and a good selection of compositions, temperature, and pressure ranges, is
820 more important than quantity.

821

822 **Acknowledgements**

823 The authors wish to thank for their support the European Metrology Programme on Innovation
824 and Research (EMPIR, co-funded by the European Union's Horizon 2020 research and
825 innovation programme and EMPIR Participating States), project 19ENG03/g07 - MefHySto; the
826 Ministerio de Economía, Industria y Competitividad, project ENE2017-88474-R; and the Junta
827 de Castilla y León, project VA280P18.

828

829 **Tables**

830

Table 1. Experimental data used for the adjustment of the reducing functions developed for the hydrogen binary systems included in the GERG-2008 model [29,30].

	Number of experimental $p\rho T$ data points used				Number of experimental VLE data points used			
hydrogen + …	Number of points	Temperature range T/K	Pressure range p/MPa	Composition range x_{H2}/mole fraction	Number of points	Temperature range T/K	Pressure range p/MPa	Composition range x_{H2}/mole fraction
… + methane [a]	1427	130 to 600	0.2 to 107	0.05 to 0.91	90	90.3 to 174	1.0 to 27.6	0.00 to 0.35
… + nitrogen	1479	270 to 573	0.1 to 307	0.15 to 0.87	19	77.4 to 113	0.5 to 15.2	0.01 to 0.39
… + carbon dioxide	316	273 to 473	0.2 to 50.7	0.01 to 0.75	68	220 to 298	1.1 to 20.3	0.00 to 0.16
… + ethane	382	275 to 422	0.2 to 26.2	0.10 to 0.80	61	139 to 283	0.7 to 53.3	0.00 to 0.40
… + propane					140	172 to 361	1.4 to 55.2	0.01 to 0.67
… + n-butane					62	328 to 394	2.8 to 16.9	0.02 to 0.27
… + isobutane	No reducing function. Linear combining rule used instead.							
… + n-pentane	No reducing function. Linear combining rule used instead.							
… + isopentane	No reducing function. Linear combining rule used instead.							
… + n-hexane	193	278 to 511	1.4 to 68.9	0.19 to 0.79	98	278 to 478	0.03 to 68.9	0.01 to 0.69
… + n-heptane					27	424 to 499	2.5 to 78.5	0.02 to 0.81
… + n-octane	No reducing function. Linear combining rule used instead.							
… + n-nonane	No reducing function. Linear combining rule used instead.							
… + n-decane					44	323 to 583	1.93 to 25.5	0.02 to 0.50
… + oxygen	No reducing function. Lorentz-Berthelot combining rule used instead.							
… + carbon monoxide	54	298	0.1 to 17.2	0.34 to 0.67	80	68.2 to 122	1.7 to 24.1	0.35 to 0.97
… + water	No reducing function. Lorentz-Berthelot combining rule used instead.							
… + hydrogen sulfide	No reducing function. Lorentz-Berthelot combining rule used instead.							
… + helium	No reducing function. Lorentz-Berthelot combining rule used instead.							
… + argon	No reducing function. Lorentz-Berthelot combining rule used instead.							

[a] The binary system hydrogen + methane is the only one with a binary-specific departure function included in the GERG-2008 model.

Table 2. Available experimental data on vapor-liquid equilibria (VLE) for binary H_2 mixtures.

Source	Year	Rank	Experimental technique	Mixture	x_{H_2} / y_{H_2}	T / K	p / MPa	Uncertainty (k = 2)
Benham et al. [118]	1957	1	Vapor-Recirculating VLE Cell - Mass Spectrometry	$CH_4 + H_2$ / $CH_4 + C_3H_8 + H_2$ / $CH_4 + C_3H_6 + H_2$ [b]	0 – 0.35 / 0 – 0.99	116 – 255	3.4 – 27.6	$10^6 \cdot U(x,y)$ = (3499 - 9990) mol·mol^{-1}; $U(T)$ = (200 - 2000) mK; $U(p)$ = 68950 Pa
Cosway et al. [119]	1959	1	Vapor-Recirculating VLE Cell - Mass Spectrometry	$CH_4 + C_2H_6 + H_2$ / $CH_4 + N_2 + H_2$ / $CH_4 + C_2H_6 + N_2 + H_2$ [b]	0 - 0.12 / 0 - 0.99	144 – 200	3.4 – 6.9	$10^6 \cdot U(x,y)$ = (1157 - 9974) mol·mol^{-1}; $U(T)$ = (200 - 2000) mK; $U(p)$ = 68950 Pa
Freeth et al. [120]	1931	1	Compression Vessel with a Volumenometer and Piezometer	$CH_4 + H_2$ [b]	0.004 – 0.10 / 0.97 – 0.99	90.6	1.7 – 20.8	$10^6 \cdot U(x,y)$ = (38 - 9905) mol·mol^{-1}; $U(T)$ = 100 mK; $U(p)$ = (1700 - 20800) Pa
Hong et al. [63]	1981	1	Cryogenic VLE Cell – Gas Chromatography	$CH_4 + H_2$ [b]	0.006 – 0.49 / 0.034 – 0.97	108 – 183	0.07 – 28.4	$10^6 \cdot U(x,y)$ = 3300 mol·mol^{-1}; $U(T)$ = 20 mK; $U(p) \leq$ 57000 Pa
Hu et al. [121]	2014	1	Static Analytic VLE Cell - Gas Chromatography	$CH_4 + H_2$ / $CH_4 + N_2 + H_2$ [b]	0.002 – 0.04 / 0.53 – 0.98	100 – 120	0.2 – 4.4	$10^6 \cdot U(x,y)$ = 400 mol·mol^{-1}; $U(T)$ = 200 mK; $U(p)$ = 5000 Pa
Sagara et al. [122]	1972	1	Static Analytic VLE Cell - Gas Chromatography	$CH_4 + H_2$ / $C_2H_6 + H_2$ / CH_4	0.003 – 0.23 / 0.03 - 0.99	103 – 248	1.0 – 10.8	$10^6 \cdot U(x,y)$ = 9950 mol·mol^{-1}; $U(T)$ = 200 mK;

				+ C_2H_4 + H_2 / C_2H_6 + C_2H_4 + H_2 [b]				$U(p)$ = 10132.5 Pa
Tsang et al. [62]	1980	1	Vapor-Recirculating VLE Cell (Phase Envelope)	CH_4 + H_2 [b]	0.002 - 0.61 / 0.16 - 0.99	92.3 – 180	0.2 – 138	$10^6 \cdot U(x,y)$ = 5000 mol·mol^{-1}; $U(T)$ = 40 mK; $U(p)$ = (2200 - 1400000) Pa
Yorizane et al. [123]	1980	1	Vapor-Recirculating VLE Cell (Phase Envelope) – Gas Chromatography	CH_4 + H_2 / N_2 + H_2 / CO + H_2 / CH_4 + N_2 + H_2 / CH_4 + CO + H_2 / N_2 + CO + H_2 [b]	0.05 – 0.53 / 0.63 – 0.99	93.1 – 103	10.1 – 15.2	$10^6 \cdot U(x,y)$ = (920 - 19730) mol·mol^{-1}; $U(T)$ = 200 mK; $U(p)$ = 202650 Pa
Akers et al. [124]	1960	2	Vapor-recycle Method - Vapor-Recirculating VLE Cell – Thermal Conductivity Analysis - Gas Chromatography	N_2 + H_2 / CO + H_2 / N_2 + CO + H_2 [b]	0.03 – 0.34 / 0.08 - 0.93	83 – 122	2.2 – 13.8	$10^6 \cdot U(x,y)$ = (104 - 3728) mol·mol^{-1}; $U(T)$ = 200 mK; $U(p)$ = 68947.6 Pa
Kremer et al. [125]	1983	1	High-pressure Low-temperature VLE Cell with View Section – Gas Chromatography	CH_4 + N_2 + H_2 / CH_4 + CO + H_2 [b]	0.0 – 0.29 / 0.0 – 0.96	80 – 144	2.9 – 10.0	$10^6 \cdot U(x,y)$ = (5800 - 19000) mol·mol^{-1}; $U(T)$ = 100 mK; $U(p)$ = (17000 - 60000) Pa
Maimoni [126]	1961	1	Vapor-Recirculating VLE Cell with Mercury Variable-	N_2 + H_2 [b]	0.01 – 0.11 / 0.38 - 0.83	90 – 95	0.6 – 4.59	$U(x,y)$ = N.A.; $U(T)$ = N.A.; $U(p)$ = N.A.

Omar et al. [127]	1962	2	Volume – Optical Interferometer Flow Method - Vapor-Recirculating VLE Cell (Vapor Phase)	$N_2 + H_2$ [b]	0.88 - 0.99	63 – 75	0.02 – 0.243	$U(y)$ = N.A.; $U(T)$ = N.A.; $U(p)$ = 10132.5 Pa
Streett et al. [65]	1978	1	Vapor-Recirculating VLE Cell – Thermal Conductivity Gas Analysis (Phase Envelope)	$N_2 + H_2$ [b]	0.002 – 0.54 / 0.25 - 0.97	63.2 – 110	1.0 – 57.2	$10^6 \cdot U(x,y)$ = 1000 mol·mol^{-1}; $U(T)$ = 40 mK; $U(p)$ = N.A.
Verschoyle [82]	1931	1	Compression Vessel with a Volumenometer and Piezometer	$N_2 + H_2$ / $CO + H_2$ / $N_2 + CO + H_2$ [b]	0 – 0.55 / 0 – 0.99	63 – 88	0.01 – 22.8	$10^6 \cdot U(x,y)$ = (5490 - 9870) mol·mol^{-1}; $U(T)$ = 200 mK; $U(p)$ = 10132.5 Pa
Yorizane et al. [128]	1971	1	Vapor-Recirculating VLE Cell (Phase Envelope) – Gas Chromatography	$N_2 + H_2$ [b]	0.05 – 0.47 / 0.62 – 0.94	77 – 88	1.7 – 19.0	$10^6 \cdot U(x,y)$ = (980 - 18840) mol·mol^{-1}; $U(T)$ = 200 mK; $U(p)$ = 202650 Pa
Bezanehtak et al. [129]	2002	1	Analytical VLE Cell – Gas Chromatography (Phase Envelope)	$CO_2 + H_2$	0.009 - 0.16 / 0.04 - 0.51	278 – 298	4.8 – 19.3	$U(x,y)$ = N.A.; $U(T)$ = N.A.; $U(p)$ = N.A.
Fandiño et al. [34]	2015	1	Static Analytical VLE Cell – Gas Chromatography (Phase Envelope)	$CO_2 + H_2$	0 – 0.18 / 0 - 0.93	218 – 303	0.6 - 15.4	$10^6 \cdot U(x,y)$ = (100 - 4300) mol·mol^{-1}; $U(T)$ = 10 mK; $U(p)$ = 6000 Pa
Kaminishi et al. [130]	1966	2	N.A. (Phase Envelope)	$CO_2 + H_2$	0.01 – 0.18 / 0.04 – 0.88	233 – 298	5.1 – 20.0	$U(x)$ = N.A.; $U(T)$ = N.A.; $U(p)$ = N.A.
Ke et al. [131] [f]	2017	2	Synthetic VLE Cell – Optic Fiber Sensor (Phase Envelope)	$CO_2 + Ar + H_2$	0.03	268 – 301	3.3 – 9.1	$10^6 \cdot U(x,y)$ = 180 mol·mol^{-1}; $U(T)$ = 100 mK;

								$U(p)$ = 50000 Pa
Ke et al. [132] [f]	2014	2	Synthetic VLE Cell – Optic Fiber Sensor (Phase Envelope)	$CO_2 + H_2$	0.05	273 - 293	3.5 – 10.5	$10^6 \cdot U(x,y)$ = 250 mol·mol^{-1}; $U(T)$ = 100 mK; $U(p)$ = 50000 Pa
Ke et al. [133] [f]	2005	2	Synthetic VLE Cell - Shear Mode Piezoelectric Sensor (Phase Envelope)	$CO_2 + H_2$	0.09	293 – 312	8.5 – 13.5	$10^6 \cdot U(x,y)$ = 910 mol·mol^{-1}; $U(T)$ = 500 mK; $U(p)$ = N.A.
Spano et al. [134]	1968	1	Vapor-Recirculating VLE Cell (Phase Envelope) – Gas Chromatography	$CO_2 + H_2$	0.001 – 0.14 / 0.11 – 0.93	220 – 290	1.1 – 20.3	$10^6 \cdot U(x,y)$ = (35 - 46675) mol·mol^{-1}; $U(T)$ = 200 mK; $U(p)$ = 30397.5 Pa
Tenorio et al. [135]	2015	1	Synthetic VLE Cell – Optic Fiber Sensor (Phase Envelope)	$CO_2 + H_2$ / CO_2 + $N_2 + H_2$	0.03 – 0.05	253 – 303	2.0 - 10.6	$10^6 \cdot U(x,y)$ = 200 mol·mol^{-1}; $U(T)$ = 100 mK; $U(p)$ = 50000 Pa
Tsang et al. [70]	1981	1	Vapor-Recirculating VLE Cell (Phase Envelope)	$CO_2 + H_2$	0.001 – 0.56 / 0.16 – 0.93	220 - 290	0.9 – 171	$10^6 \cdot U(x,y)$ = 5000 mol·mol^{-1}; $U(T)$ = 40 mK; $U(p)$ = (9300 - 1700000) Pa
Tsankova et al. [136]	2019	1	Microwave Re-entrant Resonance Cavity (Dew Points)	$CO_2 + H_2$	0.05 – 0.25	250 – 297	1.9 – 7.1	$10^6 \cdot U(y)$ = 700 mol·mol^{-1}; $U(T)$ = 81 mK; $U(p)$ = 21800 Pa
Yorizane et al. [137]	1970	1	Vapor-Recirculating VLE Cell (Phase Envelope) – Gas Chromatography	$CO_2 + H_2$	0.05 – 0.47 / 0.28 – 0.65	273.15	6.1 – 37.5	$10^6 \cdot U(x,y)$ = (940 - 13020) mol·mol^{-1}; $U(T)$ = 200 mK; $U(p)$ = 202650 Pa

Heintz et al. [138]	1982	1	Vapor-Recirculating High-Pressure VLE Cell (Phase Envelope)	$C_2H_6 + H_2$ [b]	0.007 – 0.75 / 0.20 – 1.0	92.5 – 280	3.2 – 559	$10^6 \cdot U(x,y) \leq 20000$ mol·mol^{-1}; $U(T)$ = 40 mK; $U(p)$ = (31800 - 5595000) Pa
Hiza et al. [75]	1968	1	Vapor-Recirculating VLE Cell (Phase Envelope) – Gas Chromatography	$C_2H_6 + H_2$ [b]	0.007 – 0.077 / 0.93 – 0.99	108 – 190	0.5 – 15.6	$10^6 \cdot U(x,y)$ = (134 - 19999) mol·mol^{-1}; $U(T)$ = 40 mK; $U(p)$ = N.A.
Williams et al. [139]	1954	1	Vapor-Recirculating VLE Cell (Phase Envelope) – Infrared Spectrometry	$C_2H_6 + H_2$ / $C_2H_4 + H_2$ / $C_3H_8 + H_2$ / $C_3H_6 + H_2$ / $C_2H_6 + C_2H_4 + H_2$ / $C_2H_4 + C_3H_6 + H_2$ / $C_3H_8 + C_3H_6 + H_2$ [b]	N.A. / N.A.	88.7 – 297	1.7 – 55.2	$10^6 \cdot U(x,y) \geq 150$ mol·mol^{-1}; $U(T)$ = (100 - 1000) mK; $U(p)$ = (8619 - 275791) Pa
Burriss et al. [76]	1953	1	Static VLE Cell with Mercury Variable-Volume (Phase Envelope) – Gas gravimetry	$C_3H_8 + H_2$	0.01 – 0.57 / 0.13 – 0.94	278 – 361	2.5 – 52.8	$U(x,y)$ = N.A.; $U(T)$ = 40 mK; $U(p)$ = 2757.9 Pa
Trust et al. [140]	1971	1	Static Analytical VLE Cell (Phase Envelope) – Gas Chromatography	$C_3H_8 + H_2$ / $CO + C_3H_8 + H_2$ [b]	0.002 – 0.35 / 0.03 – 0.99	88.1 – 348	1.0 – 20.7	$U(x,y)$ = N.A.; $U(T)$ = 100 mK; $U(p)$ = 41368.5 Pa
Aroyan et al. [79]	1951	1	Flow Method - Vapor-Recirculating VLE Cell (Phase	n-$C_4H_{10} + H_2$ [b]	0.008 – 0.34 / 0.87 – 1.0	144 – 297	2.1 – 54.1	$10^6 \cdot U(x,y)$ = (2000 - 5000) mol·mol^{-1}; $U(T)$ = 500 mK;

			Envelope) – Gas gravimetry					$U(p)$ = 137895 Pa
Klink et al. [141]	1975	1	Static Analytical VLE Cell with Mercury Variable-Volume – Gas Chromatography	n-C_4H_{10} + H_2	0.02 – 0.27 / 0.21 – 0.93	328 – 394	2.8 – 16.9	$10^6 \cdot U(x,y)$ = 80000 mol·mol^{-1}; $U(T)$ = 100 mK; $U(p)$ = 10132.5 Pa
Nelson et al. [142]	1943	2	High Pressure Bomb – Oxidation Analyses	n-C_4H_{10} + H_2	0.020 – 0.11 / 0.42 – 0.83	297 – 389	2.2 – 10.7	$10^6 \cdot U(x,y)$ = N.A.; $U(T)$ = N.A.; $U(p)$ = N.A.
Dean et al. [80]	1946	2	Static Analytical VLE Cell with Mercury Variable-Volume – Distillation columns + Calibrated balloons	i-C_4H_{10} + H_2	0.02 – 0.25 / 0.25 – 0.96	311 – 394	3.4 – 20.7	$10^6 \cdot U(x,y)$ = N.A; $U(T)$ = N.A.; $U(p)$ = N.A.
Connolly et al. [143]	1986	2	Mercury Glass Capillary (Solubility)	n-C_5H_{12} + H_2	0.03 – 0.12	308 – 463	2.9 – 14.1	$U(x,y)$ = N.A.; $U(T)$ = N.A.; $U(p)$ = N.A.
Freitag et al. [144]	1986	1	VLE Cell with View Section – Gas Chromatography	CH_4 + CO_2 + H_2 / n-C_5H_{12} + CO_2 + H_2 / n-C_5H_{12} + H_2	0.0 - 0.27 / 0.0 - 0.99	227 – 373	0.3 – 27.6	$10^6 \cdot U(x,y) \leq$ (30000 - 110000) mol·mol^{-1}; $U(T)$ = 250 mK; $U(p)$ = (2100 - 170000) Pa
Brunner et al. [145]	1985	1	Static VLE Cell with Stripping + VLE Cell with View Section (Solubility)	n-C_6H_{14} + H_2	0 – 0.09	298 – 373	0.02 - 9.8	$10^6 \cdot U(x)$ = 3800 mol·mol^{-1}; $U(T)$ = 200 mK; $U(p) \leq$ 39000 Pa
Fu et al. [146]	1994	2	Cocurrent-Flow Type - VLE Packed Columns - Gas Chromatography	n-C_6H_{14} + H_2 / n-C_6H_{14} + DCPD + H_2	0.02 – 0.05 / 0.91 – 0.99	311 – 378 / 313 – 363	3.4 / 2.1 – 5.5	$U(x,y)$ = N.A.; $U(T)$ = 400 mK; $U(p)$ = 6000 Pa

Gao et al. [147]	2001	2	Static VLE Cell with Mercury Variable-Volume (Bubble Points)	n-C_6H_{14} + H_2	0.01 – 0.14	344 – 410	1.2 – 15.1	$10^6 \cdot U(x) = 2000$ mol·mol^{-1}; $U(T) = 200$ mK; $U(p) = (40000 - 400000)$ Pa
Katayama et al. [148]	1976	2	Static VLE Cell with Mercury Variable-Volume (Solubility)	n-C_6H_{14} + H_2	N.A.	213 – 298	Atmospheric	$U(x,y)$ = N.A.; $U(T)$ = N.A.; $U(p)$ = N.A.
Nichols et al. [81]	1957	1	Static Analytical VLE Cell with Mercury Variable-Volume – Weighing bombs + Calibrated balloons	n-C_6H_{14} + H_2	0.03 – 0.77 / 0.31 - 0.99	278 – 478	3.4 – 68.9	$10^6 \cdot U(x,y) = 4000$ mol·mol^{-1}; $U(T) = 40$ mK; $U(p) = 2757.9$ Pa
Tsang et al. [83]	1981	1	Vapor-Recirculating VLE Cell (Phase Envelope)	CO + H_2 [b]	0.008 – 0.56 / 0.11 - 0.99	70 – 125	0.5 – 52.9	$10^6 \cdot U(x,y) = 5000$ mol·mol^{-1}; $U(T) = 40$ mK; $U(p) = 530000$ Pa
Kling et al. [87]	1991	2	Static High-Pressure VLE Cell of Variable Volume (Solubility)	H_2O + H_2	0.0004 – 0.0022	323 – 423	3.2 – 15.4	$U(x)$ = N.A.; $U(T) = 40$ mK; $U(p)$ = N.A.
Purwanto et al. [149]	1996	2	Stirred Autoclave (Solubility)	H_2O + H_2	N.A.	298 – 323	0.1	$U(x)$ = N.A.; $U(T) = 2000$ mK; $U(p) = 2000$ Pa
Setthanan et al. [86]	2006	1	Ambient Pressure Saturator + Gas Extraction System (Standard ASTM D2780-92) - (Solubility)	H_2O + H_2	$(1.3 - 1.4) \cdot 10^{-5}$	298 – 353	Standard Atmospheric Pressure	$10^6 \cdot U(x) = 0.81$ mol·mol^{-1}; $U(T)$ = N.A.; $U(p)$ = N.A.
Shoor et al. [89]	1969	2	VLE Cell - Gas Chromatography	H_2O + H_2	0.000013 – 0.000014	298 – 353	0.1	$U(x,y)$ = N.A.; $U(T)$ = N.A.; $U(p)$ = N.A.

Symons [150]	1971	2	Gas Stripping VLE Cell – Gas Chromatography (Solubility)	$H_2O + H_2$	0.000015	298.15	0.1	$10^6 \cdot U(x,y) = 0.580$ mol·mol^{-1}; $U(T)$ = N.A.; $U(p)$ = N.A.
Wiebe et al. [88]	1934	1	High-Pressure VLE Cell - Volumetric Determination	$H_2O + H_2$	0.00033 – 0.014	273 – 373	2.5 – 101.3	$10^6 \cdot U(x,y) = (3.3 – 140)$ mol·mol^{-1}; $U(T)$ = N.A.; $U(p)$ = N.A.
Yorizane et al. [90]	1969	1	Vapor-Recirculating VLE Cell (Phase Envelope) – Gas Chromatography	$H_2S + H_2$	0.002 – 0.020 / 0.32 - 0.99	243 – 273	1.0 – 5.1	$10^6 \cdot U(x,y) = (40 - 19800)$ mol·mol^{-1}; $U(T)$ = 200 mK; $U(p)$ = 202650 Pa
Hiza [92]	1972	2	Vapor-Recirculating VLE Cell – Gas Chromatography	He (4) + H_2 / He (3) + H_2 [c]	0.01 – 0.05	20 – 28	0.09 – 2.1	$U(x)$ = N.A.; $U(T)$ = 2000 mK; $U(p)$ = 2000 Pa
Hiza [93]	1981	2	Vapor-Recirculating VLE Cell – Gas Chromatography	He (4) + H_2 / He (3) + H_2 [c]	0.01 – 0.05	20 – 28	0.09 – 2.1	$U(x)$ = N.A.; $U(T)$ = 2000 mK; $U(p)$ = 2000 Pa
Sneed et al. [94]	1968	1	Vapor-Recirculating VLE Cell - Mass Spectrometry	He + H_2 [c]	0.64 - 0.99 / 0.03 – 0.70	15.5 – 30	2.0 – 10.4	$10^6 \cdot U(x,y) = (250 - 9910)$ mol·mol^{-1}; $U(T)$ = 20 mK; $U(p)$ = 10342.1 Pa
Sonntag et al. [96]	1964	1	Vapor-Recirculating VLE Cell - Mass Spectrometry	He + H_2 [d]	0.82 – 0.99 / 0.03 – 0.94	20.4 – 31	0.2 – 3.5	$U(x,y)$ = N.A.; $U(T)$ = 40 mK; $U(p)$ = 6894.8 Pa
Streett et al. [95]	1964	2	Vapor-Recirculating VLE Cell - Mass Spectrometry	He + H_2 [c]	0.79 - 0.99 / 0.03 – 0.97	15.5 – 32	0.2 – 3.4	$U(x,y)$ = N.A.; $U(T)$ = 40 mK; $U(p)$ = 6894.8 Pa
Yamanishi et al. [91]	1992	1	Cryogenic VLE Cell – Gas Chromatography	He + H_2 [c]	0.9982 – 0.9997 / 0.37 - 0.72	15.8 – 20	0.06 – 0.16	$10^6 \cdot U(x,y) = 180$ mol·mol^{-1}; $U(T)$ = 200 mK; $U(p)$ = 130 Pa

Calado et al. [97]	1979	1	Vapor-Recirculating VLE Cell - Thermal Conductivity Gas Analysis (Phase Envelope)	Ar + H_2 [b]	0 – 0.62 / 0 – 0.98	83.1 – 141	0.08 – 51.8	$10^6 \cdot U(x,y)$ = 5000 mol·mol^{-1}; $U(T)$ = 40 mK; $U(p)$ = 100000 Pa
Volk et al. [98]	1960	1	Static VLE Autoclave – Volumetric Determination (Solubility)	Ar + H_2 [b]	0.02 – 0.13	87 – 140	1.7 – 10.2	$10^6 \cdot U(x)$ = (378 - 2598) mol·mol^{-1}; $U(T)$ = 100 mK; $U(p)$ = 5066.25 Pa
Heck et al. [100]	1966	1	Vapor-Recirculating VLE Cell - Gas Chromatography (Phase Envelope)	Ne + H_2 [c]	0.014 - 0.96	26 - 42.5	0.21 - 2.5	$10^6 \cdot U(x,y)$ = (560 - 38000) mol·mol^{-1}; $U(T)$ = 100 mK; $U(p)$ = (1000 - 10000) Pa
Streett et al. [99]	1965	1	Vapor-Recirculating VLE Cell – Thermal Conductivity Gas Analysis (Phase envelope)	Ne + H_2 [c]	0.0083 – 0.99	24.6 - 33.7	0.17 - 1.4	$10^6 \cdot U(x,y)$ = (17 - 2000) mol·mol^{-1}; $U(T)$ = 20 mK; $U(p)$ = (350 - 29000) Pa
Zelfde et al. [101]	1974	2	Variable Volume Calorimeter – Synthetic Mixtures (Vapor Pressure)	Ne + H_2 [b]	0.0010 - 0.0087	20.4 - 26.6	0.014 - 0.11	$U(x,y)$ = N.A.; $U(T)$ = N.A.; $U(p)$ = N.A.
Moore et al. [151]	1972	2	Static Analytical VLE Cell – Distillation columns + Weighing + Calibrated balloons + (Solubility)	NH_3 + H_2	0.000012 – 0.000096	203 - 303	0.1	$U(x,)$ = N.A.; $U(T)$ = N.A.; $U(p)$ = N.A.
Reamer et al. [112]	1959	1	Static VLE Cell with Mercury Variable-Volume (Phase Envelope) – Gas gravimetry	NH_3 + H_2	0.0021 - 0.15 / 0.053 - 0.97	278 - 394	1.5 - 4.2	$10^6 \cdot U(x,y)$ = 4000 mol·mol^{-1}; $U(T)$ = 40 mK; $U(p)$ = (900 - 2500) Pa

Wiebe et al. [110]	1934	1	Static Analytical VLE Cell – Distillation columns + Weighing + Calibrated balloons + (Solubility)	$NH_3 + H_2$	0.0034 – 0.30	298 - 373	5 - 101	$U(x,y)$ = N.A.; $U(T)$ = N.A.; $U(p)$ = N.A.
Wiebe et al. [111]	1937	1	Static Analytical VLE Cell – Distillation columns + Weighing + Calibrated balloons + (Solubility)	$NH_3 + H_2$	0.0025 - 0.038	273	5 - 101	$U(x,y)$ = N.A.; $U(T)$ = N.A.; $U(p)$ = N.A.

[a] N.A.: not available.
[b] Not specified concentration of para/ortho hydrogen.
[c] Normal hydrogen.
[d] Parahydrogen.
[e] Orthohydrogen.
[f] Numerical data not available in the source.

Table 3. Available experimental data on density and compressibility factors for binary H_2 mixtures.

Source	Year	Rank	Experimental technique	Mixture	x_{H_2} / y_{H_2}	T / K	p / MPa	Uncertainty (k = 2)
Hernández-Gómez et al. [152]	2018	1	Single-Sinker Magnetic Suspension Densimeter	$CH_4 + H_2$	0.05 – 0.50	240 – 350	1.0 - 19.9	$U(\rho)$ = (440 - 5600) ppm; $10^6 \cdot U(y) < 400$ mol·mol^{-1}; $U(T)$ = 4 mK; $U(p)$ = 5000 Pa
Jaeschke et al. [153]	1996	1	Several Methods (Pycnometer and Direct-Weighing Gas-density Meter, Pressure-relative Volume Expansion Technique or Burnett type Apparatus, Optical Interferometry, Sinker Magnetic Suspension Densimeter)	$CH_4 + H_2$ / $CO_2 + H_2$ / $C_2H_6 + H_2$	0.15 – 0.75	270 – 353	0.2 – 30.5	$U(\rho)$ = N.A.; $U(y)$ = N.A.; $U(T)$ = N.A.; $U(p)$ = N.A.
Jett et al. [154]	1994	2	Low-Temperature Cryogenic Isochoric Apparatus + High-Temperature Burnett type Apparatus	$CH_4 + H_2$ [b]	0.05	140 – 273	0.8 – 68.2	$U(\rho)$ = N.A.; $U(x)$ = N.A.; $U(T)$ = N.A.; $U(p)$ = N.A.
Machado et al. [64]	1988	1	Gas Expansion PVT Apparatus – Burnett type Apparatus	$CH_4 + H_2$ [b]	0.08 – 0.91	130 – 159	5.3 – 106	$U(\rho)$ = 4000 ppm; $10^6 \cdot U(x)$ = 6000 mol·mol^{-1}; $U(T)$ = 60 mK; $U(p)$ = (11000 - 210000) Pa
Magee et al. [155]	1985	1	Burnett type Apparatus	$CH_4 + H_2$	0.20	273 – 600	0.3 – 71.5	$U(\rho)$ = 1000 ppm; $10^6 \cdot U(y)$ = 1000 mol·mol^{-1}; $U(T)$ = (55 - 120) mK; $U(p)$ = (700 - 12000) Pa

Magee et al. [156]	1986	2	Burnett type Apparatus	$CH_4 + H_2$ [b]	0.20	157 – 273	1.8 – 70	$U(\rho)$ = 1000 ppm; $10^6 \cdot U(y)$ = 1000 mol·mol^{-1}; $U(T)$ = (55 - 120) mK; $U(p)$ = (700 - 12000) Pa
Mason et al. [78]	1961	2	Burnett type Apparatus	$CH_4 + H_2$ / $C_2H_6 + H_2$ / $C_3H_8 + H_2$ / $C_4H_{10} + H_2$ / $C_5H_{12} + H_2$ / $C_2H_4 + H_2$ / $C_3H_6 + H_2$	0.28 - 0.76	289	0.1	$U(\rho)$ = N.A.; $U(y)$ = N.A.; $U(T)$ = N.A.; $U(p)$ = N.A.
Mihara et al. [157]	1977	1	Burnett type Apparatus	$CH_4 + H_2$ / $C_2H_6 + H_2$ / $C_3H_8 + H_2$	0.22 – 0.84	298 – 348	0.2 – 9.3	$U(\rho)$ = 1400 ppm; $10^6 \cdot U(y)$ = 20000 mol·mol^{-1}; $U(T)$ = 20 mK; $U(p)$ = 1000 Pa
Mueller et al. [158]	1961	2	Burnett type Apparatus	$CH_4 + H_2$ [b]	0.20 – 0.78	144 – 283	0.3 – 48.3	$U(\rho)$ = 1300 ppm; $10^6 \cdot U(x)$ = 1000 mol·mol^{-1}; $U(T)$ = 20 mK; $U(p)$ = (110 - 19305) Pa
Bartlett et al. [159,160]	1928 / 1930	1	Burnett type Apparatus	$N_2 + H_2$	0.75	203 – 572	0.1 – 101	$U(\rho)$ = 3000 ppm; $U(x)$ = N.A.; $U(T)$ = N.A.; $U(p)$ = N.A.
Bartlett et al. [161,162]	1927	1	Burnett type Apparatus	$N_2 + H_2$	0.06 – 0.88	273	0.1 – 101	$U(\rho)$ = 2000 ppm; $U(x)$ = N.A.; $U(T)$ = N.A.; $U(p)$ = N.A.
Bennett et al. [68]	1952	1	Burnett type Apparatus	$N_2 + H_2$	0.25 – 0.75	298 – 398	99.9 – 307	$U(\rho)$ = 3700 ppm; $10^6 \cdot U(x)$ = 2000 mol·mol^{-1}; $U(T)$ = N.A. mK; $U(p)$ = N.A Pa

Hernández-Gómez et al. [163]	2017	1	Single-Sinker Magnetic Suspension Densimeter	$N_2 + H_2$	0.05 – 0.50	240 – 350	1.0 – 20.1	$U(\rho)$ = (330 - 4400) ppm; $10^6 \cdot U(y) < 100$ mol·mol^{-1}; $U(T)$ = 4 mK; $U(p)$ = 5000 Pa
Jaeschke et al. [164]	1991	1	Burnett type Apparatus and Two Coupled Grating Interferometers (Refractive Index)	$N_2 + H_2$	0.15 – 0.75	270 – 353	0.3 – 30.2	$U(\rho)$ = 1400 ppm; $10^6 \cdot U(y) \leq 300$ mol·mol^{-1}; $U(T)$ = 20 mK; $U(p) \leq 6000$ Pa
Kestin et al. [165]	1982	2	Gravimetric Method	$N_2 + H_2$	0.28 – 0.74	296 & 299.7	0.8 – 9.9	$U(\rho)$ = N.A.; $U(y)$ = N.A.; $U(T)$ = N.A.; $U(p)$ = N.A.
Mastinu et al. [66]	1967	2	Pycnometer – Mass spectrometry	$N_2 + H_2$ [b]	0.006 - 0.020	77.4	1.2	$U(\rho)$ = 1000 ppm; $U(x)$ = N.A.; $U(T)$ = N.A.; $U(p)$ = N.A.
Michels et al. [67]	1949	1	Pycnometer (piezometer)	$N_2 + H_2$	0.75	273 – 423	≤ 34.5	$U(\rho)$ = N.A.; $U(x)$ = N.A.; $U(T)$ = N.A.; $U(p)$ = N.A.
Verschoyle [166]	1926	1	Compression Vessel with a Volumenometer and Piezometer	$N_2 + H_2$	0.25 – 0.75	273 – 293	3.7 – 20.8	$U(\rho)$ = 1000 ppm; $U(x)$ = N.A.; $U(T)$ = 100 mK; $U(p)$ = (3703 - 20819) Pa
Wiebe et al. [167]	1938	1	Burnett type Apparatus	$N_2 + H_2$	0.26 – 0.87	273 – 573	2.5 – 101	$U(\rho)$ = N.A.; $U(x)$ = N.A.; $U(T)$ = N.A.; $U(p)$ = N.A.
Zandbergen et al. [104]	1967	2	Burnett type Apparatus	$N_2 + H_2$ / Ar + H_2 [b]	0.14 – 0.74	170 – 292	0.2 – 10.0	$U(\rho)$ = N.A.; $U(x)$ = N.A.; $U(T)$ = N.A.; $U(p)$ = N.A.

Ababio et al. [168]	1993	1	Gravimetric Method using a Calibrated High-Pressure Cell and a Mass Comparator	$CO_2 + H_2$	0.35 – 0.50	303 – 343	0.6 – 12.7	$U(\rho)$ = N.A.; $10^6 \cdot U(x)$ = 1200 mol·mol^{-1}; $U(T)$ = 10 mK; $U(p)$ = 200 Pa.
Alsiyabi (PhD Thesis) [169]	2013	2	High-Pressure Vibrating U-Tube Densimeter	$CO_2 + H_2$	0.03 - 0.05	283 – 423	7.9 - 49.2	$U(\rho)$ = N.A.; $10^6 \cdot U(x)$ = 6000 mol·mol^{-1}; $U(T)$ = N.A.; $U(p)$ = N.A.
Cheng et al. [74]	2019	1	Modified Burnett type Apparatus	$CO_2 + H_2$ / $CH_4 + CO_2 + H_2$	0.60 – 0.70	673	0.6 – 25.1	$U(\rho)$ = 4700 ppm; $10^6 \cdot U(x)$ = 20000 mol·mol^{-1}; $U(T)$ = 200 mK; $U(p)$ = (2000 - 6000) Pa
Cipollina et al. [72]	2007	2	Fixed Volume Calibrated Pressurized Cell (Gravimetric procedure)	$CO_2 + H_2$ / $CO + H_2$ / $CO_2 + CO + H_2$	0.05 - 0.24	308 – 343	8.8 – 49.3	$U(\rho)$ = N.A.; $10^6 \cdot U(y)$ = 5000 mol·mol^{-1}; $U(T)$ = 600 mK; $U(p)$ = 100000 Pa
Mallu et al. [73]	1990	2	Burnett type Apparatus	$CO_2 + H_2$	0.23 – 0.86	323 – 423	0.1 – 6.0	$U(\rho) \leq$ 1600 ppm; $U(x)$ = N.A.; $U(T)$ = N.A.; $U(p)$ = N.A.
Pinho et al. [170]	2015	2	Microfluidic Capillary Device	$CO_2 + H_2$	0.10 – 0.20	307	12 – 12.8	$U(\rho)$ = 60000 ppm; $U(x)$ = N.A.; $U(T)$ = N.A.; $U(p)$ = N.A.
Sanchez-Vicente et al. [171]	2013	2	High-Pressure Vibrating U-Tube Densimeter	$CO_2 + H_2$	0.02 – 0.10	288 – 333	1.5 – 22.7	$U(\rho)$ = (1060 – 41000) ppm; $10^6 \cdot U(x)$ = 5000 mol·mol^{-1}; $U(T)$ = N.A; $U(p)$ = N.A.
Souissi et al. [71]	2017	1	Two-Sinker Magnetic Suspension Densimeter	$CO_2 + H_2$	0.05	273 – 323	0.5 – 6.0	$U(\rho)$ = 1500 ppm; $10^6 \cdot U(y) <$ 400 mol·mol^{-1}; $U(T)$ = 5 mK;

								$U(p)$ = (35 - 420) Pa
Tsankova et al. [136]	2019	1	Microwave Re-entrant Resonance Cavity	$CO_2 + H_2$	0.05 – 0.25	251 – 313	0.5 – 8.2	$U(\rho) \leq 3300$ ppm; $10^6 \cdot U(y) = 700$ mol·mol^{-1}; $U(T) = 20$ mK; $U(p) = 1400$ Pa
Zhang et al. [172]	2002	2	Gravimetric Method using a Calibrated High-Pressure Cell and an Analytical Balance	$CO_2 + H_2$	0.003	308	5.5 – 12.9	$U(\rho)$ = N.A.; $U(x)$ = N.A.; $U(T) = 60$ mK; $U(p) = 20000$ Pa
Freitag et al. [144]	1986	2	Computed from Refractive-Index Measurements using a VLE Cell with View Section	$CH_4 + CO_2 + H_2$ / n-C_5H_{12} + $CO_2 + H_2$ / n-$C_5H_{12} + H_2$	0.0 - 0.27 / 0.0 - 0.99	227 – 373	0.3 – 27.6	$U(\rho)$ = (20000 - 40000) ppm; $10^6 \cdot U(x) \leq$ (30000 - 110000) mol·mol^{-1}; $U(T) = 250$ mK; $U(p)$ = (2100 - 170000) Pa
Nichols et al. [81]	1957	1	Pycnometer	n-$C_6H_{14} + H_2$	0.19 – 0.79	278 – 511	1.4 – 68.9	$U(\rho)$ = (2500 - 5000) ppm; $10^6 \cdot U(x) = 4000$ mol·mol^{-1}; $U(T) = 40$ mK; $U(p) = 2757.9$ Pa
Scott [84]	1929	2	Pycnometer	$CO + H_2$	0.33 – 0.66	298	0.1 – 17.2	$U(\rho)$ = N.A.; $U(x)$ = N.A.; $U(T)$ = N.A.; $U(p)$ = N.A.
Townend et al. [85]	1931	2	Pycnometer	$CO + H_2$	0.33 – 0.67	273 – 298	0.1 – 60.8	$U(\rho)$ = N.A.; $U(x)$ = N.A.; $U(T)$ = N.A.; $U(p)$ = N.A.
Scholz et al. [102]	2020	1	Two-sinker Magnetic Suspension Densimeter	$Ar + H_2$	0.06 – 0.55	273 – 323	0.5 - 9.0	$U(\rho) = 150$ ppm; $10^6 \cdot U(x) = 1500$ mol·mol^{-1}; $U(T) = 5.0$ mK; $U(p)$ = (36 - 630) Pa

Tanner et al. [103]	1930	2	Pycnometer	Ar + H_2	0.17	298 – 447	3.0 - 12.7	$U(\rho)$ = N.A.; $U(x)$ = N.A.; $U(T)$ = N.A.; $U(p)$ = N.A.
Güsewell et al. [106]	1970	1	Pycnometer	Ne + H_2 [c]	0.8 - 0.9	25 - 31	0.33 - 0.98	$U(\rho)$ = 10000 ppm; $U(x)$ = N.A.; $U(T)$ = 40 mK; $U(p)$ = 2900 Pa
Streett [105]	1973	2	Burnett type Apparatus	Ne + H_2 [c]	0.027 - 0.94	25 - 31.1	0.42 - 10.3	$U(\rho)$ = 2000 ppm; $10^6 \cdot U(x)$ = (50 - 1900) $mol \cdot mol^{-1}$; $U(T)$ = 20 mK; $U(p)$ = (420 - 10300) Pa
Hongo et al. [109]	1978	2	Calculated data from ideal reduced molar volumes	NH_3 + H_2	0.19 – 0.80	298 - 373	0.12 - 6.6	$U(\rho)$ = N.A.; $U(x)$ = N.A.; $U(T)$ = N.A.; $U(p)$ = N.A.
Kazarnovskiy et al. [108]	1968	1	Pycnometer (piezometer)	NH_3 + H_2	0.43 – 0.65	423 - 573	8.4 - 155	$U(\rho)$ = 10000 ppm; $U(x)$ = N.A.; $U(T)$ = 300 mK; $U(p)$ = (59000 - 1100000) Pa

[a] N.A.: not available.
[b] Not specified concentration of para/ortho hydrogen.
[c] Normal hydrogen.
[d] Parahydrogen.
[e] Orthohydrogen.

Table 4. Available experimental data on speed of sound and other calorific properties for binary H_2 mixtures.

Source	Year	Rank	Experimental technique (Calorific property)	Mixture	x_{H_2} / y_{H_2}	T / K	p / MPa	Uncertainty (k = 2)
Maurer [173]	2021	1	Spherical Acoustic Resonator (Speed of Sound)	$CH_4 + H_2$	0.05	250 - 350	0.5 – 10.1	$U_r(w)$ = (360 - 1060) ppm; $10^6 \cdot U(x)$ = 8 mol·mol^{-1}; $U(T)$ = 40 mK; $U(p)$ = (600 - 2400) Pa
Lozano-Martín et al. [174]	2020	1	Spherical Acoustic Resonator (Speed of Sound)	$CH_4 + H_2$	0.05 - 0.50	273 - 375	0.4 - 20.2	$U_r(w)$ = 220 ppm; $10^6 \cdot U(x)$ = 40 mol·mol^{-1}; $U(T)$ = 4.6 mK; $U(p)$ = (240 - 1700) Pa
Randelman et al. [115]	1988	2	Flow Joule-Thomson Valve Apparatus (Joule-Thomson Coefficients)	$CH_4 + H_2$	0.13 - 0.57	274 - 295	2.2 - 13.8	$U(\mu_{JT})$ = N.A.; $10^6 \cdot U(x)$ = 2100 mol·mol^{-1}; $U(T)$ = 28 mK; $U(p)$ = 40000 Pa.
Wormald et al. [114]	1977	2	Flow Calorimeter (Excess Enthalpies)	$CH_4 + H_2$ / $N_2 + H_2$ [b]	0.21 - 0.92	201 - 298	1.1 - 11.2	$U(H^E)$ = 40000 ppm; $10^6 \cdot U(x)$ = (2100 - 9200) mol·mol^{-1}; $U(T)$ = 40 mK; $U(p)$ = 40000 Pa
Knapp et al. [113]	1976	1	Flow Calorimeter (Molar Heat Capacity)	$N_2 + H_2$ [b]	0.1 - 0.78	100 - 200	3.0 – 7.0	$U(C_{p,m})$ = 40000 ppm; $10^6 \cdot U(x)$ = (1400 - 10920) mol·mol^{-1}; $U(T)$ = (40 - 80) mK; $U(p)$ = (12000 - 28000) Pa
Lozano-Martín et al. [f]	2021	1	Spherical Acoustic Resonator (Speed of Sound)	$N_2 + H_2$	0.05 - 0.50	260 - 350	0.5 - 19.9	$U(w)$ = 240 ppm; $10^6 \cdot U(x)$ = 70 mol·mol^{-1}; $U(T)$ = 5.2 mK; $U(p)$ = (240 – 1620) Pa

Van Itterbeek et al. [69]	1949	1	Ultrasonic Interferometer (Speed of sound)	$N_2 + H_2$ / $O_2 + H_2$ / $CO + H_2$ [b]	0.12 - 0.84	75 - 90	lim. $p \rightarrow 0$	$U(w)$ = N.A.; $U(x)$ = N.A.; $U(T)$ = N.A.; $U(p)$ = N.A.
Alsiyabi [169]	2013	2	Ultrasonic Cell - Time of Flight (Speed of Sound)	$CO_2 + H_2$	0.05	268 - 301	9.7 - 40.7	$U(w)$ = N.A.; $10^6 \cdot U(x)$ = 6000 mol·mol^{-1}; $U(T)$ = N.A.; $U(p)$ = N.A.
Maurer [173]	2021	1	Spherical Acoustic Resonator (Speed of Sound)	$CO_2 + H_2$	0.25 - 0.74	250 - 350	0.5 – 10.1	$U_r(w)$ = (380 - 1030) ppm; $10^6 \cdot U(x)$ = (12 - 53) mol·mol^{-1}; $U(T)$ = 40 mK; $U(p)$ = (600 - 2400) Pa
Van Itterbeek et al. [107]	1946	1	Ultrasonic Interferometer (Speed of sound)	$He + H_2$ / $Ar + H_2$ [b]	0.14 - 0.81	20.3 - 90	lim. $p \rightarrow 0$	$U(w)$ = N.A.; $U(x)$ = N.A.; $U(T)$ = N.A.; $U(p)$ = N.A.
Brouwer et al. [175]	1970	2	Flow Calorimeter (Molar Heat Capacity)	$Ne + H_2$ [c]	0.03 - 0.84	24.5 - 30.5	0.19 - 0.92	$U(C_{p,m})$ = N.A.; $U(x)$ = N.A.; $U(T)$ = N.A.; $U(p)$ = N.A.
Güsewell et al. [106]	1970	1	Parallel-plate Ultrasonic Resonator (Speed of sound)	$Ne + H_2$ [c]	0.8 - 0.9	25 - 31	0.33 - 0.98	$U_r(w)$ = 10000 ppm; $U(x)$ = N.A.; $U(T)$ = 40 mK; $U(p)$ = 2900 Pa

[a] N.A.: not available.
[b] Not specified concentration of para/ortho hydrogen.
[c] Normal hydrogen.
[d] Parahydrogen.
[e] Orthohydrogen.
[f] Not yet published.

Table 5. Statistical analysis of the deviation of the experimental sets of vapor-liquid equilibrium (VLE) data of binary mixtures containing hydrogen with respect to the improved GERG-2008 EoS [30][39]: Average absolute deviations (AAD), Bias, RMS and Max AD. The deviations are presented as 10^2 mol/mol for bubble-point data (x) and dew-point data (y).

Source	Number of data[a]	AAD	Bias	RMS	Max AD	AAD within experimental uncertainty[b]
		CH_4+H_2				
Benham et al. 1957 (x) [118]	13	1.7	-0.79	2.9	8.1	N
Benham et al. 1957 (y) [118]	13	1.5	0.82	2.0	4.7	N
Cosway et al. 1959 (x) [119]	3	0.23	-0.23	0.31	0.53	Y
Cosway et al. 1959 (y) [119]	3	3.0	3.0	3.2	4.7	N
Freeth et al. 1931 (x) [120]	15	0.88	-0.62	1.4	2.8	N
Freeth et al. 1931 (y) [120]	20	0.44	0.40	0.62	1.7	Y
Hong et al. 1981 (x) [63]	129	0.82	0.12	2.3	15	N
Hong et al. 1981 (y) [63]	133	1.2	0.74	2.5	14	N
Hu et al. 2014 (x) [121]	23	0.20	-0.20	0.26	0.55	N
Hu et al. 2014 (y) [121]	23	5.2	-4.2	6.0	12	N
Sagara et al. 1972 (x) [122]	28	0.57	-0.24	0.77	2.2	Y
Sagara et al. 1972 (y) [122]	28	1.8	1.8	2.4	5.4	N
Tsang et al. 1980 (x) [62]	169	1.4	-0.60	5.7	53	N
Tsang et al. 1980 (y) [62]	168	1.2	0.11	3.0	22	N
Yorizane et al. 1980 (x) [123]	3	0.81	-0.54	1.2	2.0	N
Yorizane et al. 1980 (y) [123]	3	0.20	0.18	0.24	0.34	Y
		N_2+H_2				
Akers et al. 1957 (x) [124]	10	0.40	-0.16	0.54	1.2	N
Akers et al. 1957 (y) [124]	10	1.1	-0.93	1.3	2.4	N
Kremer et al. 1983 (x) [125]	3	0.35	-0.35	0.37	0.50	Y
Kremer et al. 1983 (y) [125]	3	0.57	-0.57	0.60	0.84	Y
Maimoni 1961 (x) [126]	11	0.060	-0.093	0.097	0.15	UNR
Maimoni 1961 (y) [126]	15	0.12	-0.069	0.22	0.65	UNR
Omar et al. 1962 (y) [127]	24	0.46	0.038	0.87	3.7	UNR
Streett et al. 1978 (x) [65]	66	1.0	-0.46	1.8	7.5	N
Streett et al. 1978 (y) [65]	64	1.4	0.013	2.3	9.6	N
Verschoyle 1931 (x) [82]	61	1.7	-1.6	4.9	30	N
Verschoyle 1931 (y) [82]	53	1.6	-0.033	3.8	20	N
Yorizane et al. 1971 (x) [128]	17	2.2	-1.9	2.8	6.3	N
Yorizane et al. 1971 (y) [128]	17	1.7	-1.2	1.8	2.6	Y
		CO_2+H_2				
Bezanehtak et al. 2002 (x) [129]	41	1.0	-1.0	1.1	1.6	UNR

Bezanehtak et al. 2002 (y) [129]	33	2.5	2.6	4.0	7.8	UNR
Fandiño et al. 2015 (x) [34]	85	0.13	-0.0014	0.35	2.5	Y
Fandiño et al. 2015 (y) [34]	85	0.45	0.22	0.66	1.8	N
Kaminishi et al. 1966 (x) [130]	20	4.3	-0.0070	5.9	14	UNR
Kaminishi et al. 1966 (y) [130]	21	13	-0.38	18	41	UNR
Spano et al. 1968 (x) [134]	45	0.18	0.18	0.49	2.3	Y
Spano et al. 1968 (y) [134]	49	1.2	-1.1	2.8	14	Y
Tenorio et al. 2015 (x) [135]	37	0.15	-0.29	0.42	1.6	N
Tenorio et al. 2015 (y) [135]	36	0.15	0.16	0.41	1.3	N
Tsang et al. 1981 (x) [70]	113	1.1	-1.0	3.0	15	N
Tsang et al. 1981 (y) [70]	118	2.7	2.6	6.4	25	N
Tsankova et al. 2019 (y) [136]	27	0.70	-0.70	0.90	1.8	N
Yorizane et al. 1970 (x) [137]	11	2.8	-2.9	5.7	17	N
Yorizane et al. 1970 (y) [137]	11	2.0	1.2	3.3	8.7	N
		$C_2H_6+H_2$				
Cosway et al. 1959 [119] / Williams et al. 1954 [139] (x)	5	0.63	-0.076	0.69	1.2	N
Cosway et al. 1959 [119]/ Williams et al. 1954 [139] (y)	5	0.14	0.14	0.18	0.34	N
Heintz et al. 1982 (x) [138]	63	0.52	-1.0	2.9	7.7	Y
Heintz et al. 1982 (y) [138]	63	0.44	1.8	3.8	20	Y
Hiza et al. 1968 (x) [75]	31	0.43	-1.2	1.5	2.8	Y
Hiza et al. 1968 (y) [75]	70	0.012	0.0057	0.049	0.34	Y
Sagara et al. 1972 (x) [122]	16	0.47	0.17	0.58	1.2	Y
Sagara et al. 1972 (y) [122]	16	0.53	0.53	0.65	1.6	Y
		$C_3H_8+H_2$				
Burris et al. 1953 (x) [76]	50	1.3	2.0	3.7	12	UNR
Burris et al. 1953 (y) [76]	54	2.5	3.2	6.5	17	UNR
Trust et al. 1971 (x) [140]	73	0.77	-0.78	1.8	4.7	UNR
Trust et al. 1971 (y) [140]	54	0.72	0.52	3.1	9.7	UNR
		$C_4H_{10}+H_2$				
Aroyan et al. 1951 (x) [79]	31	2.0	-2.9	3.8	8.3	N
Aroyan et al. 1951 (y) [79]	28	0.13	0.18	0.32	1.1	Y
Klink et al. 1975 (x) [141]	60	1.0	0.80	1.2	2.5	Y
Klink et al. 1975 (y) [141]	60	2.7	2.6	3.7	12	Y
Nelson et al. 1943 (x) [142]	13	1.0	0.71	1.1	2.4	UNR
Nelson et al. 1943 (y) [142]	5	1.7	4.4	5.0	6.9	UNR
		$iC_4H_{10}+H_2$				

Dean et al. 1946 (*x*) [80]	22	9.5	-9.5	10.8	19.0	UNR
Dean et al. 1946 (*y*) [80]	22	7.1	5.8	12.5	42.6	UNR
		$C_5H_{12}+H_2$				
Connolly et al. 1986 (x) [143]	81	6.3	-6.3	6.9	11.5	UNR
Freitag et al. 1986 (x) [144]	29	4.8	-6.1	8.5	24	Y
Freitag et al. 1986 (y) [144]	30	0.89	1.1	1.5	4.2	Y
		$C_6H_{14}+H_2$				
Brunner et al. 1985 (x) [145]	24	0.57	0.49	0.89	2.1	Y
Fu et al. 1994 (x) [146]	3	0.67	0.46	0.78	1.2	UNR
Fu et al. 1994 (y) [146]	3	0.24	0.24	0.24	0.27	UNR
Gao et al. 2001 (x) [147]	34	1.8	1.8	2.0	3.8	N
Nichols et al. 1957 (x) [81]	59	1.6	0.54	3.5	12.6	UNR
Nichols et al. 1957 (y) [81]	59	1.4	2.5	4.5	17.7	UNR
		$CO+H_2$				
Akers et al. 1957 (x) [124]	11	0.28	0.10	0.31	0.53	Y
Akers et al. 1957 (y) [124]	11	0.90	-0.26	1.0	1.8	N
Tsang et al. 1981 (x) [83]	127	0.58	-0.32	1.0	4.8	Y
Tsang et al. 1981 (y) [83]	127	0.80	0.07	1.4	5.0	N
Verschoyle et al.1931 (x) [82]	67	1.1	-0.32	1.8	7.7	N
Verschoyle et al.1931 (y) [82]	77	1.4	-0.47	2.9	10.2	N
		H_2O+H_2				
Kling et al. 1991 (x) [87]	10	0.12	-0.12	0.13	0.22	UNR
Setthanan et al. 2006 (x) [86]	3	0.0010	-0.0013	0.0014	0.0014	N
Shoor et al. 1969 (x) [89]	2	0.00086	-0.0013	0.0013	0.0013	UNR
Wiebe et al. 1934 (x) [88]	40	0.51	-0.51	0.67	1.4	N
		H_2S+H_2				
Yorizane et al. 1969 (x) [90]	11	0.84	-0.84	1.0	2.0	N
Yorizane et al. 1969 (y) [90]	11	2.9	1.2	3.7	6.5	N
		$He+H_2$				
Hiza et al. 1972 (x) [92]	21	0.22	0.30	0.31	0.46	UNR
Hiza et al. 1981 (x) [93]	24	0.11	-0.19	0.21	0.44	UNR
Hiza et al. 1981 (y) [93]	16	1.1	-2.7	3.0	4.4	UNR
Sneed et al. 1968 (x) [94]	60	2.4	2.0	3.7	14	N
Sneed et al. 1968 (y) [94]	60	7.1	-7.1	9.1	21	N
Sonntag et al. 1964 (x) [96]	48	0.38	0.26	1.2	6.0	UNR
Sonntag et al. 1964 (y) [96]	49	4.4	-5.4	6.3	16	UNR
Streett et al. 1964 (x) [95]	88	0.42	0.33	1.2	7.3	UNR
Streett et al. 1964 (y) [95]	86	2.4	-2.6	3.7	12	UNR

Yamanishi et al. 1992 (x) [91]	24	0.024	0.023	0.029	0.064	Y
Yamanishi et al. 1992 (y) [91]	11	2.1	4.4	5.7	12	N
		$Ar+H_2$				
Calado et al. 1979 (x) [97]	132	19	-21	27	62	N
Calado et al. 1979 (y) [97]	127	8.5	9.4	14	57	N
Volk et al. 1960 (x) [98]	119	6.0	-6.1	6.6	11	N
		$Ne+H_2$				
Heck et al. (x) [100]	40	1.3	-2.2	4.0	14	Y
Heck et al. (y) [100]	58	1.9	-2.2	5.0	14	Y
Streett et al. (x) [99]	50	1.6	-2.6	5.1	19	N
Streett et al. (y) [99]	77	2.8	-3.5	5.2	16	N
Zelfde et al. (x) [101]	98	0.20	-0.20	0.24	0.52	UNR
		NH_3+H_2				
Moore et al. 1972 (x) [151]	4	0.00038	-0.0011	0.0013	0.0021	UNR
Reamer et al. 1959 (x) [112]	55	0.15	0.072	0.19	0.48	Y
Reamer et al. 1959 (y) [112]	104	0.78	0.54	1.2	3.8	Y
Wiebe et al. 1934 (x) [110]	72	1.1	-0.80	2.7	12	UNR
Wiebe et al. 1937 (x) [111]	11	0.35	0.29	0.44	0.78	UNR

[a] Data of pure fluid as well as data for which deviations in terms of mol-% could not be calculated are not considered.

[b] Y = yes, N = no, UNR = uncertainty not reported.

Table 6. Statistical analysis of the deviation of the experimental sets of density and compressibility factors data of binary mixtures containing hydrogen with respect to the improved GERG-2008 EoS [30][39]: Average absolute relative deviations (AARD), Bias, RMS and Max ARD.

Source	Number of data[a]	AARD / %	Bias / %	RMS / %	Max ARD / %	AAD within experimental uncertainty[b]
			CH_4+H_2			
Hernández-Gómez et al. 2018 [152]	391	0.048	-0.021	0.065	0.25	Y
Jett et al. 1994 [154]	168	0.64	0.36	1.0	6.2	UNR
Machado et al. 1988 [64]	296	1.4	-0.42	1.8	11	N
Magee et al. 1985 [155]	172	0.25	-0.23	0.29	1.1	N
Magee et al. 1986 [156]	173	0.75	-0.71	1.3	3.4	N
Mason et al. 1961 [78]	2	0.014	-0.0074	0.015	0.021	UNR
Mihara et al. 1977 [90]	153	0.13	-0.13	0.20	0.79	Y
Mueller et al. 1961 [158]	344	0.86	-0.81	1.7	11	N
			N_2+H_2			
Bartlett et al. 1928 – 1930 [159,160]	103	0.198	0.077	0.272	0.742	Y
Bartlett et al. 1927 (x2) [161,162]	72	0.158	0.096	0.202	0.471	Y
Bennett et al. 1952 [68]	77	0.296	-0.060	0.387	1.793	Y
Hernández-Gómez et al. 2017 [163]	399	0.038	-0.027	0.050	0.154	Y
Jaeschke et al. 1991 [164]	197	0.011	-0.001	0.016	0.092	Y
Kestin et al. 1982 [165]	54	1.091	1.008	1.185	2.756	UNR
Mastinu 1967 [66]	10	0.923	0.923	0.946	1.165	N
Michels et al. 1949 [67]	119	0.058	0.058	0.059	0.081	UNR
Verschoyle 1926 [166]	63	0.075	0.028	0.091	0.195	Y
Wiebe et al. 1938 [167]	175	0.118	0.096	0.155	0.457	UNR
Zandbergen et al. 1967 [104]	100	0.240	0.053	0.361	2.009	UNR
			CO_2+H_2			
Ababio et al. 1993 [168]	53	0.11	-0.023	0.14	0.41	UNR
Alsiyabi 2013 [169]	67	2.7	-0.10	3.4	12	UNR
Cheng et al. 2019 [74]	16	0.41	0.023	0.57	1.5	Y
Cipollina et al. 2007 [72]	48	0.51	-0.16	0.58	1.0	UNR
Mallu et al. 1990 [73]	130	0.41	-0.45	0.55	1.7	N
Pinho et al. 2015 [170]	2	2.1	0.76	3.2	3.8	Y
Sanchez-Vicente et al. 2013 [171]	488	1.4	0.39	2.0	6.5	Y
Souissi et al. 2017 [71]	19	0.19	-0.19	0.21	0.37	Y

Tsankova et al. 2019 [136]	66	0.39	-0.21	0.46	1.2	Y
Zhang et al. 2002 [172]	20	2.2	1.3	2.7	5.1	UNR
			$C_2H_6+H_2$			
Mason et al. 1961 [78]	2	0.017	-0.017	0.017	0.019	UNR
Mihara et al. 1977 [157]	154	0.23	-0.23	0.35	1.5	N
			$C_3H_8+H_2$			
Mason et al. 1961 [78]	2	0.031	0.031	0.031	0.033	UNR
Mihara et al. 1977 [157]	73	0.12	-0.12	0.16	0.43	Y
			$C_4H_{10}+H_2$			
Mason et al. 1961 [78]	4	0.14	0.14	0.16	0.24	UNR
			$C_5H_{12}+H_2$			
Freitag et al. 1986 [144]	55	10	7.5	13	28	N
Mason et al. 1961 [78]	2	0.37	0.37	0.37	0.37	UNR
			$C_6H_{14}+H_2$			
Nichols et al. 1957 [81]	421	2.0	0.034	2.8	13	N
			$CO+H_2$			
Cipollina et al. 2007 [72]	48	2.40	-0.63	3.1	6.5	UNR
Scott 1929 [84]	54	0.25	-0.13	0.34	0.72	UNR
Townend et al. 1931 [85]	120	0.16	-0.054	0.24	0.79	UNR
			$Ar+H_2$			
Scholz et al. 2020 [102]	144	0.32	0.32	0.41	1.1	N
Tanner et al. 1930 [103]	24	0.64	0.64	0.70	1.1	UNR
Zandbergen et al. 1967 [104]	122	1.4	1.3	2.4	9.3	UNR
			$Ne+H_2$			
Güsewell et al. [106]	12	5.8	6.2	6.4	8.9	N
Streett [105]	217	5.4	3.1	6.8	27	N
			NH_3+H_2			
Hongo et al. [109]	120	0.67	-0.16	0.87	2.6	UNR
Kazarnovskiy et al. [108]	52	1.1	-0.55	1.2	2.8	Y

[a] Data of pure fluid as well as data for which deviations in terms of density or compressibility factor could not be calculated are not considered.

[b] Y = yes, N = no, UNR = uncertainty not reported.

Table 7. Statistical analysis of the deviation of the experimental sets of speed of sound and other calorific properties data of binary mixtures containing hydrogen with respect to the improved GERG-2008 EoS [30][39]: Average absolute relative deviations (AARD), Bias, RMS and Max ARD.

Property	Source	Number of data[a]	AARD / %	Bias / %	RMS / %	Max ARD / %	AAD within experimental uncertainty[b]
			CH_4+H_2				
Speed of sound	Maurer 2021 [173]	45	0.028	0.023	0.029	0.047	Y
Speed of sound	Lozano-Martín et al. 2020 [174]	233	0.042	-0.019	0.058	0.26	N
Joule-Thomson coefficient	Randelmand et al. 1988 [115]	56	28	28	31	78	UNR
Excess Enthalpy	Wormald et al. 1977 [114]	72	8.1	-7.9	10	22	N
			N_2+H_2				
Speed of sound	Itterbeek et al. 1949 [69]	19	0.29	0.087	0.42	1.4	UNR
Molar heat capacity	Knapp et al. 1976 [113]	78	1.6	-1.2	2.5	12	Y
Speed of sound	Lozano-Martín et al. 2021	174	0.025	-0.010	0.046	0.27	Y
Excess Enthalpy	Wormald et al. 1977 [114]	63	4.6	1.4	6.2	22	Y
			CO_2+H_2				
Speed of sound	Alsiyabi et al. 2013 [169]	55	6.1	6.3	6.7	19	N
Speed of sound	Maurer 2021 [173]	95	0.063	-0.043	0.10	0.45	Y
			O_2+H_2				
Speed of sound	Itterbeek et al. 1949 [69]	12	0.24	-0.23	0.41	1.3	UNR
			$CO+H_2$				
Speed of sound	Itterbeek et al. 1949 [69]	16	0.21	-0.15	0.27	0.69	UNR
			$He+H_2$				
Speed of sound	Itterbeek et al. 1946 [107]	4	0.20	0.20	0.26	0.48	UNR
			$Ar+H_2$				
Speed of sound	Itterbeek et al. 1946 [107]	12	0.27	-0.25	0.35	0.70	UNR

			$Ne+H_2$				
Molar heat capacity	Brouwer et al. [175]	77	5.2	-5.8	35	42	UNR
Spee of sound	Güsewell et al. [106]	12	1.1	0.81	1.7	4.3	Y

[a] Data of pure fluid as well as data for which deviations in terms of the corresponding calorific property could not be calculated are not considered.

[b] Y = yes, N = no, UNR = uncertainty not reported.

Figures

Figure 1. Relative deviations in density of experimental (p, ρ, T) data of a 3% H_2-enriched natural gas mixture, ρexp, from density values calculated from the GERG-2008 EoS, $\rho GERG$, versus pressure p: □, T = 260 K; ◇, T = 275 K; △, T = 300 K; ×, T = 325 K; ○, T = 350 K. From Hernández-Gómez et el. [48]. Error bars on the 260-K isotherm indicate the expanded uncertainty (k = 2) of the experimental density data. The claimed uncertainty of the GERG-2008 EoS for this composition is 0.1%.

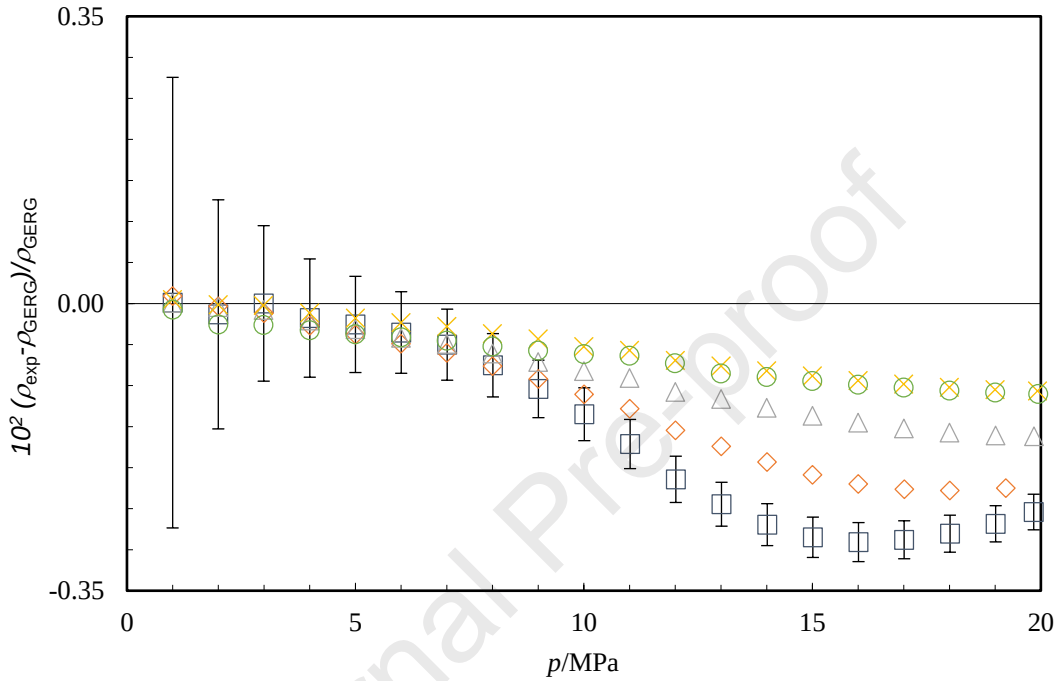

Figure 2. Deviations of bubble-point data (a) and dew-point data (b) for the binary mixtures (CH_4 + H_2) with respect to the improved GERG-2008 EoS [30][39]: + Benham et al. (1957), ○ Cosway et al. (1959), - Freeth et al. (1931), □ Hong et al. (1981), ◇ Hu et al. (2014), ✶ Sagara et al. (1972), × Tsang et al. (1980), Δ Yorizane et al. (1980).

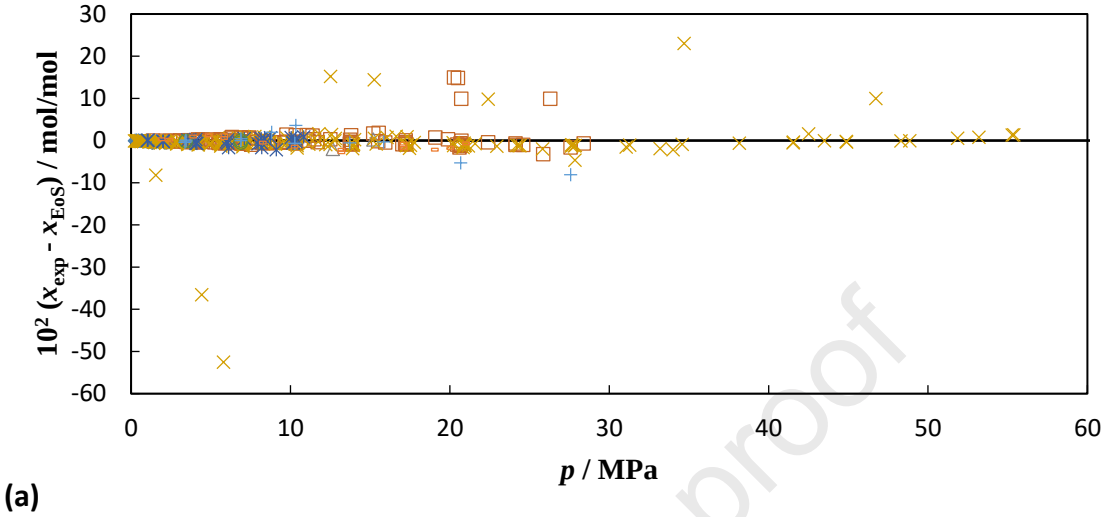

(a)

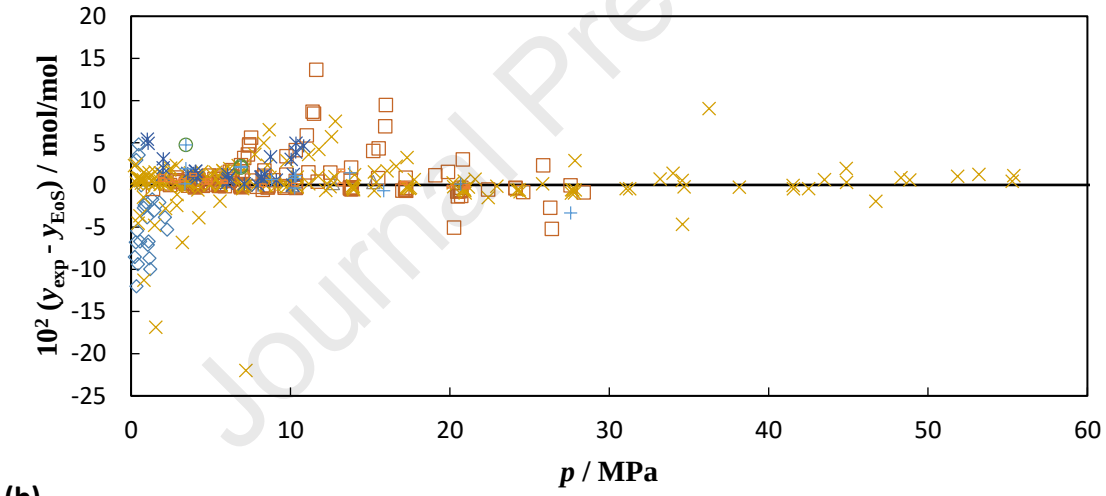

(b)

Figure 3. Deviations of bubble-point data (a) and dew-point data (b) for the binary mixtures (N_2 + H_2) with respect to the improved GERG-2008 EoS [30][39]: ○ Akers et al. (1957), ◇ Kremer et al. (1983), ∗ Maimoni (1961), × Omar et al. (1962), □ Street et al. (1978), + Verschoyle (1931), Δ Yorizane et al. (1971).

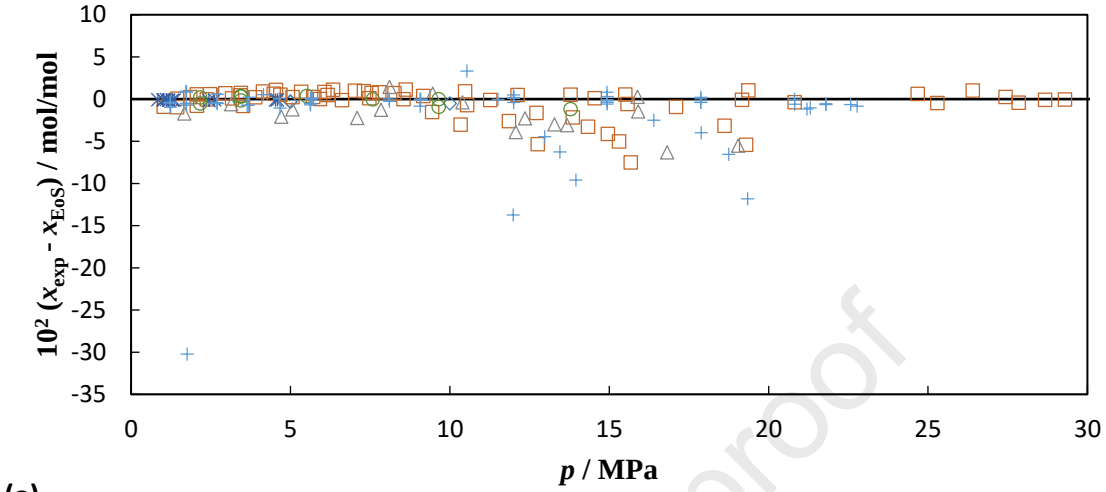

(a)

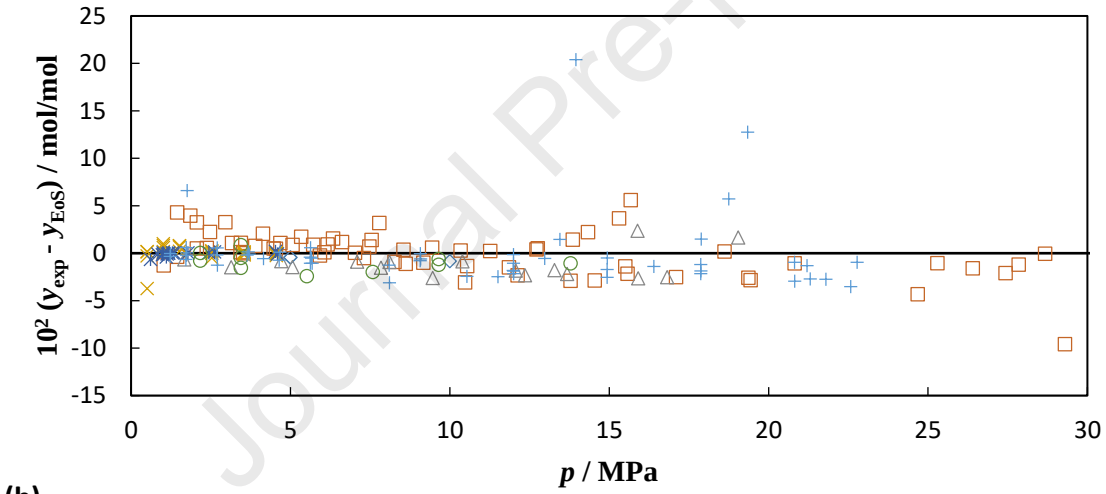

(b)

Figure 4. Deviations of bubble-point data (a) and dew-point data (b) for the binary mixtures (CO_2 + H_2) with respect to the improved GERG-2008 EoS [30][39]: × Bezanehtak et al. (2002), Δ Fandiño et al. (2015), - Kaminishi et al. (1966), + Spano et al. (1968), □ Tenorio et al. (2015), ◇ Tsankova et al. (2019), ∗ Tsang et al. (1981), ○ Yorizane et al. (1970).

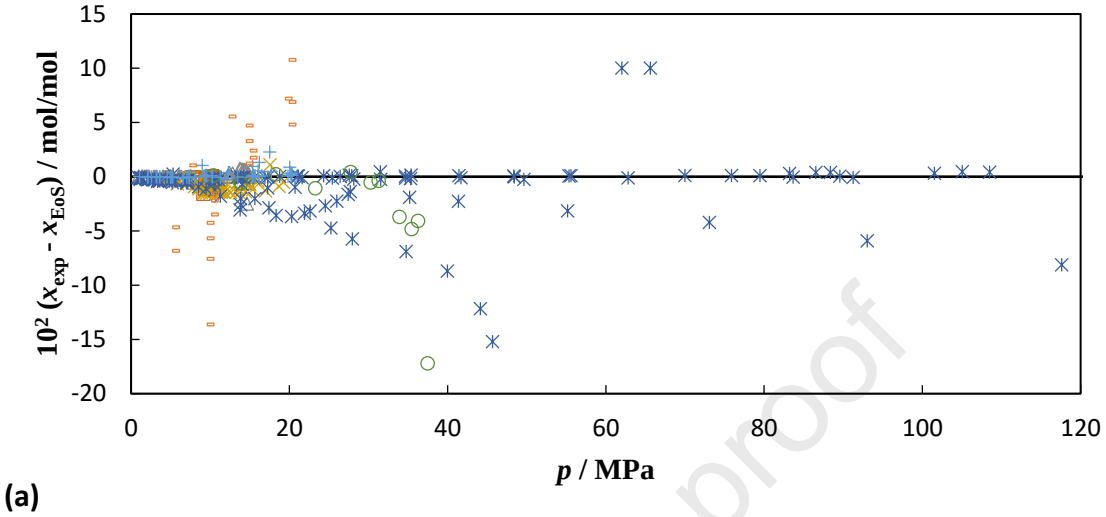

(a)

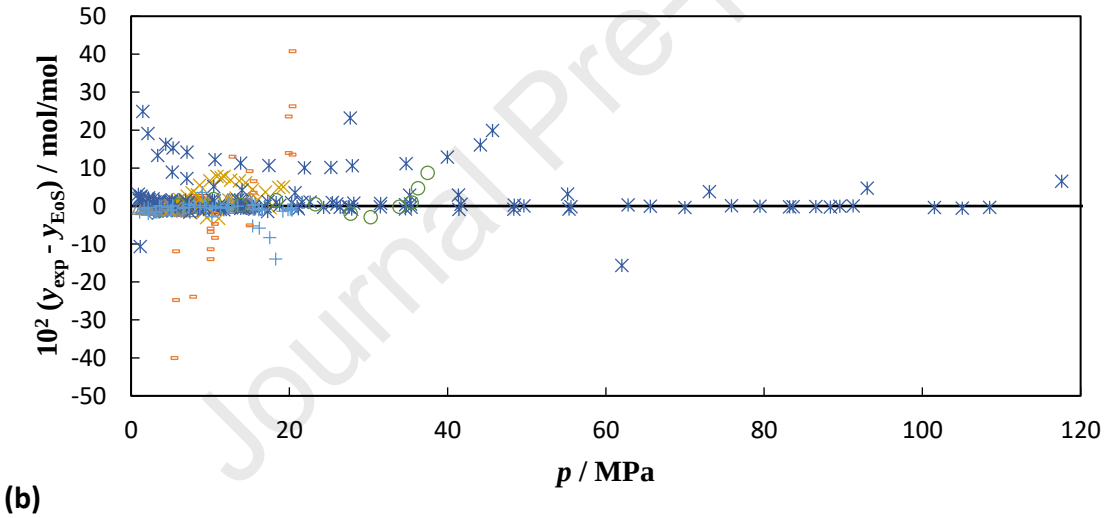

(b)

Figure 5. Deviations of bubble-point data (a) and dew-point data (b) for the binary mixtures (C_2H_6 + H_2) and (C_3H_8 + H_2) with respect to the improved GERG-2008 EoS [30][39]: × Cosway et al. / Williams et al. (C_2H_6 + H_2,1954), ◇ Heintz et al. (C_2H_6 + H_2, 1982), Δ Hiza et al. (C_2H_6 + H_2, 1968), □ Sagara et al. (C_2H_6 + H_2, 1972), ○ Burris et al. (C_3H_8 + H_2,1953), ∗ Trust et al. (C_3H_8 + H_2,1971).

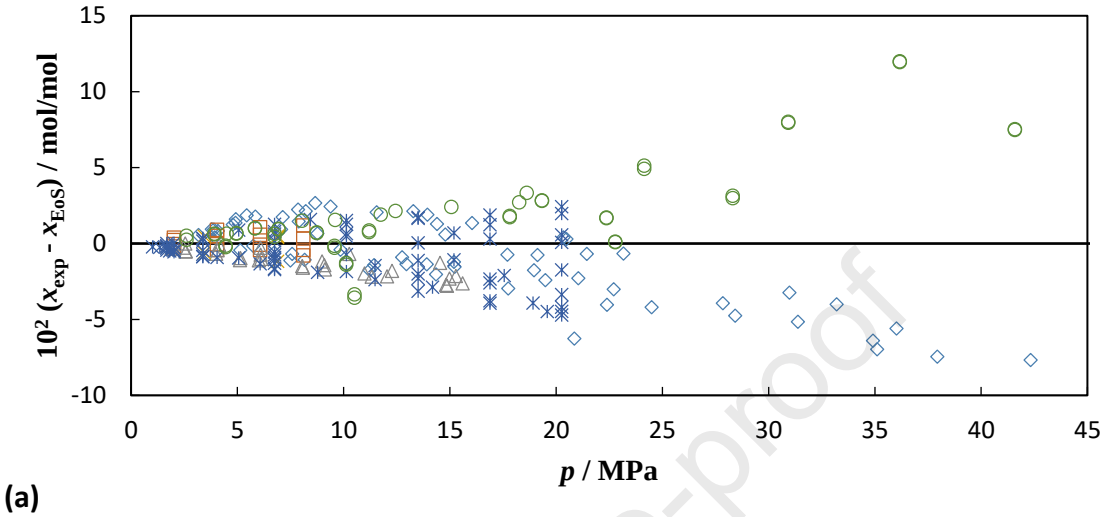

(a)

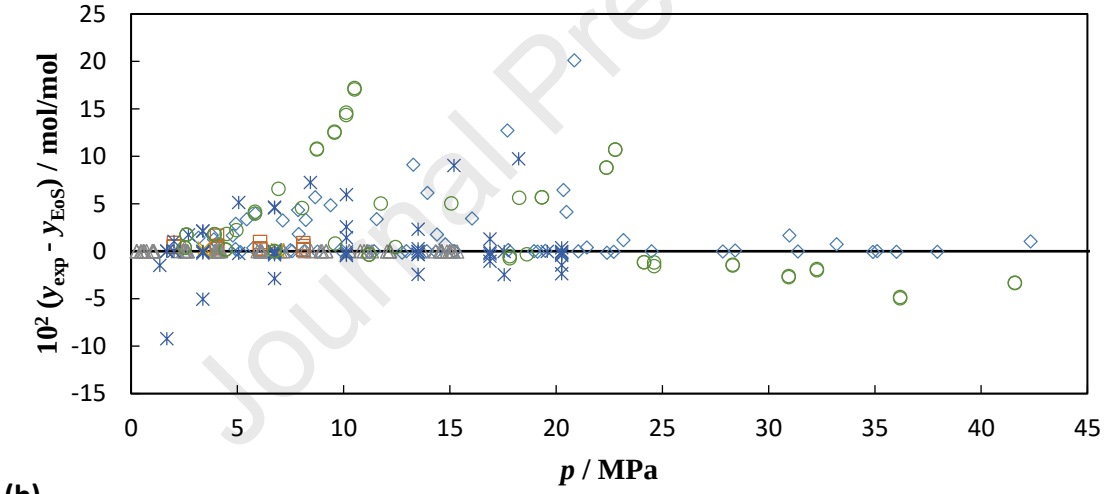

(b)

Figure 6. Deviations of bubble-point data (a) and dew-point data (b) for the binary mixtures (n-C_4H_{10} + H_2), (i-C_4H_{10} + H_2), (n-C_5H_{12} + H_2), and (n-C_6H_{14} + H_2) with respect to the improved GERG-2008 EoS [30][39]: □ Aroyan et al. (n-C_4H_{10} + H_2, 1951), ◇ Klink et al. (n-C_4H_{10} + H_2, 1975), Δ Nelson et al. (n-C_4H_{10} + H_2, 1943), × Dean et al. (i-C_4H_{10} + H_2, 1946), ○ Connolly et al. (n-C_5H_{12} + H_2, 1986), ∗ Freitag et al. (n-C_5H_{12} + H_2, 1986), − Brunner et al. (n-C_6H_{14} + H_2, 1985), - Fu et al. (n-C_6H_{14} + H_2, 1994), + Gao et al. (n-C_6H_{14} + H_2, 2001), ◇ Nichols et al. (n-C_6H_{14} + H_2, 1957).

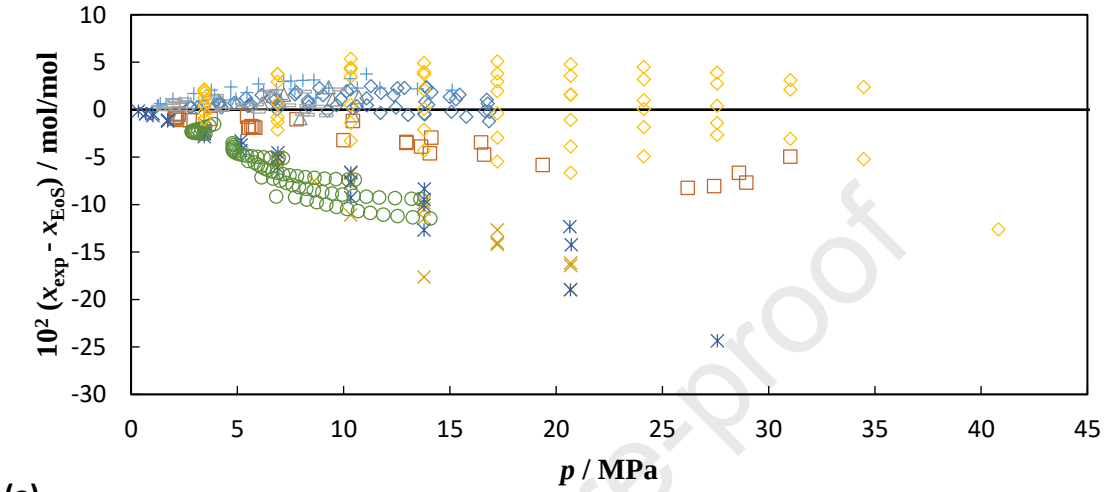

(a)

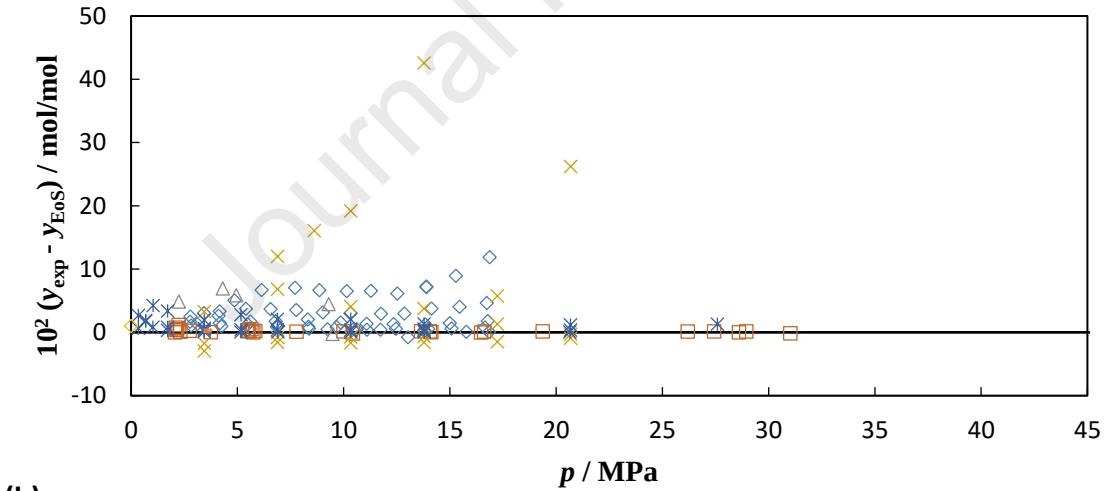

(b)

Figure 7. Deviations of bubble-point data (a) and dew-point data (b) for the binary mixtures (CO + H_2) with respect to the improved GERG-2008 EoS [30][39]: Δ Akers et al. (CO + H_2, 1957), ◇ Tsang et al. (CO + H_2, 1981), □ Verschoyle et al. (CO + H_2, 1931).

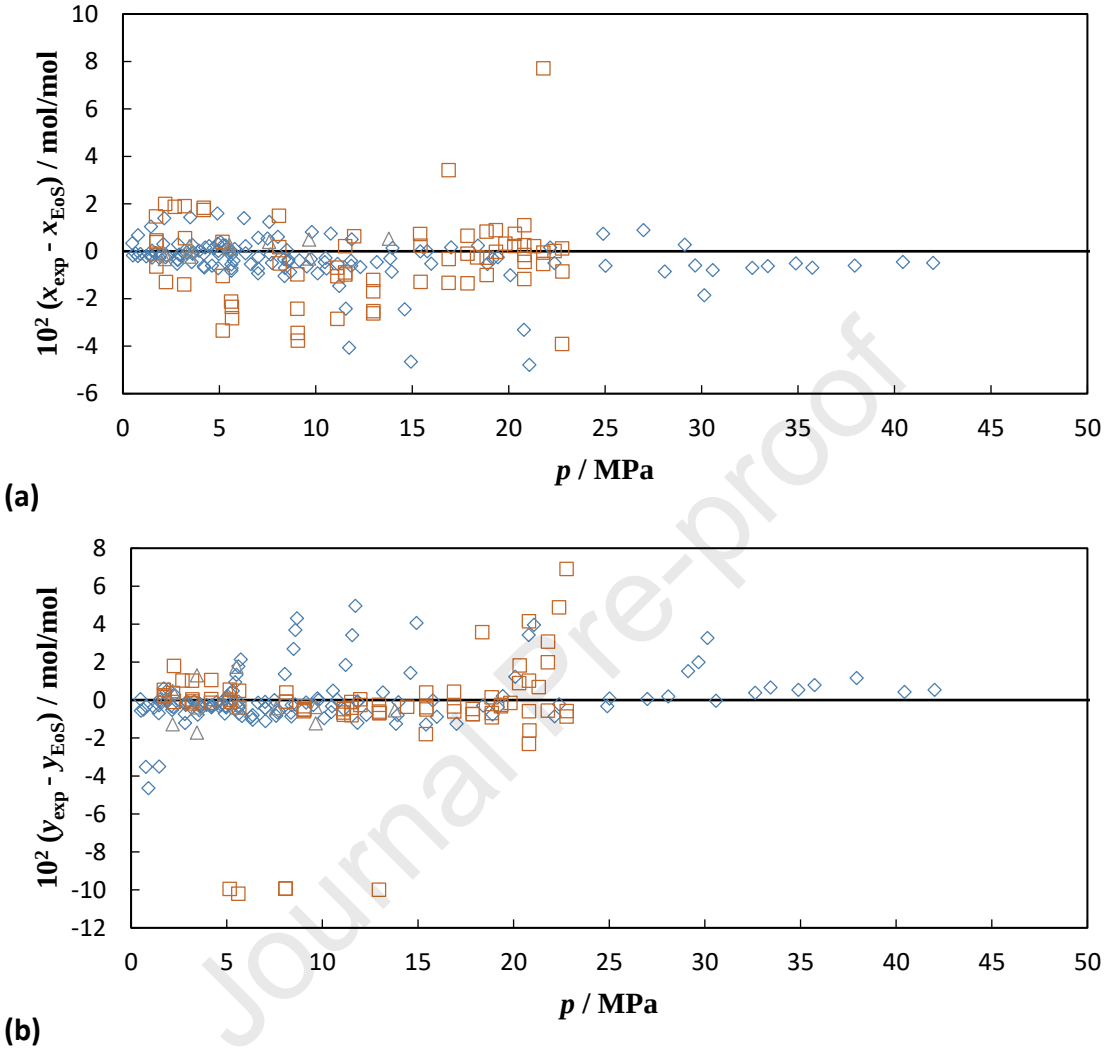

Figure 8. Deviations of bubble-point data (a) and dew-point data (b) for the binary mixtures (H_2O + H_2) and (H_2S + H_2) with respect to the improved GERG-2008 EoS [30][39]: □ Kling et al. (H_2O + H_2, 1991), ◇ Setthanan et al. (H_2O + H_2, 2006), ∗ Shoor et al. (H_2O + H_2, 1969), Δ Wiebe et al. (H_2O + H_2, 1934), × Yorizane et al. (H_2S + H_2, 1969).

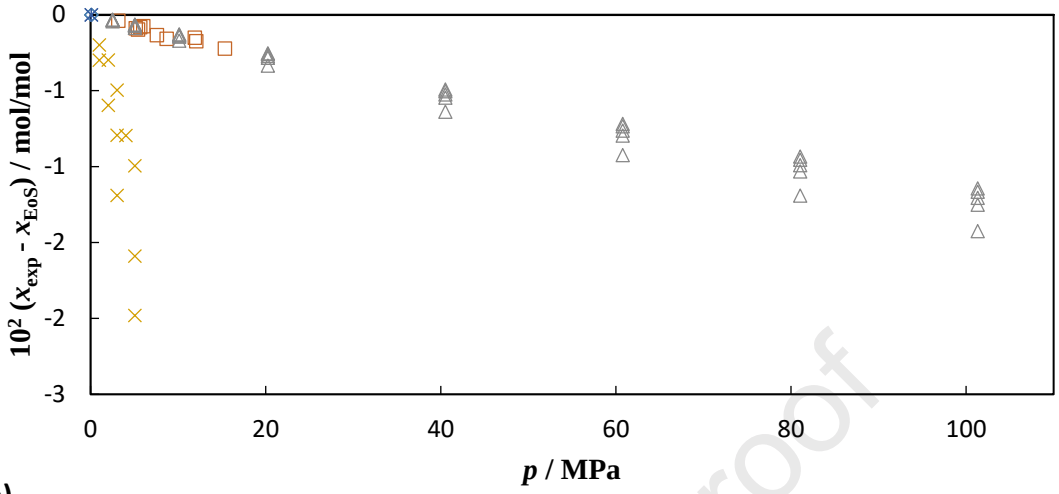

(a)

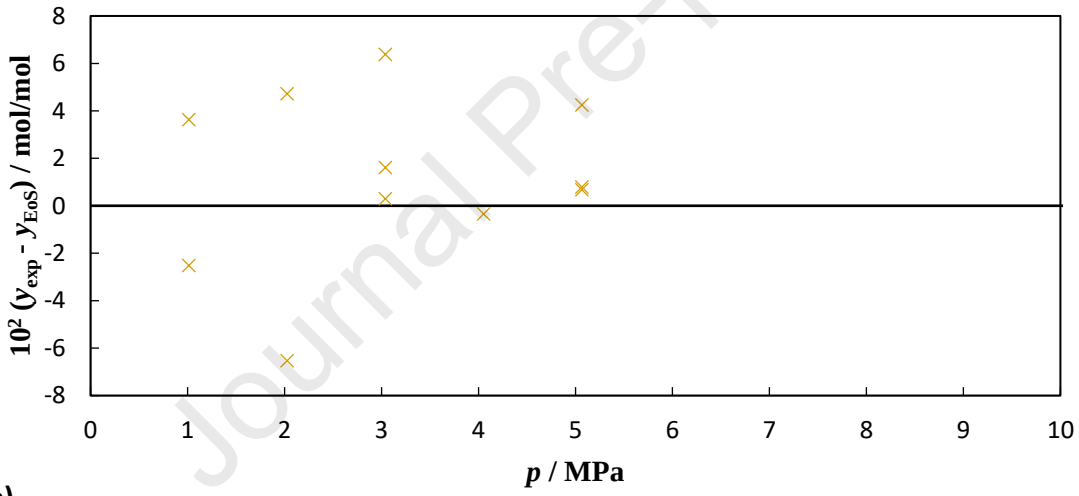

(b)

Figure 9. Deviations of bubble-point data (a) and dew-point data (b) for the binary mixtures (He + H_2), (Ar + H_2) and (Ne + H_2) with respect to the improved GERG-2008 EoS [30][39]: ☐ Hiza et al. (He + H_2, 1972), ☐ Hiza et al. (He + H_2, 1981), Δ Sneed et al. (He + H_2, 1968), ✶ Sonntag et al. (He + H_2, 1964), × Street et al. (He + H_2, 1964), ◇ Yamanishi et al. (He + H_2, 1992), + Calado et al. (Ar + H_2, 1960), ○ Volk et al. (Ar + H_2, 1979), − Heck et al. (Ne + H_2, 1966), - Street et al. (Ne + H_2, 1965), ◇ Zelfde et al. (Ne + H_2, 1974).

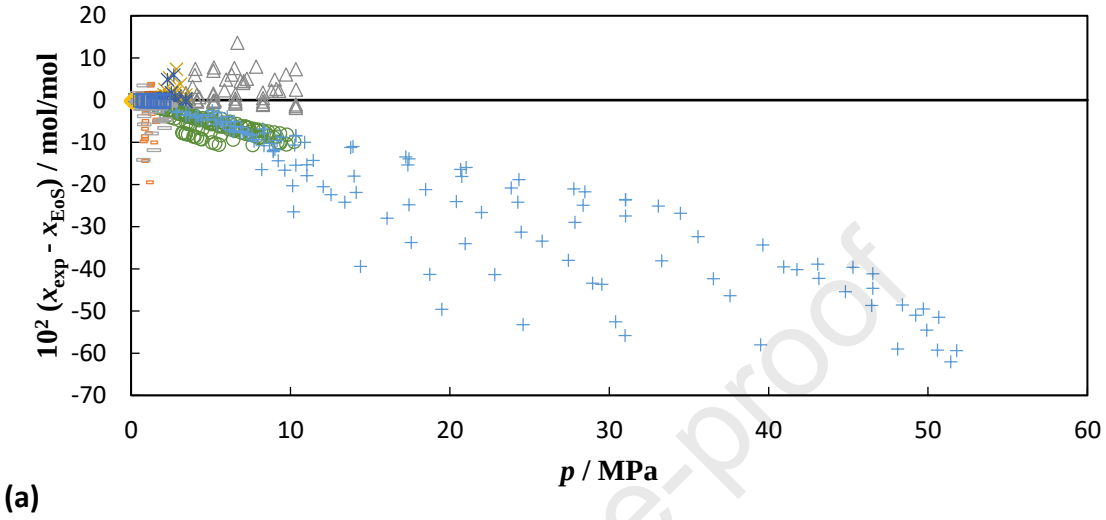

(a)

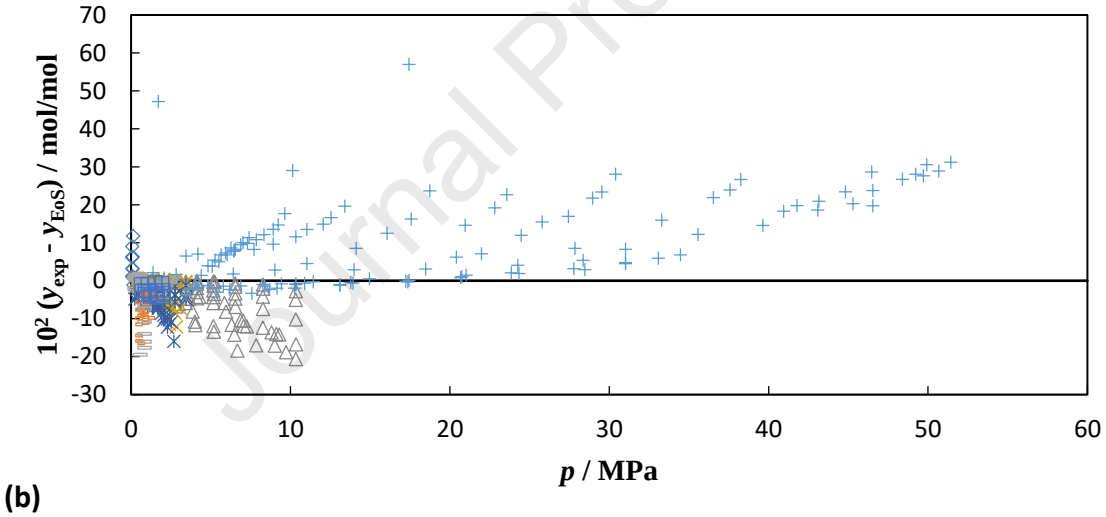

(b)

Figure 10. Deviations of bubble-point data (a) and dew-point data (b) for the binary mixtures (NH_3 + H_2) with respect to the improved GERG-2008 EoS [30][39]: × Moore et al. (1972), Δ Reamer et al. (1959), ◇ Wiebe et al. (1934), □ Wiebe et al. (1937).

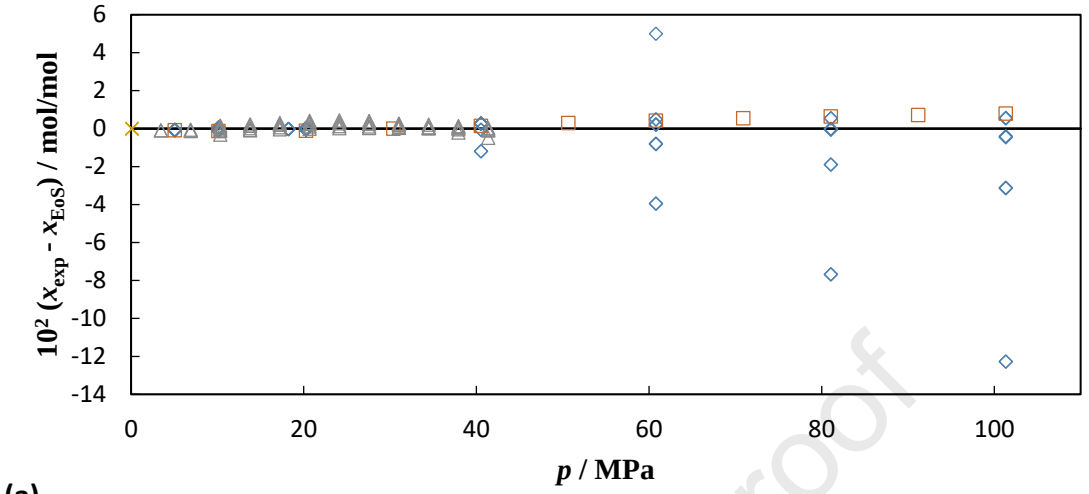

(a)

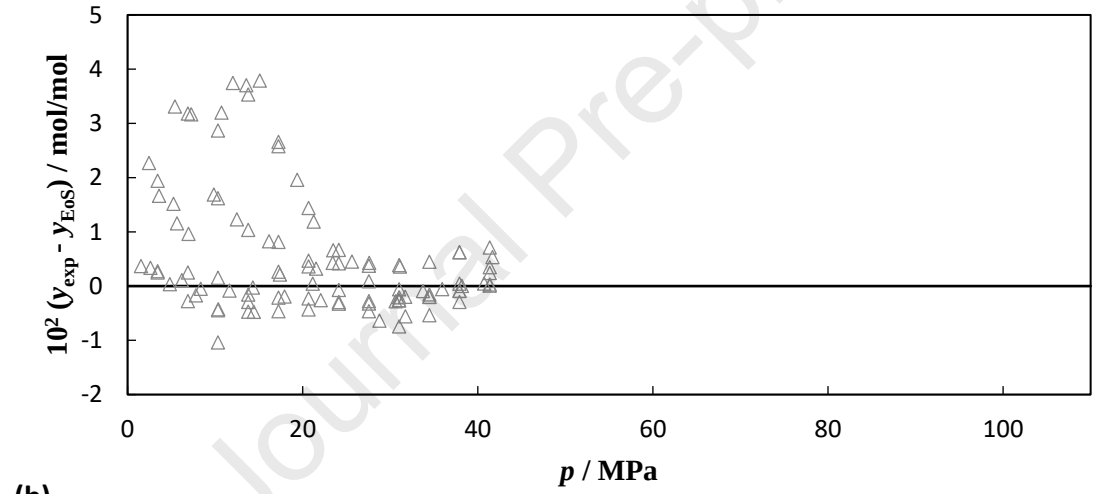

(b)

Figure 11. Percentage deviations of homogeneous density data for the binary mixtures (CH_4 + H_2) with respect to the improved GERG-2008 EoS [30][39]: ○ Hernández-Gómez et al. (2018), × Jett et al. (1994), ✳ Machado et al. (1988), ◇ Magee et al. (1985), □ Magee et al. (1986), ＋ Mason et al. (1961), Δ Mihara et al. (1977), - Mueller et al. (1961).

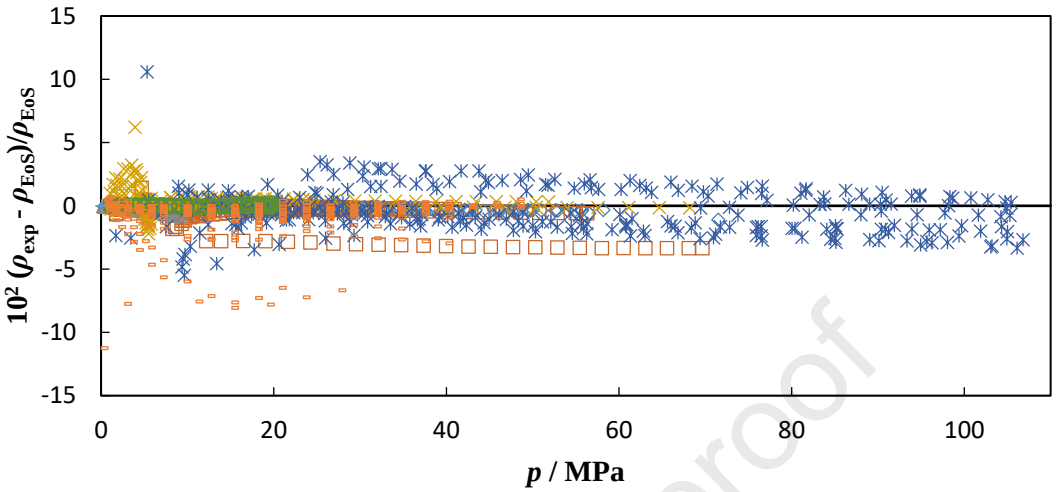

Figure 12. Percentage deviations of homogeneous density data for the binary mixtures (N_2 + H_2) with respect to the improved GERG-2008 EoS [30][39]: ┼ Bartlett et al. (1928/1930), ○ Bartlett et al. (1927), × Bennett et al. (1952), ◇ Hernández-Gómez et al. (2017), - Jaeschke et al. (1991), □ Kestin et al. (1982), ◇ Mastinu (1967), □ Michels et al. (1949), Δ Verschoyle et al. (1926), − Wiebe et al. (1938), ✳ Zandbergen et al. (1967).

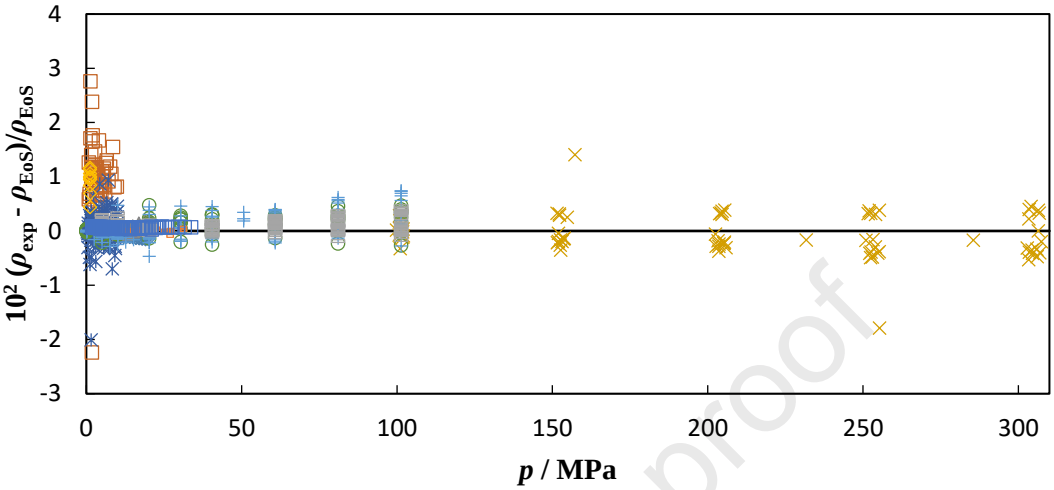

Figure 13. Percentage deviations of homogeneous density data for the binary mixtures (CO_2 + H_2) with respect to the improved GERG-2008 EoS [30][39]: □ Ababio et al. (1993), ◇ Alsiyabi (2013), - Cheng et al. (2019), × Cipollina et al. (2007), ◇ Mallu et al. (1990), ○ Pinho et al. (2015), ∗ Sanchez-Vicente et al. (2013), + Souissi et al. (2017), − Tsankova et al. (2019), Δ Zhang et al. (2002).

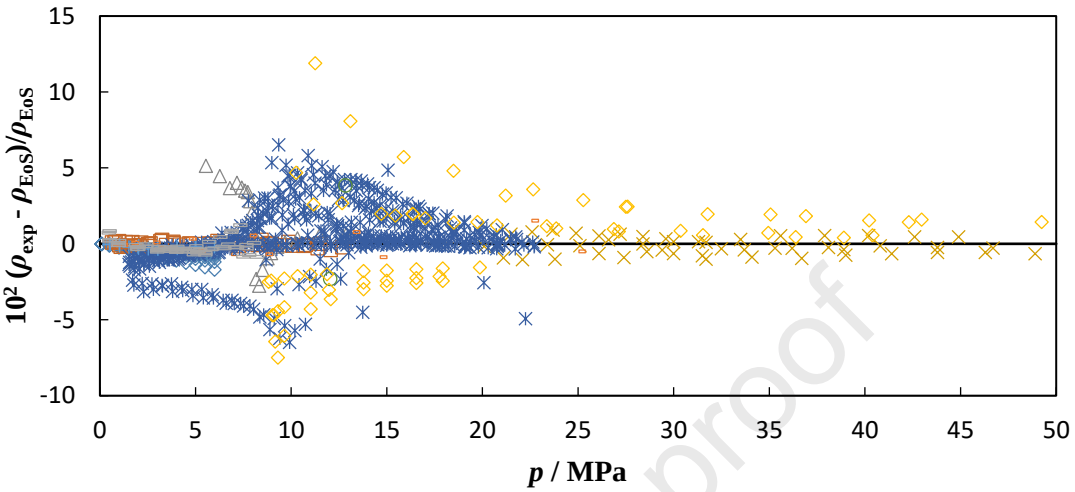

Figure 14. Percentage deviations of homogeneous density data for the binary mixtures (C_2H_6 + H_2) and (C_3H_8 + H_2) with respect to the improved GERG-2008 EoS [30][39]: □ Mason et al. (C_2H_6 + H_2, 1961), ◇ Mihara et al. (C_2H_6 + H_2, 1977), × Mason et al. (C_3H_8 + H_2, 1961), Δ Mihara et al. (C_3H_8 + H_2, 1977).

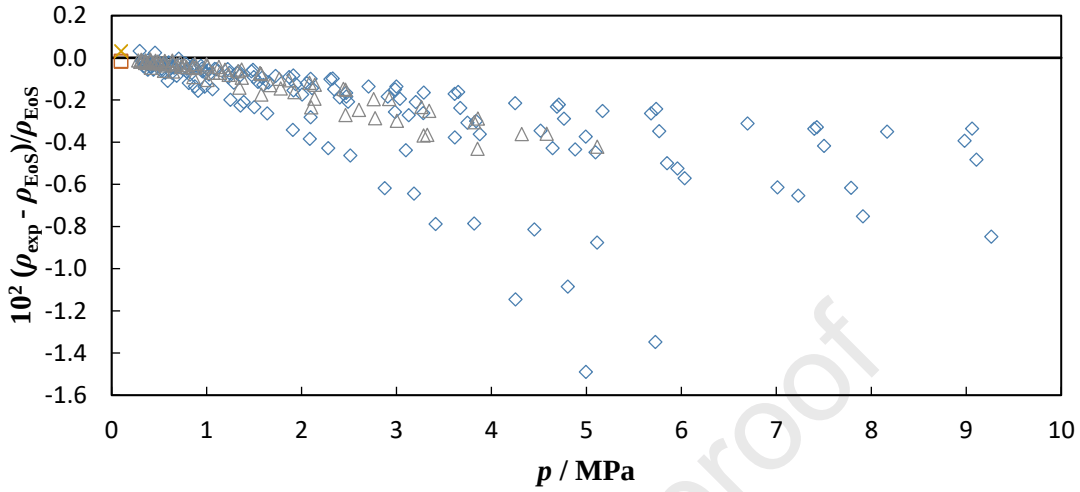

Figure 15. Percentage deviations of homogeneous density data for the binary mixtures (C_4H_{10} + H_2), (C_5H_{12} + H_2) and (C_6H_{14} + H_2) with respect to the improved GERG-2008 EoS [30][39]: ◇ Mason et al. (C_4H_{10} + H_2, 1961), Δ Freitag et al. (C_5H_{12} + H_2, 1986), □ Mason et al. (C_5H_{12} + H_2, 1961), × Nichols et al. (C_6H_{14} + H_2, 1957).

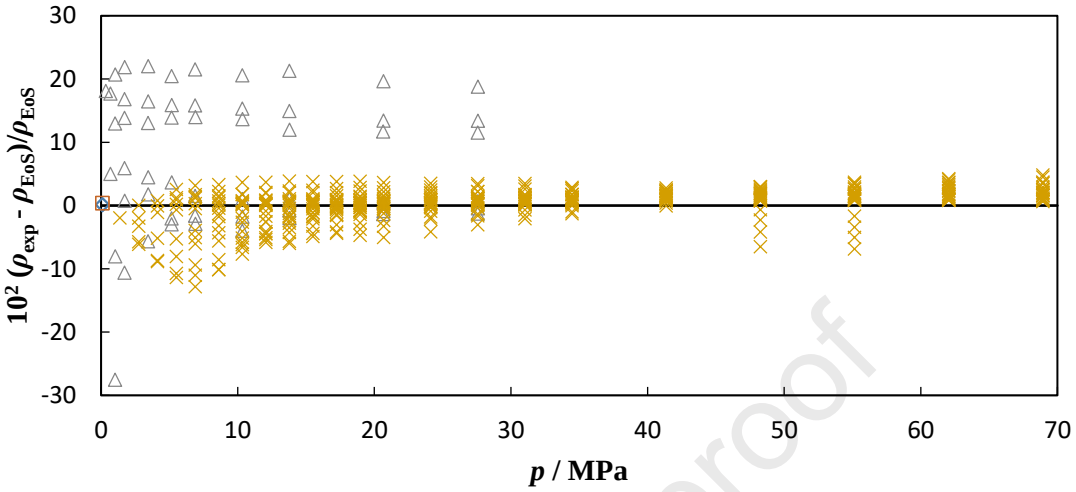

Figure 16. Percentage deviations of homogeneous density data for the binary mixtures (CO + H_2), (Ar + H_2), and (Ne + H_2) with respect to the improved GERG-2008 EoS [30][39]: ◇ Cipollina et al. (CO + H_2, 2007), Δ Scott et al. (CO + H_2, 1929), □ Townend et al. (CO + H_2, 1931), × Scholz et al. (Ar + H_2, 2020), ∗ Tanner et al. (Ar + H_2, 1930), ○ Zandbergen et al. (Ar + H_2, 1967), - Güsewell et al. (Ne + H_2, 1970), ┼ Street (Ne + H_2, 1973).

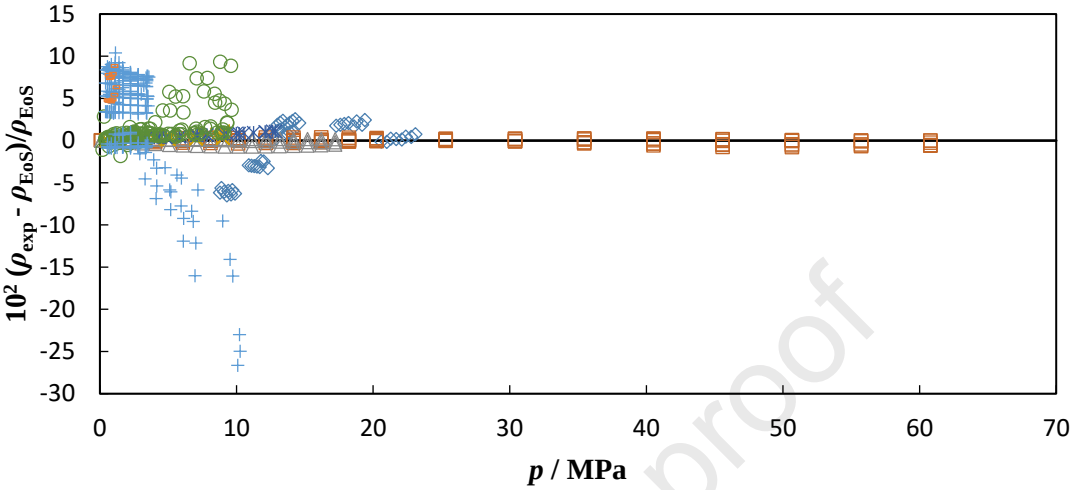

Figure 17. Percentage deviations of homogeneous density data for the binary mixtures (NH_3 + H_2) with respect to the improved GERG-2008 EoS [30][39]: ◇ Hongo et al.(1978), □ Kanarnovskiy et al. (1968).

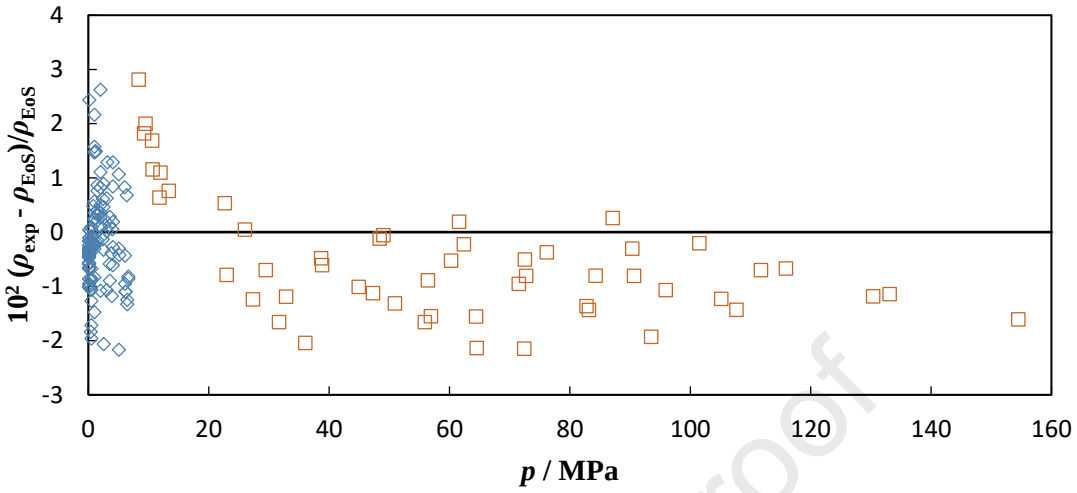

Figure 18. Percentage deviations of speed of sound data for the binary mixtures ($CH_4 + H_2$), ($N_2 + H_2$), ($CO_2 + H_2$), ($O_2 + H_2$), ($CO + H_2$), ($He + H_2$), ($Ar + H_2$) and ($Ne + H_2$) with respect to the improved GERG-2008 EoS [30][39]: ○ Maurer ($CH_4 + H_2$, 2021), ◇ Lozano-Martín et al. ($CH_4 + H_2$, 2020), × Itterbeek et al. ($N_2 + H_2$, 1949), Δ Lozano-Martín et al. ($N_2 + H_2$, 2021), ✳ Alsiyabi et al. ($CO_2 + H_2$, 2013), - Maurer ($CO_2 + H_2$, 2021), ＋ Itterbeek et al. ($O_2 + H_2$, 1949), − Itterbeek et al. ($CO + H_2$, 1949), □ Itterbeek et al. ($He + H_2$, 1946), ◇ Itterbeek et al. ($Ar + H_2$, 1946), □ Güsewell et al. ($Ne + H_2$, 1970).

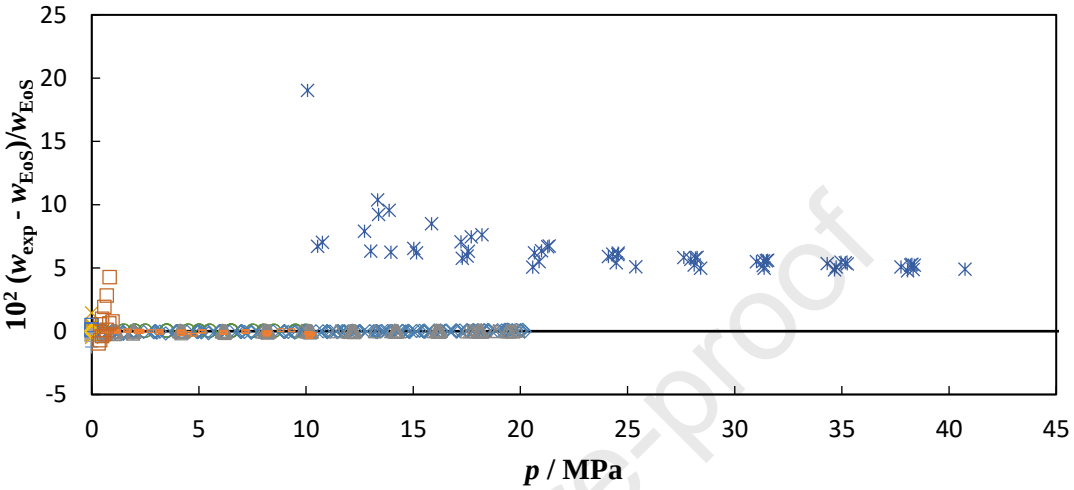

Figure 19. Percentage deviations of molar isobaric heat capacity data for the binary mixtures (N_2 + H_2) and (Ne + H_2) with respect to the improved GERG-2008 EoS [30][39]: ◇ Knapp et al. (N_2 + H_2, 1976), □ Brouwer et al. (Ne + H_2, 1970).

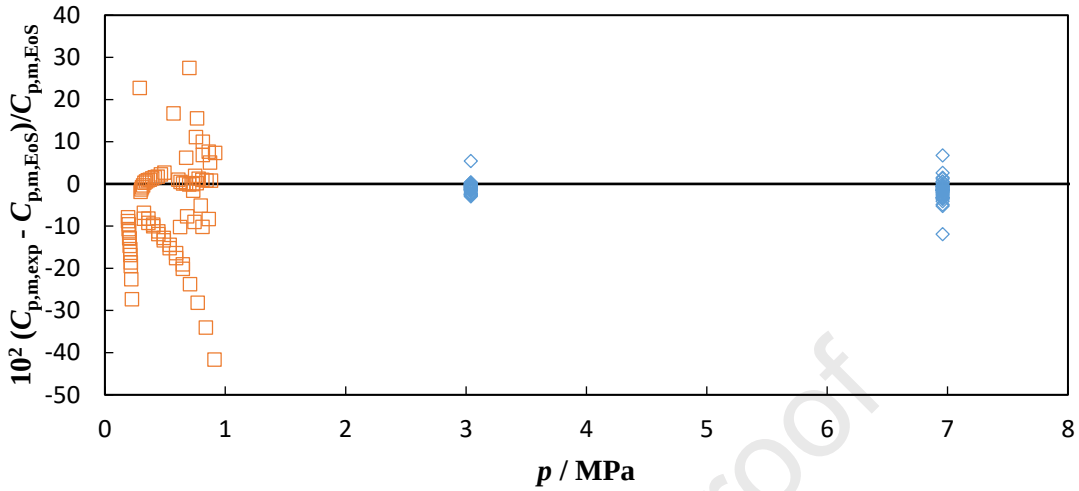

Figure 20. Percentage deviations of excess enthalpy data for the binary mixtures ($CH_4 + H_2$) and ($N_2 + H_2$) with respect to the improved GERG-2008 EoS [30][39]: Δ Wormald et al. ($CH_4 + H_2$, 1977), ◇ Wormald et al. ($N_2 + H_2$, 1977).

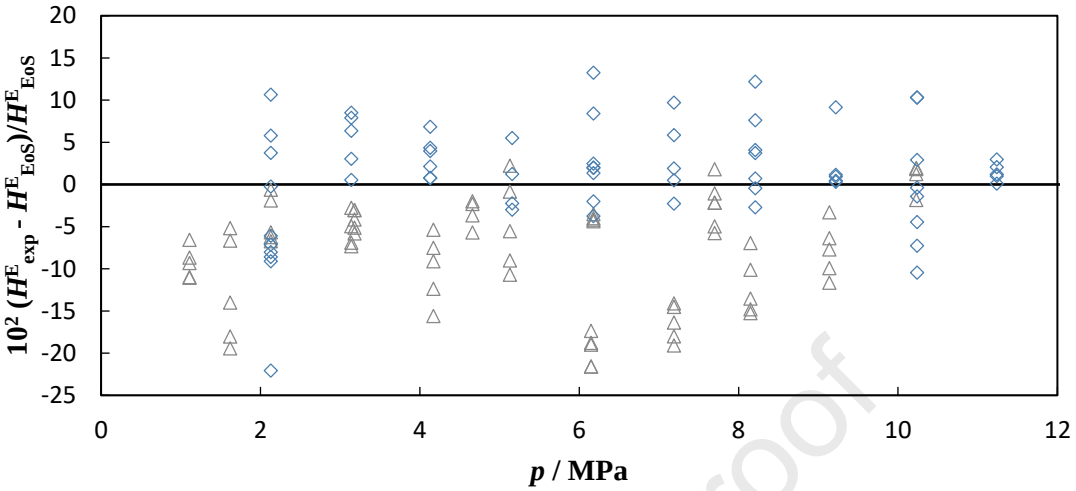

Figure 21. Percentage deviations of Joule-Thomson data for the binary mixtures (CH_4 + H_2) with respect to the improved GERG-2008 EoS [30][39]: ☐ Randelmand et al. (1988).

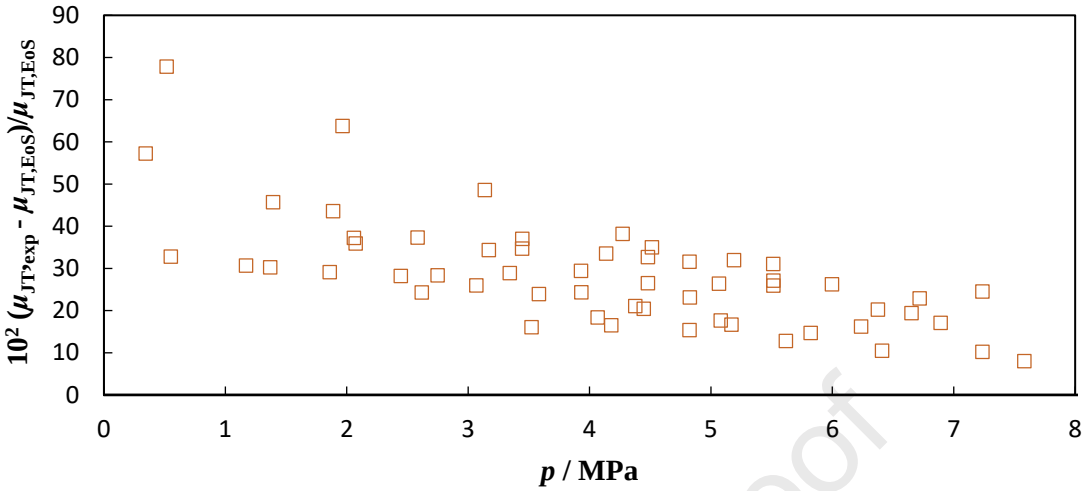

References

[1] IEA IEA. The Future of Hydrogen. Paris: 2019. https://doi.org/10.1787/1e0514c4-en.

[2] Velazquez Abad A, Dodds PE. Green hydrogen characterisation initiatives: Definitions, standards, guarantees of origin, and challenges. Energy Policy 2020. https://doi.org/10.1016/j.enpol.2020.111300.

[3] Hendriks E, Kontogeorgis GM, Dohrn R, De Hemptinne JC, Economou IG, Žilnik LF, et al. Industrial requirements for thermodynamics and transport properties. Ind Eng Chem Res 2010;49:11131–41. https://doi.org/10.1021/ie101231b.

[4] Kontogeorgis GM, Dohrn R, Economou IG, de Hemptinne J-C, ten Kate A, Kuitunen S, et al. Industrial Requirements for Thermodynamic and Transport Properties: 2020. Ind Eng Chem Res 2021;60:4987–5013. https://doi.org/10.1021/acs.iecr.0c05356.

[5] Hassanpouryouzband A, Joonaki E, Edlmann K, Heinemann N, Yang J. Thermodynamic and transport properties of hydrogen containing streams. Sci Data 2020;7:222. https://doi.org/10.1038/s41597-020-0568-6.

[6] Lozano-Martín D, Moreau A, Vega-Maza D, Chamorro CR. Thermophysical Properties of Hydrogen Mixtures Relevant for the Development of the Hydrogen Economy: Analysis of Available Experimental Data and Thermodynamic Models. SSRN Electron J 2021. https://doi.org/10.2139/ssrn.3939438.

[7] Nikolaidis P, Poullikkas A. A comparative overview of hydrogen production processes. Renew Sustain Energy Rev 2017;67:597–611. https://doi.org/10.1016/j.rser.2016.09.044.

[8] Das D, Veziroğlu TN. Hydrogen production by biological processes: A survey of literature. Int J Hydrogen Energy 2001. https://doi.org/10.1016/S0360-3199(00)00058-6.

[9] Steinfeld A. Solar thermochemical production of hydrogen - A review. Sol Energy 2005. https://doi.org/10.1016/j.solener.2003.12.012.

[10] Kothari R, Buddhi D, Sawhney RL. Comparison of environmental and economic aspects of various hydrogen production methods. Renew Sustain Energy Rev 2008. https://doi.org/10.1016/j.rser.2006.07.012.

[11] Alstrum-Acevedo JH, Brennaman MK, Meyer TJ. Chemical approaches to artificial photosynthesis. 2. Inorg Chem 2005. https://doi.org/10.1021/ic050904r.

[12] Razi F, Dincer I. A critical evaluation of potential routes of solar hydrogen production for sustainable development. J Clean Prod 2020. https://doi.org/10.1016/j.jclepro.2020.121582.

[13] Abdin Z, Zafaranloo A, Rafiee A, Mérida W, Lipiński W, Khalilpour KR. Hydrogen as an energy vector. Renew Sustain Energy Rev 2020. https://doi.org/10.1016/j.rser.2019.109620.

[14] Dingenen F, Verbruggen SW. Tapping hydrogen fuel from the ocean: A review on photocatalytic, photoelectrochemical and electrolytic splitting of seawater. Renew Sustain Energy Rev 2021;142:110866. https://doi.org/10.1016/j.rser.2021.110866.

[15] Handwerker M, Wellnitz J, Marzbani H. Comparison of Hydrogen Powertrains with the Battery Powered Electric Vehicle and Investigation of Small-Scale Local Hydrogen Production Using Renewable Energy. Hydrogen 2021;2:76–100. https://doi.org/10.3390/hydrogen2010005.

[16] Ross DK. Hydrogen storage: The major technological barrier to the development of hydrogen fuel cell cars. Vacuum 2006;80:1084–9.

https://doi.org/10.1016/j.vacuum.2006.03.030.

[17] Balali Y, Stegen S. Review of energy storage systems for vehicles based on technology, environmental impacts, and costs. Renew Sustain Energy Rev 2021;135:110185. https://doi.org/10.1016/j.rser.2020.110185.

[18] Chabab S, Théveneau P, Coquelet C, Corvisier J, Paricaud P. Measurements and predictive models of high-pressure H2 solubility in brine (H2O+NaCl) for underground hydrogen storage application. Int J Hydrogen Energy 2020;45:32206–20. https://doi.org/10.1016/j.ijhydene.2020.08.192.

[19] Yue M, Lambert H, Pahon E, Roche R, Jemei S, Hissel D. Hydrogen energy systems: A critical review of technologies, applications, trends and challenges. Renew Sustain Energy Rev 2021;146:111180. https://doi.org/10.1016/j.rser.2021.111180.

[20] Hassan IA, Ramadan HS, Saleh MA, Hissel D. Hydrogen storage technologies for stationary and mobile applications: Review, analysis and perspectives. Renew Sustain Energy Rev 2021;149:111311. https://doi.org/10.1016/j.rser.2021.111311.

[21] Quarton CJ, Samsatli S. Power-to-gas for injection into the gas grid: What can we learn from real-life projects, economic assessments and systems modelling? Renew Sustain Energy Rev 2018;98:302–16. https://doi.org/10.1016/j.rser.2018.09.007.

[22] Griffiths S, Sovacool BK, Kim J, Bazilian M, Uratani JM. Industrial decarbonization via hydrogen: A critical and systematic review of developments, socio-technical systems and policy options. Energy Res Soc Sci 2021;80:102208. https://doi.org/10.1016/j.erss.2021.102208.

[23] Dahal K, Brynolf S, Xisto C, Hansson J, Grahn M, Grönstedt T, et al. Techno-economic review of alternative fuels and propulsion systems for the aviation sector. Renew Sustain Energy Rev 2021;151:111564. https://doi.org/10.1016/j.rser.2021.111564.

[24] Leachman JW, Jacobsen RT, Penoncello SG, Lemmon EW. Fundamental equations of state for parahydrogen, normal hydrogen, and orthohydrogen. J Phys Chem Ref Data 2009;38:721–48. https://doi.org/10.1063/1.3160306.

[25] Lemmon EW, Bell IH, Huber ML, McLinden MO, Lemmon, E.W., Bell, I.H., Huber, M.L., McLinden MO. NIST Standard Reference Database 23: Reference Fluid Thermodynamic and Transport Properties-REFPROP, Version 10.0. Natl Inst Stand Technol Stand Ref Data Progr 2018.

[26] Jacobsen RT, Leachman JW, Penoncello SG, Lemmon EW. Current status of thermodynamic properties of hydrogen. Int J Thermophys 2007;28:758–72. https://doi.org/10.1007/s10765-007-0226-7.

[27] Younglove BA. Thermophysical properties of fluids. I. Argon, ethylene, parahydrogen, nitrogen, nitrogen trifluoride, and oxygen. J Phys Chem Ref Data 1982;Suppl. No.:1–353.

[28] Klimeck R. Entwicklung einer Fundamentalgleichung für Erdgase für das Gas- und Flüssigkeitsgebiet sowie das Phasengleichgewicht. Ph.D. Dissertation. Ruhr-Universität Bochum, Bochum, Germany, 2000.

[29] Kunz O, Klimeck R, Wagner W, Jaeschke M. GERG Technical Monograph 15 The GERG-2004 wide-range equation of state for natural gases and other mixtures. Düsseldorf: 2007.

[30] Kunz O, Wagner W. The GERG-2008 Wide-Range Equation of State for Natural Gases and Other Mixtures: An Expansion of GERG-2004. J Chem Eng Data 2012;57:3032–91. https://doi.org/10.1021/je300655b.

[31] Sakoda N, Shindo K, Shinzato K, Kohno M, Takata Y, Fujii M. Review of the thermodynamic properties of hydrogen based on existing equations of state. Int J Thermophys 2010;31:276–96. https://doi.org/10.1007/s10765-009-0699-7.

[32] Neumann T, Thol M, Bell IH, Lemmon EW, Span R. Fundamental Thermodynamic Models for Mixtures Containing Ammonia. Fluid Phase Equilib 2020;511:112496. https://doi.org/10.1016/j.fluid.2020.112496.

[33] Demetriades TA, Graham RS. A new equation of state for CCS pipeline transport: Calibration of mixing rules for binary mixtures of CO2 with N2, O2 and H2. J Chem Thermodyn 2016;93:294–304. https://doi.org/10.1016/j.jct.2015.07.045.

[34] Fandiño O, Trusler JPM, Vega-Maza D. Phase behavior of (CO2+H2) and (CO2+N2) at temperatures between (218.15 and 303.15)K at pressures up to 15MPa. Int J Greenh Gas Control 2015;36:78–92. https://doi.org/10.1016/j.ijggc.2015.02.018.

[35] Blackham TM. A GENERALIZED HELMHOLTZ ENERGY FUNCTIONAL FORM FOR THERMODYNAMIC. 2016.

[36] Aasen A, Hammer M, Lasala S, Jaubert JN, Wilhelmsen Ø. Accurate quantum-corrected cubic equations of state for helium, neon, hydrogen, deuterium and their mixtures. Fluid Phase Equilib 2020;524:112790. https://doi.org/10.1016/j.fluid.2020.112790.

[37] Aasen A, Hammer M, Ervik Å, Müller EA, Wilhelmsen Ø. Equation of state and force fields for Feynman-Hibbs-corrected Mie fluids. I. Application to pure helium, neon, hydrogen, and deuterium. J Chem Phys 2019;151:1–19. https://doi.org/10.1063/1.5111364.

[38] Aasen A, Hammer M, Müller EA, Wilhelmsen Ø. Equation of state and force fields for Feynman-Hibbs-corrected Mie fluids. II. Application to mixtures of helium, neon, hydrogen, and deuterium. J Chem Phys 2020;152. https://doi.org/10.1063/1.5136079.

[39] Beckmüller R, Thol M, Bell IH, Lemmon EW, Span R. New Equations of State for Binary Hydrogen Mixtures Containing Methane, Nitrogen, Carbon Monoxide, and Carbon Dioxide. J Phys Chem Ref Data 2021;50:1–22. https://doi.org/10.1063/5.0040533.

[40] International Organisation for Standardization G. ISO 20765-2 Natural gas -Calculation of thermodynamic properties -Part 2: Single-phase properties (gas, liquid, and dense fluid) for extended ranges of application 2015.

[41] Span R. Multiparameter Equations of State — An Accurate Source of Thermodynamic Property Data. Springer-Verlag; 2000.

[42] Thol M, Bell IH. Empirical Fundamental Equations of State for Pure Fluids and Mixtures. 2020. https://doi.org/10.2514/5.9781624105814.0365.0408.

[43] Span R, Wagner W. Equations of State for Technical Applications. II. Results for Nonpolar Fluids. Int J Thermophys 2003;24:41–109. https://doi.org/10.1023/A:1022310214958.

[44] Lemmon EW, Span R. Short Fundamental Equations of State for 20 Industrial Fluids. J Chem Eng Data 2006;51:785–850. https://doi.org/10.1021/je050186n.

[45] K. E. Starling and J. L. Savidge. Compressibility factors of natural gas and other related hydrocarbon gases - AGA Transmission Measurement Committee Report 8, 1992.

[46] Demetriades TA, Drage TC, Graham RS. Developing a new equation of state for carbon capture and storage pipeline transport. Proc Inst Mech Eng Part E J Process Mech Eng 2013. https://doi.org/10.1177/0954408913481552.

[47] Köster A, Thol M, Vrabec J. Molecular Models for the Hydrogen Age: Hydrogen, Nitrogen, Oxygen, Argon, and Water. J Chem Eng Data 2018;63:305–20. https://doi.org/10.1021/acs.jced.7b00706.

[48] Hernández-Gómez R, Tuma D, Lozano-Martín D, Chamorro CR. Accurate experimental (p, ρ, T) data of natural gas mixtures for the assessment of reference equations of state when dealing with hydrogen-enriched natural gas. Int J Hydrogen Energy 2018;43:21983–98. https://doi.org/10.1016/j.ijhydene.2018.10.027.

[49] Richter M, Ben Souissi MA, Span R, Schley P. Accurate (p, σ, T, x) measurements of hydrogen-enriched natural-gas mixtures at T = (273.15, 283.15, and 293.15) K with pressures up to 8 MPa. J Chem Eng Data 2014;59:2021–9. https://doi.org/10.1021/je500181v.

[50] Deiters UK, Bell IH. Unphysical Critical Curves of Binary Mixtures Predicted with GERG Models. Int J Thermophys 2020;41:1–19. https://doi.org/10.1007/s10765-020-02743-3.

[51] Alkhatib III, AlHajaj A, Almansoori A, Vega LF. Accurate Predictions of the Effect of Hydrogen Composition on the Thermodynamics and Transport Properties of Natural Gas. Ind Eng Chem Res 2022:acs.iecr.2c00363. https://doi.org/10.1021/acs.iecr.2c00363.

[52] Peng DY, Robinson DB. A New Two-Constant Equation of State. Ind Eng Chem Fundam 1976;15:59–64. https://doi.org/10.1021/i160057a011.

[53] Lopez-Echeverry JS, Reif-Acherman S, Araujo-Lopez E. Peng-Robinson equation of state: 40 years through cubics. Fluid Phase Equilib 2017;447:39–71. https://doi.org/10.1016/j.fluid.2017.05.007.

[54] Twu CH, Coon JE, Cunningham JR. A new generalized alpha function for a cubic equation of state Part 1. Peng-Robinson equation. Fluid Phase Equilib 1995;105:49–59. https://doi.org/10.1016/0378-3812(94)02601-V.

[55] Gross J, Sadowski G. Perturbed-chain SAFT: An equation of state based on a perturbation theory for chain molecules. Ind Eng Chem Res 2001;40:1244–60. https://doi.org/10.1021/ie0003887.

[56] Gross J, Sadowski G. Application of the perturbed-chain SAFT equation of state to associating systems. Ind Eng Chem Res 2002;41:5510–5. https://doi.org/10.1021/ie010954d.

[57] Gross J, Sadowski G. Reply to Comment on "perturbed-Chain SAFT: An Equation of State Based on a Perturbation Theory for Chain Molecules." Ind Eng Chem Res 2019;58:5744–5. https://doi.org/10.1021/acs.iecr.9b01515.

[58] FELIPE J. BLAS and LOURDES F. VEGA. Thermodynamic behaviour of homonuclear and heteronuclear Lennard-Jones chains with association sites from simulation and theory. Mol Phys 1997;92:135–50. https://doi.org/10.1080/002689797170707.

[59] Alkhatib III, Pereira LMC, Torne J, Vega LF. Polar soft-SAFT: Theory and comparison with molecular simulations and experimental data of pure polar fluids. Phys Chem Chem Phys 2020;22:13171–91. https://doi.org/10.1039/d0cp00846j.

[60] Wagner W, Kleinrahm R. Densimeters for very accurate density measurements of fluids over large ranges of temperature, pressure, and density. Metrologia 2004;41. https://doi.org/10.1088/0026-1394/41/2/S03.

[61] Cheng S, Li F, Shang F, Ma W, Jin H, Sakoda N, et al. A Review of Experimental Researches on the Thermophysical Properties of Hydrogen-Containing Mixtures at High

Temperatures and High Pressures. J Chem Eng Data 2021;66:3361–85. https://doi.org/10.1021/acs.jced.1c00366.

[62] Tsang CY, Clancy P, Calado JCG, Streett WB. Phase equilibria in the H2/CH4 system at temperatures from 92.3 to 180.0 K and pressures to 140 MPa. Chem Eng Commun 1980;6:365–83. https://doi.org/10.1080/00986448008912543.

[63] Hong JH, Kobayashi R. Vapor-Liquid Equilibrium Study of the H2-CH4 System at Low Temperatures and Elevated Pressures. J Chem Eng Data 1981;26:127–31. https://doi.org/10.1021/je00024a007.

[64] Machado JRS, Streett WB, Deiters U. PVT Measurements of Hydrogen/Methane Mixtures at High Pressures. J Chem Eng Data 1988;33:148–52. https://doi.org/10.1021/je00052a027.

[65] Streett WB, Calado JCG. Liquid-vapour equilibrium for hydrogen + nitrogen at temperatures from 63 to 110 K and pressures to 57 MPa. J Chem Thermodyn 1978;10:1089–100. https://doi.org/10.1016/0021-9614(78)90083-6.

[66] Mastinu G. Apparatus to determine excess molar volumes. Application to the H 2-N2 mixture. Rev Sci Instrum 1967;38:1114–6. https://doi.org/10.1063/1.1720980.

[67] Michels A, Wassenaar T. ISOTHERMS OF A NITROGEN-HYDROGEN MIXTURE B E T W E E N 0 ~ A N D 150 ~ U P T O 340 A T M O S P H E R E S Summary Compressibility isotherms of a l : 3 nitrogen-hydrogen mixture have been up to densities of 180 Amagat (pressures up to 340 atm). The result n.d.:258–62.

[68] Bennett CO, Dodge BF. Compressibilities of Mixtures of Hydrogen and Nitrogen Above 1000 Atmospheres. Ind Eng Chem 1952;44:180–5. https://doi.org/10.1021/ie50505a051.

[69] Van Itterbeek A, Van Doninck W. Measurements on the velocity of sound in mixtures of hydrogen, helium, oxygen, nitrogen and carbon monoxide at low temperatures. Proc Phys Soc Sect B 1949;62:62–9. https://doi.org/10.1088/0370-1301/62/1/308.

[70] Tsang CY, Street WB. Phase equilibria in the H2/CO2 system at temperatures from 220 to 290 K and pressures to 172 MPa. Chem Eng Sci 1981;36:993–1000. https://doi.org/10.1016/0009-2509(81)80085-1.

[71] Ben Souissi MA, Kleinrahm R, Yang X, Richter M. Vapor-Phase (p, ρ, T, x) Behavior and Virial Coefficients for the Binary Mixture (0.05 Hydrogen + 0.95 Carbon Dioxide) over the Temperature Range from (273.15 to 323.15) K with Pressures up to 6 MPa. J Chem Eng Data 2017;62:2973–81. https://doi.org/10.1021/acs.jced.7b00213.

[72] Cipollina A, Anselmo R, Scialdone O, Filardo G, Galia A. Experimental P-T-ρ measurements of supercritical mixtures of carbon dioxide, carbon monoxide, and hydrogen and semiquantitative estimation of their solvent power using the solubility parameter concept. J Chem Eng Data 2007;52:2291–7. https://doi.org/10.1021/je700307r.

[73] Mallu BV, Viswanath DS. Compression factors and second virial coefficients of H2, CH4, {xCO2 + (1 − x)H2}, and {xCO2 + (1 − x)CH4}. J Chem Thermodyn 1990;22:997–1006. https://doi.org/10.1016/0021-9614(90)90189-W.

[74] Cheng S, Shang F, Ma W, Jin H, Sakoda N, Zhang X, et al. Density Data of Two (H2 + CO2) Mixtures and a (H2 + CO2 + CH4) Mixture by a Modified Burnett Method at Temperature 673 K and Pressures up to 25 MPa. J Chem Eng Data 2019;64:1693–704. https://doi.org/10.1021/acs.jced.8b01206.

[75] Hiza MJ, Heck CK, Kidnay AJ. Liquid-Vapor and Solid-Vapor Equilibrium in the System Hydrogen - Ethane. Adv Cryog Eng 1968;13:343–56.

[76] Burriss WL, Hsu NT, Reamer HH, Sage BH. Phase Behavior of the Hydrogen-Propane System. Ind Eng Chem 1953;45:210–3. https://doi.org/10.1021/ie50517a060.

[77] MIHARA S, SAGARA H, ARAI Y, SAITO S. THE COMPRESSIBILITY FACTORS OF HYDROGEN METHANE, HYDROGEN-ETHANE AND HYDROGEN-PROPANE GASEOUS MIXTURES. J Chem Eng Japan 1977;10:395–9. https://doi.org/10.1252/jcej.10.395.

[78] Mason DMA, Eakin BE. Compressibility Factor of Fuel Gases at 60° F. and 1 Atm. J Chem Eng Data 1961;6:499–504. https://doi.org/10.1021/je60011a006.

[79] Aroyan HJ, Katz DL. Low Temperature Vapor-Liquid Equilibria in Hydrogen-n-Butane System. Ind Eng Chem 1951;43:185–9. https://doi.org/10.1021/ie50493a050.

[80] Dean MR, Tooke JW. Vapor-Liquid Equilibria in Three Hydrogen-Paraffin Systems. Ind Eng Chem 1946;38:389–93. https://doi.org/10.1021/ie50436a014.

[81] Nichols WB, Reamer HH, Sage BH. Volumetric and phase behavior in the hydrogen–n-hexane system. AIChE J 1957;3:262–7. https://doi.org/10.1002/aic.690030223.

[82] Transactions P. The ternary system carbon monoxide-nitrogen-hydrogen and the component binary systems between temperatures of -185° and -215° C., and between pressures of 0 and 225 atm. Philos Trans R Soc London Ser A, Contain Pap a Math or Phys Character 1931;230:189–220. https://doi.org/10.1098/rsta.1932.0006.

[83] Tsang CY, Streett WB. Phase equilibria in the H2 CO system at temperatures from 70 to 125 K and pressures to 53 MPa. Fluid Phase Equilib 1981;6:261–73. https://doi.org/10.1016/0378-3812(81)85008-X.

[84] Scott GA, A PRSL. The isotherms of hydrogen, carbon monoxide and their mixtures. Proc R Soc London Ser A, Contain Pap a Math Phys Character 1929;125:330–44. https://doi.org/10.1098/rspa.1929.0171.

[85] Townend DTA, Bhatt LA. Isotherms of hydrogen, carbon monoxide and their mixtures. Proc R Soc London Ser A, Contain Pap a Math Phys Character 1931;134:502–12. https://doi.org/10.1098/rspa.1931.0210.

[86] Setthanan U, Morris DR, Lister DH. Solubilities of H2 in H2O and D2 in D 2O with dissolved boric acid and lithium hydroxide. Can J Chem 2006;84:65–8. https://doi.org/10.1139/v06-010.

[87] Kling G, Maurer G. The solubility of hydrogen in water and in 2-aminoethanol at temperatures between 323 K and 423 K and pressures up to 16 MPa. J Chem Thermodyn 1991;23:531–41. https://doi.org/10.1016/S0021-9614(05)80095-3.

[88] Wiebe R, Gaddy VL. The Solubility of Hydrogen in Water at 0, 50, 75 and 100° from 25 to 1000 Atmospheres. J Am Chem Soc 1934;56:76–9. https://doi.org/10.1021/ja01316a022.

[89] Shoor SK, Walker RD, Gubbins KE. Salting out of nonpolar gases in aqueous potassium hydroxide solutions. J Phys Chem 1969;73:312–7. https://doi.org/10.1021/j100722a006.

[90] Yorizane M, Sadamoto S, Masuoka H, Eto Y. Gas Solubilities in Methanol at High Pressure. J Soc Chem Ind Japan 1969;72:2174–7. https://doi.org/10.1246/nikkashi1898.72.10_2174.

[91] Yamanishi T, Okuno K, Naruse Y, Sada E. Liquid-vapor equilibrium in binary systems for He in n-H2, HD, and n-D2 under ordinary pressure. J Phys Chem 1992;96:2284–9.

[92] Hiza MJ. Technical Note 621 - Liquid-Vapor Equilibrium in the Binary Systems of He-4 and He-3 with n-D2 and n-H2. 1972.

[93] Hiza MJ. Liquid-vapor equilibria in binary systems containing 4He or 3He with nH2 or nD2. Fluid Phase Equilib 1981;6:203–27. https://doi.org/10.1016/0378-3812(81)85005-4.

[94] Sneed CM, Sonntag RE, Van Wylen GJ. Helium-hydrogen liquid-vapor equilibrium to 100 atm. J Chem Phys 1968;49:2395–404. https://doi.org/10.1063/1.1670414.

[95] Streett WB, Sonntag RE, Van Wylen GJ. Liquid-vapor equilibrium in the system normal hydrogen-helium. J Chem Phys 1964;40:1390–5. https://doi.org/10.1063/1.1725322.

[96] Sonntag RE, Van Wylen GJ, Crain RW. Liquid-vapor equilibrium in the system equilibrium hydrogen-helium. J Chem Phys 1964;41:2399–402. https://doi.org/10.1063/1.1726277.

[97] Calado JCG, Streett WB. Liquid-vapor equilibrium in the system H2Ar at temperatures from 83 to 141 K and pressures to 52 MPa. Fluid Phase Equilib 1979;2:275–82. https://doi.org/10.1016/0378-3812(79)80012-6.

[98] Volk H, Halsey GD. Solubility of hydrogen and deuterium in liquid argon. J Chem Phys 1960;33:1132–9. https://doi.org/10.1063/1.1731347.

[99] Streett WB, Jones CH. Liquid Phase Separation and Liquid—Vapor Equilibrium in the System Neon—Hydrogen. J Chem Phys 1965;42:3989–94. https://doi.org/10.1063/1.1695872.

[100] Heck CK, Barrick PL. LIQUID-VAPOR PHASE EQUILffiRIA OF THE NEON-NORMAL HYDROGEN SYSTEM 1966:349–55.

[101] Van't Zelfde P, Dokoupil Z. Some vapour-pressure measurements of the condensed system Ne-H2 near the triple point of Ne. Physica 1974;74:423–34. https://doi.org/10.1016/0031-8914(74)90135-9.

[102] Scholz CW, Span R. Vapor-Phase (p , ρ, T , x) Behavior of the (Hydrogen + Argon) System . J Chem Eng Data 2020. https://doi.org/10.1021/acs.jced.0c00355.

[103] Laboratories C. The pressures of gaseous mixtures. Part III. Proc R Soc London Ser A, Contain Pap a Math Phys Character 1930;126:268–88. https://doi.org/10.1098/rspa.1930.0007.

[104] Zandbergen P, Beenakker JJM. Experimental determination of the volume change on mixing for gaseous N2-H2, Ar-H2 and Ar-N2 between 170 and 292°K up to 100 ATM. Physica 1967;33:343–65. https://doi.org/10.1016/0031-8914(67)90169-3.

[105] Streett WB. An experimental study of the equation of state of liquid mixtures of neon + normal hydrogen. J Chem Thermodyn 1973;5:313–23. https://doi.org/10.1016/S0021-9614(73)80019-9.

[106] Güsewell D, Schmeissner F, Schmid J. Density and sound velocity of saturated liquid neon-hydrogen and neon-deuterium mixtures between 25 and 31 K. Cryogenics (Guildf) 1970;10:150–4. https://doi.org/10.1016/0011-2275(70)90087-1.

[107] Van Itterbeek A, Van Doninck W. Velocity of sound in mixtures of argon, helium and hydrogen at low temperatures. Proc Phys Soc 1946;58:615–23. https://doi.org/10.1088/0959-5309/58/5/309.

[108] Kazarnovskii YS, Simonov GB, Arsitov GE. Compressibility of Nitrogen-Hydrogen-Ammonia Mixtures at high Pressures and Temperatures. Zh Fiz Khim 1968;14:774–81.

[109] Hongo M, Iwasaki H. VISCOSITY OF HYDROGEN AND OF HYDROGEN-AMMONIA MIXTURES UNDER PRESSURES 1978;48:1–9.

[110] Wiebe R, Tremearne TH. The Solubility of Hydrogen in Liquid Ammonia at 25, 50, 75 and 100° and at Pressures to 1000 Atmospheres. J Am Chem Soc 1934;56:2357–60. https://doi.org/10.1021/ja01326a039.

[111] Wiebe R, Gaddy VL. The Solubility in Liquid Ammonia of Hydrogen at 0° and of Nitrogen at 0, 50, 75, 90 and 100° at Pressures to 1000 Atmospheres. Critical Phenomena of Ammonia-Nitrogen Mixtures 1. J Am Chem Soc 1937;59:1984–7. https://doi.org/10.1021/ja01289a055.

[112] Reamer HH, Sage BH. Phase Behavior in the Hydrogen-Ammonia System. J Chem Eng Data 1959;4:152–4. https://doi.org/10.1021/je60002a012.

[113] Knapp H, Schmölling K, Neumann A. Measurement of the molal heat capacity of H2 N2 mixtures. Cryogenics (Guildf) 1976;16:231–7. https://doi.org/10.1016/0011-2275(76)90266-6.

[114] Wormald CJ, Lewis KL, Mosedale S. The excess enthalpies of hydrogen + methane, hydrogen + nitrogen, methane + nitrogen, methane + argon, and nitrogen + argon at 298 and 201 K at pressures up to 10.2 MPa. J Chem Thermodyn 1977;9:27–42. https://doi.org/10.1016/0021-9614(77)90194-X.

[115] Randelman RE, Wenzel LA. Joule-Thomson Coefficients of Hydrogen and Methane Mixtures. J Chem Eng Data 1988;33:293–9. https://doi.org/10.1021/je00053a021.

[116] Li H, Jakobsen JP, Wilhelmsen Ø, Yan J. PVTxy properties of CO2 mixtures relevant for CO2 capture, transport and storage: Review of available experimental data and theoretical models. Appl Energy 2011;88:3567–79. https://doi.org/10.1016/j.apenergy.2011.03.052.

[117] Li H, Dong B, Yu Z, Yan J, Zhu K. Thermo-physical properties of CO2 mixtures and their impacts on CO2 capture, transport and storage: Progress since 2011. Appl Energy 2019;255:113789. https://doi.org/10.1016/j.apenergy.2019.113789.

[118] Benham AL, Katz DL. Vapor-liquid equilibria for hydrogen–light-hydrocarbon systems at low temperatures. AIChE J 1957;3:33–6. https://doi.org/10.1002/aic.690030107.

[119] Cosway HF, Katz DL. Low-temperature vapor-liquid equilibria in ternary and quaternary systems containing hydrogen, nitrogen, methane, and ethane. AIChE J 1959;5:46–50. https://doi.org/10.1002/aic.690050111.

[120] F. A. F, F.R.S., T. T. H. V. Physical constants of the system methane-hydrogen. Proc R Soc London Ser A, Contain Pap a Math Phys Character 1931;130:453–63. https://doi.org/10.1098/rspa.1931.0016.

[121] Hu M, Lin W, Gu A, Li J. Isothermal vapor-liquid equilibrium in CH4/H2/N2 system at a cryogenic temperature range from 100.0K to 125.0K. Fluid Phase Equilib 2014;366:16–23. https://doi.org/10.1016/j.fluid.2014.01.002.

[122] SAGARA H, ARAI Y, SAITO S. VAPOR-LIQUID EQUILIBRIA OF BINARY AND TERNARY SYSTEMS CONTAINING HYDROGEN AND LIGHT HYDROCARBONS. J Chem Eng Japan 1972;5:339–48. https://doi.org/10.1252/jcej.5.339.

[123] M Y, S Y, H M, I F, Fu C-T, Lu BC-Y. Phase Behavior Of Three Hydrogen-Containing Ternary Systems. Proc Adv Cryog Eng 1980;25:654–61.

[124] Akers WW, Eubanks LS. Vapor-Liquid Equilibria in the System Hydrogen-Nitrogen-Carbon Monoxide. Adv. Cryog. Eng., vol. 389, Boston, MA: Springer US; 1960, p. 275–93. https://doi.org/10.1007/978-1-4684-3105-6_32.

[125] Kremer H, Knapp H. Vapor-liquid equilibria in ternary mixtures of H2, N2, CO and CH4. Fluid Phase Equilib 1983;11:289–310. https://doi.org/10.1016/0378-3812(83)85030-4.

[126] Maimoni A. Liquid-vapor equilibria in the hydrogen-nitrogen and deuterium-nitrogen systems. AIChE J 1961;7:371–5. https://doi.org/10.1002/aic.690070306.

[127] Omar MH, Dokoupil Z. Some supplementary measurements on the vapour-liquid equilibrium of the system hydrogen-nitrogen at temperatures higher than the triple point of nitrogen. Physica 1962;28:33–43. https://doi.org/10.1016/0031-8914(62)90089-7.

[128] Yorizane M, Yoshimura S, Masuoka H, Naka T. The Measurement and Prediction of the Vapor-Liquid Equilibrium Relation at Low Temperature and High Pressure for H2-N2 System. Chem Eng 1971;35:691-696,a1. https://doi.org/10.1252/kakoronbunshu1953.35.691.

[129] Bezanehtak K, Combes GB, Dehghani F, Foster NR, omasko DL. Vapor-liquid equilibrium for binary systems of carbon dioxide + methanol, hydrogen + methanol, and hydrogen + carbon dioxide at high pressures. J Chem Eng Data 2002;47:161–8. https://doi.org/10.1021/je010122m.

[130] KAMINISHI G, TORIUMI T. Vapor-Liquid Phase Equilibrium in the CO2-112, C O2-N2 and CO2-02 Systems. J Soc Chem Ind Japan 1966;69:175–8. https://doi.org/10.1246/nikkashi1898.69.2_175.

[131] Ke J, Suleiman N, Sanchez-Vicente Y, Murphy TS, Rodriguez J, Ramos A, et al. The phase equilibrium and density studies of the ternary mixtures of CO2 + Ar + N2 and CO2 + Ar + H2, systems relevance to CCS technology. Int J Greenh Gas Control 2017;56:55–66. https://doi.org/10.1016/j.ijggc.2016.11.003.

[132] Ke J, Parrott AJ, Sanchez-Vicente Y, Fields P, Wilson R, Drage TC, et al. New phase equilibrium analyzer for determination of the vapor-liquid equilibrium of carbon dioxide and permanent gas mixtures for carbon capture and storage. Rev Sci Instrum 2014;85. https://doi.org/10.1063/1.4891796.

[133] Ke J, King PJ, George MW, Poliakoff M. Method for locating the vapor-liquid critical point of multicomponent fluid mixtures using a shear mode piezoelectric sensor. Anal Chem 2005;77:85–92. https://doi.org/10.1021/ac048970i.

[134] Spano JO, Heck CK, Barrick PL. Liquid-Vαpor Equilibria of the Hydrogen-Carbon Dioxide System. J Chem Eng Data 1968;13:168–71. https://doi.org/10.1021/je60037a007.

[135] Tenorio MJ, Parrott AJ, Calladine JA, Sanchez-Vicente Y, Cresswell AJ, Graham RS, et al. Measurement of the vapour-liquid equilibrium of binary and ternary mixtures of CO2, N2 and H2, systems which are of relevance to CCS technology. Int J Greenh Gas Control 2015;41:68–81. https://doi.org/10.1016/j.ijggc.2015.06.009.

[136] Tsankova G, Leusmann Y, Span R, Richter M. Dew Points, Dielectric Permittivities, and Densities for (Hydrogen + Carbon Dioxide) Mixtures Determined with a Microwave Re-Entrant Cavity Resonator. Ind Eng Chem Res 2019;58:21752–60. https://doi.org/10.1021/acs.iecr.9b04423.

[137] Yorizane M, Yoshimura S, Masuoka H. Vapor Liquid Equilibrium at High Pressure. Chem Eng 1970;34:953-957,a1. https://doi.org/10.1252/kakoronbunshu1953.34.953.

[138] Heintz A, Streett WB, Heintz A. Phase Equilibria in the H2/C2H6 System at Temperatures from 92.5 to 280.1 K and Pressures to 560 MPa. J Chem Eng Data 1982;27:465–9. https://doi.org/10.1021/je00030a029.

[139] Williams RB, Katz DL. Vapor-Liquid Equilibria in Binary Systems. Hydrogen with Ethylene, Ethane, Propylene, and Propane. Ind Eng Chem 1954;46:2512–20. https://doi.org/10.1021/ie50540a033.

[140] Trust DB, Kurata F. Vapor-liquid phase behavior of the hydrogen-propane and hydrogen-carbon monoxide-propane systems. AIChE J 1971;17:86–91. https://doi.org/10.1002/aic.690170119.

[141] Klink AE, Cheh HY, Amick EH. The vapor-liquid equilibrium of the hydrogen—n-butane system at elevated pressures. AIChE J 1975;21:1142–8. https://doi.org/10.1002/aic.690210614.

[142] Nelson EE, Bonnell WS. Solubility of Hydrogen in n-Butane. Ind Eng Chem 1943;35:204–6. https://doi.org/10.1021/ie50398a016.

[143] Connolly JF, Kandalic GA. Gas Solubilities, Vapor—Liquid Equilibria, and Partial Molal Volumes in Some Hydrogen-Hydrocarbon Systems. J Chem Eng Data 1986;31:396–406. https://doi.org/10.1021/je00046a008.

[144] Freitag NP, Robinson DB. Equilibrium phase properties of the hydrogen-methane-carbon dioxide, hydrogen-carbon dioxide-n-pentane and hydrogen-n-pentane systems. Fluid Phase Equilib 1986;31:183–201. https://doi.org/10.1016/0378-3812(86)90012-9.

[145] Brunner E. Solubility of Hydrogen in 10 Organic Solvents at 298.15, 323.15, and 373.15 K. J Chem Eng Data 1985;30:269–73. https://doi.org/10.1021/je00041a010.

[146] Fu MS, Tan CS. Solubility of hydrogen in a mixture of n-hexane and dicyclopentadiene from 313 to 363 K and from 2.0 to 5.5 MPa. Fluid Phase Equilib 1994;93:233–47. https://doi.org/10.1016/0378-3812(94)87011-X.

[147] Gao W, Robinson RL, Gasem KAM. Solubilities of hydrogen in hexane and of carbon monoxide in cyclohexane at temperatures from 344.3 to 410.9 K and pressures to 15 MPa. J Chem Eng Data 2001;46:609–12. https://doi.org/10.1021/je0003546.

[148] Katayama T, Nitta T. Solubilities of Hydrogen and Nitrogen in Alcohols and n-Hexane. J Chem Eng Data 1976;21:194–6. https://doi.org/10.1021/je60069a018.

[149] Purwanto, Deshpande RM, Chaudhari R V., Delmas H. Solubility of hydrogen, carbon monoxide, and 1-octene in various solvents and solvent mixtures. J Chem Eng Data 1996;41:1414–7. https://doi.org/10.1021/je960024e.

[150] Symons EA. Hydrogen Gas Solubility in the Dimethyl Sulfoxide – Water System: A Further Clue to Solvent Structure in These Media. Can J Chem 1971;49:3940–7. https://doi.org/10.1139/v71-660.

[151] Moore RG, Otto FD. The solubility of hydrogen in aliphatic amines. Can J Chem Eng 1972;50:355–60. https://doi.org/10.1002/cjce.5450500308.

[152] Hernández-Gómez R, Tuma D, Pérez E, Chamorro CR. Accurate Experimental (p, ρ, and T) Data for the Introduction of Hydrogen into the Natural Gas Grid (II): Thermodynamic Characterization of the Methane-Hydrogen Binary System from 240 to 350 K and Pressures up to 20 MPa. J Chem Eng Data 2018;63:1613–30. https://doi.org/10.1021/acs.jced.7b01125.

[153] Jaeschke M, Dorsfen H-MH, Humphreys AE. GERG TM7 - Supplement to the GERG Databank of High-Accuracy Compresion Factor Measurements. 1996.

[154] M Jett et al 1994 J.Chem.Thermodyn. - The nature of (p,Vm,T) surfaces of mixtures - (quantum + normal) and (normal + hydrogen-bonded) as summarized by their isochoric inflection loci.pdf n.d.

[155] Magee JW, Pollin AG, Martin RJ, Kobayashi R. Burnett-isochoric P-V-T measurements of a nominal 20 mol% hydrogen-80 mol% methane mixture at elevated temperatures and pressures. Fluid Phase Equilib 1985;22:155–73. https://doi.org/10.1016/0378-3812(85)85017-2.

[156] Magee JW, Kobayashi R. Isochoric (p, ϱn, T) measurements on (0.2005H2 + 0.7995CH4) at temperatures from 140 to 273.15 K and pressures to 70 MPa. J Chem Thermodyn 1986;18:847–58. https://doi.org/10.1016/0021-9614(86)90119-9.

[157] MIHARA S, SAGARA H, ARAI Y, SAITO S. The compressibility factors of hydrogen-methane, hydrogen-ethane and hydrogen-propane gaseous mixtures. J Chem Eng JAPAN 1977;10:395–9. https://doi.org/10.1252/jcej.10.395.

[158] Mueller WH, Leland TW, Kobayashi R. Volumetric properties of gas mixtures at low temperatures and high pressures by the Burnett method: The hydrogen-methane system. AIChE J 1961;7:267–72. https://doi.org/10.1002/aic.690070220.

[159] Bartlett EP, Cupples HD, Tremearne TH. The compressibility isotherms of hydrogen, nitrogen and a 3:1 mixture of these gases at temperatures between 0 and 400Å° and at pressures to 1000 atmospheres. J Am Chem Soc 1928;50:1275–88. https://doi.org/10.1021/ja01392a007.

[160] Bartlett EP, Hetherington HC, Kvalnes HM, Tremearne TH. The compressibility isotherms of hydrogen, nitrogen and A 3:1 Mixture of these gases at temperatures of -70, -50, -25 and 20° and at pressures to 1000 atmospheres. J Am Chem Soc 1930;52:1363–73. https://doi.org/10.1021/ja01367a011.

[161] Bartlett EP. The compressibility isotherms of hydrogen, nitrogen and mixtures of these gases at 0° and pressures to 1000 atmospheres. J Am Chem Soc 1927;49:687–701. https://doi.org/10.1021/ja01402a011.

[162] Bartlett EP. The compressibility isotherms of hydrogen, nitrogen and mixtures of these gases at 0° and pressures to 1000 atmospheres. A correction. J Am Chem Soc 1927;49:1955–7. https://doi.org/10.1021/ja01407a016.

[163] Hernández-Gómez R, Tuma D, Gómez-Hernández A, Chamorro CR. Accurate Experimental (p, ρ, T) Data for the Introduction of Hydrogen into the Natural Gas Grid: Thermodynamic Characterization of the Nitrogen-Hydrogen Binary System from 240 to 350 K and Pressures up to 20 MPa. J Chem Eng Data 2017;62:4310–26. https://doi.org/10.1021/acs.jced.7b00694.

[164] Jaeschke M, Hinze HM, Achtermann HJ, Magnus G. PVT data from burnett and refractive index measurements for the nitrogen-hydrogen system from 270 to 353 K and pressures to 30 MPa. Fluid Phase Equilib 1991;62:115–39. https://doi.org/10.1016/0378-3812(91)87010-7.

[165] Kestin J, Nagasaka Y, Wakeham WA. The Thermal Conductivity of Mixtures of Hydrogen with Nitrogen. Berichte Der Bunsengesellschaft Für Phys Chemie 1982;86:187–91. https://doi.org/10.1002/bbpc.19820860302.

[166] T. T. H. V. Isotherms of hydrogen, of nitrogen, and of hydrogen-nitrogen mixtures, at 0° and 20° C., up to a pressure of 200 atmospheres. Proc R Soc London Ser A, Contain Pap a Math Phys Character 1926;111:552–76. https://doi.org/10.1098/rspa.1926.0081.

[167] Wiebe R, Gaddy VL. The Compressibilities of Hydrogen and of Four Mixtures of Hydrogen and Nitrogen at 0, 25, 50, 100, 200 and 300° and to 1000 Atmospheres. J Am Chem Soc 1938;60:2300–3. https://doi.org/10.1021/ja01277a007.

[168] B D Ababio et al 1993 J.Chem.Thermodyn. - (Pressure, amount-of-substance density, temperature) of (1 - x)CO2 + xH2 using a direct method.pdf n.d.

[169] Al-Siyabi I. Effect of impurities on CO_2 stream properties. PhD Thesis Heriot-Watt Univ 2013:1–182.

[170] Pinho B, Girardon S, Bazer-Bachi F, Bergeot G, Marre S, Aymonier C. Simultaneous measurement of fluids density and viscosity using HP/HT capillary devices. J Supercrit Fluids 2015;105:186–92. https://doi.org/10.1016/j.supflu.2015.04.016.

[171] Sanchez-Vicente Y, Drage TC, Poliakoff M, Ke J, George MW. Densities of the carbon dioxide+hydrogen, a system of relevance to carbon capture and storage. Int J Greenh Gas Control 2013;13:78–86. https://doi.org/10.1016/j.ijggc.2012.12.002.

[172] Zhang J, Zhang X, Han B, He J, Liu Z, Yang G. Study on intermolecular interactions in supercritical fluids by partial molar volume and isothermal compressibility. J Supercrit Fluids 2002;22:15–9. https://doi.org/10.1016/S0896-8446(01)00107-3.

[173] Maurer A. Instrument Development and Speed of Sound Measurements in Hydrogen-Rich Mixtures Dissertation zur Erlangung des Grades Doktor-Ingenieur der Fakultät für Maschinenbau der Ruhr-Universität Bochum von Alexander Maurer aus Remscheid Bochum 2021 2021.

[174] Lozano-Martín D, Martín MC, Chamorro CR, Tuma D, Segovia JJ. Speed of sound for three binary (CH4 + H2) mixtures from p = (0.5 up to 20) MPa at T = (273.16 to 375) K. Int J Hydrogen Energy 2020;45:4765–83. https://doi.org/10.1016/j.ijhydene.2019.12.012.

[175] Brouwer JP, Vossepoel AM, Van Den Meijdenberg CJN, Beenakker JJM. Specific heat of the liquid mixtures of neon and hydrogen isotopes in the phase-separation region. II. The system Ne-D2. Physica 1970;50:125–48. https://doi.org/10.1016/0031-8914(70)90057-1.

Design of hydrogen production and use processes need reliable thermodynamic models.

A literature survey on equations of state for hydrogen mixtures is reported.

Available experimental data are tested against thermodynamic models.

The more relevant data needed to improve equations of state are identified.

Declaration of interests

☒ The authors declare that they have no known competing financial interests or personal relationships that could have appeared to influence the work reported in this paper.

☐ The authors declare the following financial interests/personal relationships which may be considered as potential competing interests: